5-2018

Characterization of Bacteriorhodopsin and Halorhodopsin Reconstituted in Lipid Bilayer Membranes

Joel Domkam Kamwa
University of Arkansas, Fayetteville

Characterization of Bacteriorhodopsin and Halorhodopsin Reconstituted in Lipid Bilayer Membranes

A dissertation submitted in partial fulfillment
of the requirements for the degree of
Doctor of Philosophy in Microelectronics-Photonics

by

Joel Domkam Kamwa
Technische Universität Darmstadt, Germany
Engineering Diploma in Material Science, 2007
University of Arkansas
Master of Science in Microelectronics-Photonics, 2014

August 2018
University of Arkansas

This dissertation is approved for recommendation to the Graduate Council.

Jiali Li, Ph.D.
Dissertation Director

Ingrid Fritsch, Ph.D.
Committee Member

Hameed Naseem, Ph.D.
Committee Member

Surendra Singh, Ph.D.
Committee Member

Rick Wise, Ph.D.
Ex-Officio Member

The following signatories attest that software used in this dissertation was legally licensed for use by Joel D. Kamwa for research purposes and publication.

Mr. Joel D. Kamwa	Dr. Jiali Li, Dissertation Director

This dissertation was submitted to http://www.turnitin.com for plagiarism review by the TurnItIn company's software. The signatories have examined the report on this dissertation that was returned by TurnItIn and attest that, in their opinion, the items highlighted by the software are incidental to common usage and are not plagiarized material.

Dr. Rick Wise, Program Director	Dr. Jiali Li, Dissertation Director

Abstract

Motivated to produce electricity with photon activated ion pumps, the main purpose of this work was to characterize the photosynthetic membrane proteins bacteriorhodopsin (proton pump) and halorhodopsin (chloride pump). The proteins were re-suspended in lipid bilayers. For this work, an experimental set-up was built which included: chambers for lipid bilayer formation and characterization, lasers for ion pump activation, and an AxoPatch electrophysiology system for small photocurrent measurement. Lipid bilayer membranes were formed using mostly folding method: folding two monolayers together. The membranes were characterized by their resistance, capacitance, and generated photocurrent. Photocurrent was generated upon illumination of lipid-protein membranes with lasers. A green (532 nm) laser was used to illuminate bacteriorhodopsin containing membranes to produce proton-based positive photocurrent, while a purple (405 nm) laser was used to illuminate halorhodopsin containing membranes to generate chloride-based negative photocurrent. The investigation included: the generation of photocurrent using formed lipid-protein membranes and their voltage dependence, the study of the effect of laser intensity and protein concentration on the photocurrent amplitude and efficiency, the TEM-imaging of photocurrent generating lipid-protein solutions, and an equation that can help predict photocurrent amplitude in the defined protein concentration range.

Acknowledgements

My profound gratitude goes especially to the members of my committee: Dr. Ingrid Fritsch, Dr. Hameed Naseem, Dr. Surendra Singh, and to the MicroEP director Dr. Rick Wise in whom I had the unique privilege to find trusted advisors, professors, and mentors. I am deeply grateful to Dr. Jiali Li for the opportunity offered to be part of her lab-group, for the advice, and for the guidance throughout this investigation. Through the atmosphere and the quality time spent together, Dr. Li's lab group became a family thorough the years; a family which is not easy to part from. For the discussions and the good time, my thanks go to my lab mates Mitu Acharjee, Dr. Harpreet Kaur, Dr. Santoshi Nandivada, and to all undergrad- and REU- students I had the privilege to guide in experimental research.

I especially want to thank Dr. Rick Wise again, and Renee Jones-Hearon for making this achievement possible, I feel blessed to have had you by my side.

I am profoundly thankful to Prof. Ken Vickers for giving me the opportunity to enter this path seven years ago.

The UoA ECS chapter and the entire MicroEP and Physics communities shall be recognized for the support throughout this entire period. This path was made possible through a STEM-scholarship followed by graduate assistantships which I am thankful for. I would also like to thank the University of Arkansas for providing the necessary resources to achieve this goal.

I would like to express my deep gratitude to my brothers, sisters and their families: Stephane & Nadege Kamwa, Orly & Micheline Tantchou, William (Cabano) & Jane Kamwa, Yves & Marie-Ange (Marange) Dsamou, Roger (LeDix) & Prudence (kiki52) Kamwa, Rodrigue (Big T) & Ingrid (Commissaire!) Tchoufong, Ibrahima & Idalia (I^2) Ouattara, Sinclair (Lumumba) & Amy Tantchou, Philipp (Felipe) & Kiki Guether, Christian (pa' a Bosch) & Annick (Mamanick) Tuetche, Aurelien (Senateur) & Tony Tchegho, Christoph (Prof) & Hugethe

Bobda, Sylvain (Chief) & Angel Tientcheu. I would like to extend my gratitude to the Wingolf fraternity in Germany, to the Cameroonian communities in Fayetteville and Germany, to the Ocean237 & families, to the TexArsolidarity and families, to the Zamis-du-mond2-briss & families, to the CamNWA-Society and families, to the Mamiton families, as well as to the whole Domkam's and Simo's descendants.

Pierre & Justine Tantchou shall be praised to the highest for being the parents they are to me and my wife.

I am eternally in debt to my father Jean-Dagobert Kamwa for the provided education and the mindset.

My son Jayden Kamwa, and my daughter Joella Kamwa, shall be applauded for making me a more disciplined and well-organized person.

To my wonderful wife and best friend, Dr. Larisse Tantchou-Kamwa: the last eighteen years have been a dream I hope never to wake up from. For the love, the serenity, the care, the support, the counsels, the friendship, and discussions, this achievement is equally yours my love.

God bless you for who you are

ALQJVMPCPASPT

Dedication

"I press on toward the goal for the prize of the upward call of God in Christ Jesus. Let those of us who are mature think this way, and if in anything you think otherwise, God will reveal that also to you. Only let us hold true to what we have attained" Philippians 3:14-16

For the pain, I caused her as, and since I indicated my intention to go back to school, I dedicate this work to my mom:

Julienne Sitchom epse. Kamwa.

Table of Contents

Table of Figures

Chapter 1: Introduction

Energy generation, conversion, and storage have never been a more central topic as today. Global warming and increasing energy demand require new types of technologies to be developed. One of the most prominent substitutes to conventional energy sources is the generation of electrical power using sunlight. Biologically inspired solutions of solar energy conversion are contributing to the improvement of ecologically friendly energy sources. This work supports this view, by leaning on the ability of certain proteins to convert into ion pumps following light photon absorption. These types of proteins have one structure in common called rhodopsin. Rhodopsin is an extremely light sensitive (sub-) protein found in animal and biological light sensing organs. There are two main type of rhodopsin including: higher animals (Bovine) rhodopsin, and archaeal (Archaic) rhodopsin. Bovine rhodopsin is found in animals' sight organ and commonly referred to as eyes' retinal. The archaeal rhodopsin is prevalent in some bacteria and mostly serves as sensory rhodopsin, or as trigger for a cation or anion pump. All types of rhodopsin include a light sensitive chromophore called retinal. The retinal is surrounded by seven spiral helices (Opsins), and is bound to amino acid residue via a Schiff base full of ion. In case of ion pumping rhodopsin, the retinal chromophore can be activated by light photons through the excitation of the retinal (Figure 1-1). The photo-activation induces a conformational change of the retinal from a ground (13-cis) state to an excited (15-trans) state [1].

Under native environmental conditions, the 13-cis ground configuration with two intermediates does not transport. Without light influence in the dark, the retinal activity of the 13-cis and the 15-trans conformation is moderated by thermal equilibrium. When illuminated, the retinas of ion pumping proteins undergo a multi-step cycle [2]. Archaeal rhodopsin is mainly responsible for two functions: emitting signal upon photo excitation, as exemplified by sensory

rhodopsin (mammal's eyes); and pumping ions through lipid bilayers upon photo excitation, as performed by bacteriorhodopsin (bR) and halorhodopsin (hR) [2].

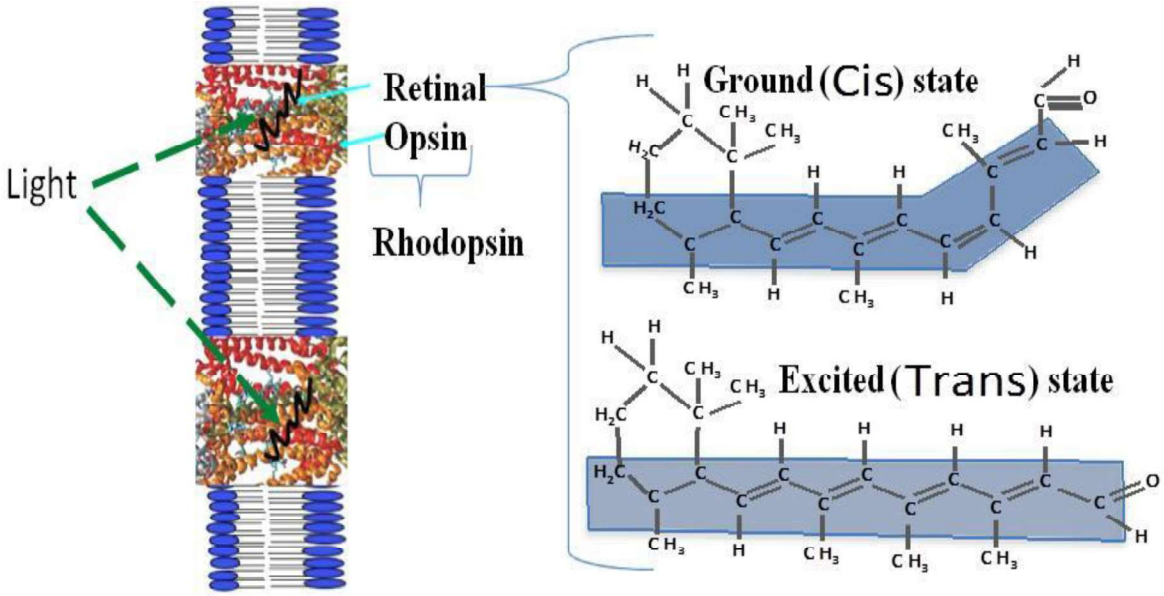

Figure 1-1:Retinal in ground (cis) and excited (trans) states.

The main purpose of this work was to characterize bacteriorhodopsin (proton pump), and halorhodopsin (chloride pump) resuspended in lipid bilayers as photosynthetic lipid-proteins membranes. A green (532 nm) laser was used to illuminate bacteriorhodopsin containing membranes and to produce proton-based positive photocurrent, while a purple (405 nm) laser was used to illuminate halorhodopsin containing membranes and to generate chloride-based negative photocurrent. TEM-imaging of photocurrent generating lipid-protein solutions, and an attempt to form an equation that can help predict photocurrent amplitude, were realized.

Chapter 2: Background of bR and hR and their current application

The photon adsorption of bR and hR containing membranes has been under investigation since the mid-1970s [3]. In early experiments, proteins with the ability to transfer ions were identified. The proteins were reconstituted onto lipid membranes, and the charge transfer from the protein during a cycle was characterized using the resulting transient capacitive current. It was evidenced that the capacitive current occurs upon activation of the protein ion pump with a laser light. The high capacitance and low conductance of lipid membranes into which the proteins are reconstituted, make the investigation of charge transfer easier. It is thus important to first investigate protein-free lipid membranes, to identify the lipid concentration at which membranes will exhibit high capacitance and resistance signals. Lipid membranes tend to be unstable, unless supported by a solid substrate [3].

Unsupported, freestanding membranes such as cell membranes are called micro-lipid membranes, while membranes on solid substrate, or membranes build across a septum, as in the present study, are generally called nano-membrane [4, 5]. Nano-membranes are formed across a pore (window) drilled in the solid substrate with a size between 100 and 280 μm [6]. Since a solid substrate can be easily manufactured, lipid bilayer can also be used in electronic devices such as semiconductors, solar cells, artificial prosthesis, and more [3, 7].

2.1 Applications

2.1.1 Artificial G-protein coupled receptors

As one of the most representative groups, which include human genes, G-Protein Coupled Receptors (GPCRs) are the target of several pharmaceutical products. The G-protein is, with a conserved set of residues, located and activated in the cytoplasmic region. Following the photo excitation of the chromophore, the set of residues goes into a conformational change and activates rhodopsin, which leads to signal transduction. The rhodopsin structure exhibits a

bundle of seven helices with a ground conformation (11-cis-retinal), which plays a crucial role in maintaining rhodopsin in the ground state. The interaction between the 11-cis-retinal and residues adjusts the wavelength at which the chromophore exhibits maximal absorption. bR was used to characterize the crystal structure of the GPCRs' rhodopsin. This finding allowed an insight in GPCRs, and revealed the arrangement of the individual receptors, as well as the mechanism governing the GPCRs activation [8].

2.1.2 Retinal prosthesis

bR is currently considered an excellent candidate for the development of retinal prosthesis. The photoactive protein is intended to slow down, or stop retinal degeneration, or in some cases replace degenerated retinal [9]. The bR based retinal prosthesis imitates the light-absorbing aptitudes of native visual pigments. The implant can generate a unidirectional proton gradient that is high enough to stimulate the undamaged neural network in the affected retina [9]. The implant consists of a multilayered oriented bR thin film that is captured between two membrane surfaces. The membrane surfaces are ion permeable and biologically inert. Oriented multilayers are necessary to absorb and convey enough protons for the neural excitation [9, 10]. The proposed bR based retinal implant can also be customized to individuals since pathologies vary from patient to patient. The prosthesis is intended to be tuned to selectively remove / replace damaged pixels, using the Q state, a bR-state with artificially extended lifetime [11].

2.1.3 Memory/storage

The bR stability was successfully tested in a wide pH range (pH1 to pH10), leading to the conclusion that bR can resist harsh environment. This was a solid argument for conducting experiments on writing and re-writing on bR films. It was proved that both processes, writing and re-writing on bR films several times, are possible without material degradation, which makes bR a good candidate for holographic recording medium [12]. bR based holographic memories

are intended to be based either on the transient M-state as a real-time processor or on the Q state (stable over months) as a long-term memory. The M-state with absorption at 410 nm is the farthest from the bR ground-state (570 nm) [13]. The switch between M-state and bR-state is called hypsochromic shift. The relaxation time of the M-state, is by approximately 10 ms, the longest and the most appropriate for holographic processing [14]. It was found that by absorbing 410 nm the M-state could directly reach the bR-state (Figure 2-1), which is typical for a photochromic pair. Photochromism is defined as the ability of two states of the same specimen with different absorption maxima to convert in each other through photonic stimulation. bR being a close to infinite protein, its photo-chromic applications would be superior to the currently used photochemical intermediate in holographic processing [11].

In order to write data on a thin bR page sample, a 570 nm green laser is used to start the photocycle. An orthogonally disposed 640 nm red laser pulses the signal in the bR thin page and converts the process into a branched photocycle. Once the O-state is at maximum, a spatial light modulator (SLM) allows the Q-state to be selectively created according to the frequency and amplitude of the intended bit/signal.

The process resembles an AND gate which allows writing only if photochemical conditions are met. To read the page, a green laser is required to activate the bR photocycle. During the O-state, a red laser without spatial light modulator, but tied to a charge-coupled detector, reads the presence (bit 0) and absence (bit 1) of Q-states on the film. To erase the data from the bR thin film page, a 380 nm blue light laser is used. The laser can be made coherent or non-coherent. In the coherent mode, the laser selectively converts the Q-states back to bR and, thus, erases only partially the data. In the non-coherent mode, the laser converts all Q-states back to bR and all are erased. Directed evolution has allowed researchers to form and erase Q-state as fast and efficient as per hardware standards [15, 16, 17].

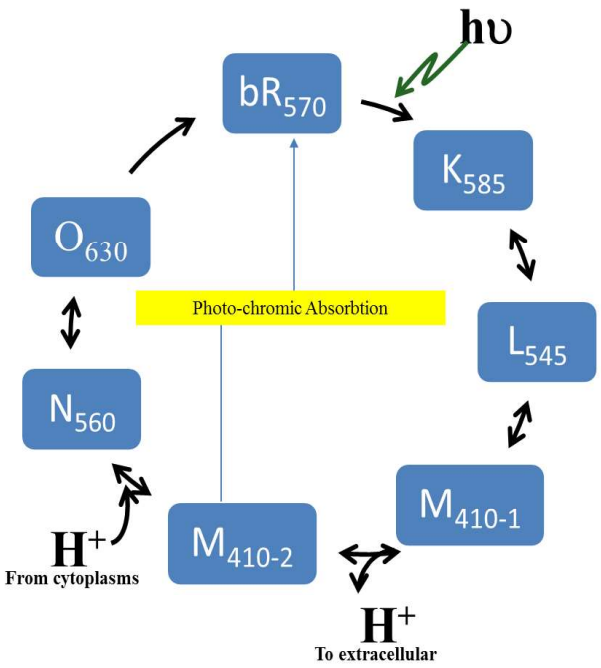

Figure 2-1: Bacteriorhodopsin (bR) photocycle steps for photo-chromic direct absorption.

The duration of the M intermediate is key in optical storage. bR mutants F171C-F219L and D96N-D96G with destabilized and stabilized M-state, respectively, have been tested by Dewang Ma et al. [13] because of their divergent M-state lifetime. It was revealed that, for the destabilized F171C & F219L, blue light flashes, during and after green light irradiation, induced high photocurrent and shorter M-state lifetime due to reduced M-state accumulation. D96N & D96G on the other hand generated small photocurrent with increased amplitude in presence of azide. This indicates a reduced proton pumping and a longer more stable accumulation of the M state. Mixing both mutants induced a disruption in Asp96 behavior. Photocurrent generated by the bR-D96G/F171C/F219L mixture was similar to the photocurrent generated by the D96N and D96G mutant type. The bR-D96G/F171C/F219L, however, exhibited negative current when irradiated with blue light only. This means that in the dark, the Schiff base is deprotonated. It was thus suggested that the new mutant bR-D96G/F171C/F219L could be used to stabilize the M-state. However, the proton pumping would be drastically impacted [13]. Using dried bR or

dried bR-polymer film, researchers found out that the photo response was not significantly different. It was thus concluded that protein immobilization might rather be the reason for the elongation of the M state decay [13].

2.1.4 bR based photoactive devices

Zhisong Lu et al. [18] were able to build a bR-based photoactive device using synthesized NaYF4:Yb,Er and NaYF4:Yb,Tm. The device was also referred to as "Up-Conversion Nanoparticle" (UCNP) incorporated with bR. In order to build the bR-based photoactive devices, bR was captured in a Purple Membrane (PM) film and deposited on gold Indium Thin Oxide (ITO). The mixture containing NaYF4:Yb,Tm and NaYF4:Yb,Er was used in three different ratios. The UCNP used could generate blue and green light under 980 nm near infrared irradiation. The generated light induced and accelerated the photocycle. This was followed by the transition from the M_{410} to the ground state. The ground state, in return, generated a stationary photocurrent. The photocurrent was controlled by adjusting, the blue and green light emissions from the UCNP over the NIR irradiation range. This approach opens possibilities to investigate the fundamentals of the bR photo-response, and further the capabilities to construct new bR-based photoactive devices [18].

2.1.5 Biomolecule-Sensitized Solar Cells (BSSCs)

In BSSCs, the anode is a porous nanoparticle (TiO_2 or ZnO) which is made photoactive by infusing it with bR. The bR, with a wide absorption range (500 to 600 nm), gets excited by light and injects electrons in the conduction band of the semiconductor material. Since the lowest unoccupied molecular orbital of TiO_2 is lower than that of the bR, the electron transition from bR to TiO_2 flows and does not require energy (Figure 2-2).

The electrons use the external circuit to transfer to the cathode. The excited bR collects a proton from the buffer and goes back to its ground state (Figure 2-2). The bR photoactive

abilities can be enhanced through modification such as: converting Glu residues into Gln at the extracellular site of bR (Thavasi et al. [19]); or by treatment of TiO_2 surface with $TiCl_4$ and controlling of bR loading (Mohammadpour and Janfaza [20]), these enhancement methods are accompanied by coating a light scattering layer of TiO_2 nanofiber. The low cost and non-toxic aspect of BSSCs justify such investigations although BSSCs are less efficient than the more popular Dye Sensitized Solar Cells (DSSC) [21, 22, 23].

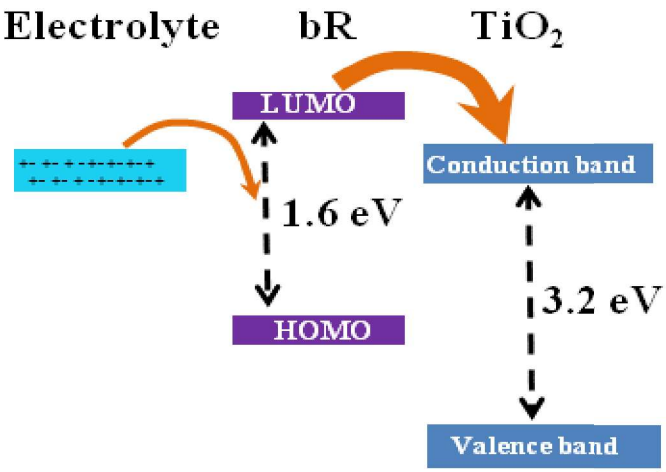

Figure 2-2: Principles of bR-based biomolecule-sensitized solar cells.

2.1.6 Bio-solar devices

bR-based solar devices are not only environmentally friendlier then common solar cells, but also more economic in manufacturing costs. Unfortunately, they are still far from reaching high power level. Research in the area of charge transfer enhancement, Quantum Dot (QD)-bR integration to harvest photons in different wavelengths, or creation of new bR-mutants with higher photo conversion efficiency and stability are necessary to take bR-based conversion devices to a competitive level [23]. Griep et al. [24] demonstrated that when a QD-bR device is irradiated with UV light during Fluorescence Resonance Energy Transfer (FRET), bR absorbs and transfers the energy. This observation was possible by fixing QDs on three different

substrates. The first substrate was made of QDs with retinal-free-bR, the second one was simply the QDs, and the third one was made of QDs with retinal-bR. It was noticed that from the three samples, only the retinal-bR sample exhibited a decrease in fluorescence on the QD spectra. Based on these results, Nabiev et al. [25] were able to show that FRET is the main QD quenching mechanism in bR-QD devices [25].

2.1.7 Durable hybrid catalyst

New, more active and durable, hybrid catalysts are envisaged for applications in metal air batteries, super capacitors, solar cells, and more. Silver (Ag) nanoparticles were deposited on top of a bR film through in situ electrolysis to produce the nano-bio electro-catalyst Ag/bR/CP. The bR film was supported by solid carbon cloth. The electro-catalyst was successfully tested for direct electrochemical hydrogen evolution [26].

2.1.8 Artificial Intelligence (AI - holographic associative processors)

The potential of the bR in transmission speed and high resolution makes it a good candidate for holographic recording [12]. Unlike serial memories found in computers, associative memories and processor mimic animal brain functions. This type of processor is specialized in searching through an entire memory bank, and to logically recall events as requested. The requested information or the closest possibles are qualified as answers. This process is also known as Artificial Intelligence (AI) [27, 28, 29]. Several research groups proposed Fourier-transform based holographic optical loops to bring this ability into devices. Hamp et al. [30], for example, have modified the bR efficiency so as to increase the M state lifetime, from biologically under a millisecond, up to the order of a second. This innovation allowed the creation of a bR based real time holographic interferometer (Figure 2-3) [31]. bR is, with exceptional holographic and photochromic properties, one of the most promising materials for the future conception of serial bio-memories [32].

2.1.9 Recording media

Nanoscale patterned arrays are good candidates to serve as recording media. With high densities (over 100 Gigabits/in^2), recording media based on nanoscale patterned arrays containing bR, will be better than existing ones with 3.7 Gigabits/in^2. Patterned arrays are usually referred to as photonic crystals. Their reaction to electromagnetic radiation is comparable to crystalline structure reacting to electrons [33]. This is particularly interesting since photonic band gap (energy point where no photon level is allowed) could be artificially fabricated. Possible applications include: spontaneous emission enhancement or inhibition, tunable optical filter, waveguide, and more [33, 34].

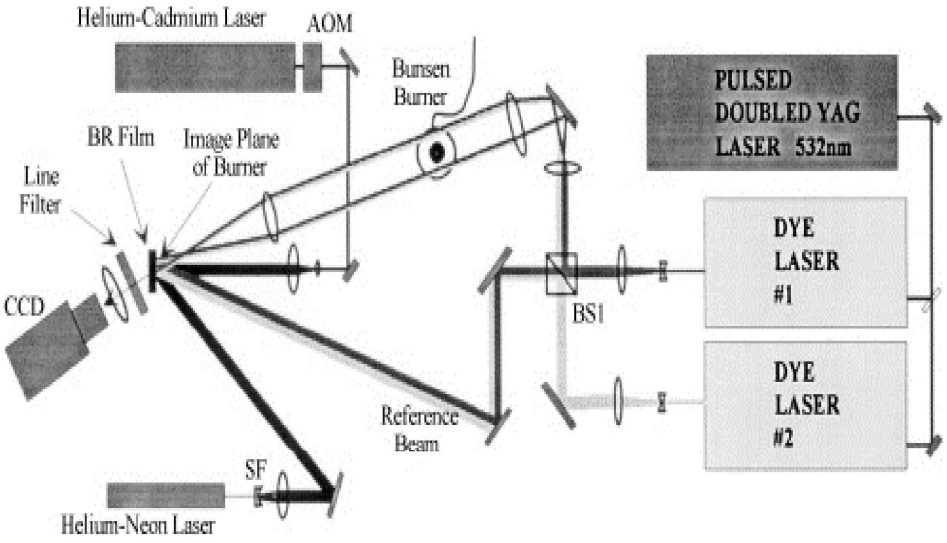

Figure 2-3: Set-up of a bR-based real time holographic interferometer.

The transient nature of the M state in the bR cycle, hinders the development of bR-based long-term memory. The Q state, a modified M state, is suspected to build a photo-chromic pair with bR, and could be used in long-term memory applications. The Q state with maximal absorption around 380 nm, can be made stable for months or years by reducing photo relaxation to its minimum [35]. Ongoing research is investigating ways to create the “blue” bR mutant that

could be used in holographic long-term memory [36].

2.1.10 Pore arrays formation for recording media

O. Jessensky et al. [37] were able to form self-organized, ordered hR-hexagonal pore arrays in anodic alumina using oxalic, and sulfuric acids as electrolyte. Both acids produced highly ordered hexagonal structures. The anodizing voltage was used to define the size of the ordered domains. This is because the expansion of aluminum during oxidation depends on the applied voltage. Hexagonal structures were obtained through the repulsive forces which arise at the metal/oxide interface caused by mechanical stress. In case of contraction and extreme volume expansion, the observed domains had no order [37].

Self-organized nanopore arrays with high aspect ratios and polycrystalline structure were fabricated by An-Ping Li et al. [38], the procedure included oxidizing aluminum in oxalic, sulfuric, and phosphoric acid in a two-step anodization process. Anodic electrolyte and applied voltage were used to control the pore distance and diameter [38]. It was shown that ordered pore arrays, formed by anodizing alumina in phosphoric acid, exhibit a polycrystalline structure compared to other formation techniques (anodizing aluminum using oxalic or sulfuric acid). The distance between pores was linearly connected to the anodic potential. The fabricated pores on porous anodic alumina exhibited a 50 to 420 nm distances between pores. Ordered domains could be observed only in case of volume expansion of aluminum during oxide formation [39].

2.1.11 Three-dimensional optical memories

The voltage dependency of the spectral change during bR photocycle pre-determines this protein for optical storage applications [13]. bR can be used in three-dimensional optical memories, when fixed in a polymer suspension. The bR/Quantum (bR/Q) photo-chromic pair can be used as binary bits, 0/1 respectively [40, 41]. The Q state is reached through the so-called branched photo cycle. This process requires two photons for activation; it is necessary to place

bR so as to be irradiated by two diode lasers in such a way that bR selectively drives information signal directly into the Q state. This "differential" absorptivity can be used to store, retrieve, and erase data from computer memory (see Section 2.1.3) [42].

2.1.12 Hydrogen generation

bR-based water splitting technologies for hydrogen production are the subject of numerous investigations [42, 44, 45]. bR is used as a bio-conjugated nano-material in either a particle or an electrode system. Adsorbing bR on a TiO_2 electrode significantly increases the system photo response. The more porous the electrode, the more the photo response is improved [22].

The Raman spectrum of bR adsorbed on the surface of Pt/TiO_2 nanoparticles (compared to the Raman spectrum of bR-free Pt/TiO_2) shows peak regions associated with the presence of retinal chromophore and anatase TiO_2. The energy level diagram of the device in the presence of the I^-/I_3 redox pair shows a possible charge injection in bR/TiO_2 [45]. bR serves as visible light harvester on Pt/TiO_2, and as optimizer of the protons-Pt catalyst interface which is responsible for the reduction of protons to hydrogen via the electron donor methanol. Photocurrent increased by 50% in the presence of I^-/I_3 redox using bR integrated TiO_2 electrodes. This increase is most probably due to charge injection from bR to TiO_2 nano-particles. 25 times increase in efficiency of hydrogen generation was realized. This implies that not only bR, but also bR impregnated TiO_2 nano-particles are photo efficient. This approach of generating hydrogen with bR-based devices is an excellent way to produce and store hydrogen as fuel using sun and salinity, which are infinite, as an energy source [45].

2.1.13 Hybrid bio electro catalyst

In situ electrolysis deposition and vesicle fusion processes were used by Zhenlu Zhao et al. [26] to fabricate a hybrid bio electro catalyst with Ag/bR and CP (poly-diallyl-dimethyl-

ammonium chloride). The researcher deposited silver (Ag) nanoparticles (AgNPs) on top of a bR monolayer supported by solid carbon cloth (CP). When tested as a cathode using light intensity with a wavelength under 550 nm, the measured over potential was 60 mV, which was lower than the bR-free cathode. The device exhibited high catalytic stability, and the interaction between silver nanoparticles and bR seemed to have enhanced the Hydrogen Evolution Reaction (HER) [26].

2.1.14 Nanotube electronics

Since their discovery in 1991, nanotubes were subject to numerous investigations. Especially because of their high electrical conductivity, biocompatibility, chemical stability, and mechanical strength [44]. bR was tested in combination with nanotubes as a nanoelectronic device by Bradley et al. [47]. Surprisingly, properties of both materials were maintained despite the interaction with each other. The asymmetry of charge distribution within bR was demonstrated using the device. It was suggested that an in vivo monitoring experiment could be performed on living cells by connecting them to the bR-based nanoelectronic devices [45].

Bertoncini and Chauvet reported on bR-integrated Single-Walled Carbon Nanotubes (SWCNTs) being used in molecular optoelectronics. The researchers used sonication to de-bundle SWCNTs before adding bR. Here also, both systems conserved their functionality. This shows that the conformational change that bR undergoes is not enough to impair the bR photoactivity [47].

2.1.15 Solid state (dry) systems

bR can be used in solid state (dry) system, even if the current flow is small. The current flow travels the same path as the protons over the retinal. This phenomenon was demonstrated by Yongdong Jin et al. [49]. When integrated in a Solid-State Planar Junction (SSPJ) as a monolayer, bR remains active and the junction becomes photoconductive. The junction

photoconductivity was related to the M-intermediate state of the bR cycle. The results showed that the bR conductance is rather negligible which means that proton transfer is mostly responsible for the processes associated with the bR presence in solid-state systems. It is complex to state that the I-V parameters depend upon the bR orientation since the zero-current photo-voltage was not measured [49].

2.1.16 Cellular Neural/Nonlinear Network (CNN) computers

The physical and chemical bR capability to act as a reversible transient holographic material was used by S. Tőkés et al. [12] to investigate its possible application on optical Cellular Neural/Nonlinear Network (CNN) computers. CNN is usually part of a Programmable Opto-Electronic Analogic Computer (POAC). The goal in this type of research is to investigate efficient bR application within POAC systems [12]. Compared to the common VanderLugt Correlator (VLC), the Joint Transform Correlator (JTC), also based on Fourier transformation, is a powerful information-processing unit used to identify patterns [50, 51, 52]. The JTC can also be used to pre-process basic operations on a CNN computer, which makes it possible to identify mathematical morphology for example [50].

2.1.17 bR based TiO_2 nanowire FET

Li et al. [53] investigated a promising approach for the application of bR-nano hybrid materials in bioelectronics. Based on a Field Effect Transistors (FET) fabricated with a bR-modified TiO_2 nanowire, the researchers investigated the effect of bR on the transistor performance. The results showed that the presence of the bR as bio-dipole was able to improve the FET performance. Following the changes induced by the bR on the TiO_2, an increase of more than 4 x 10^{-4} cm^2 V^{-1} s^{-1} was observed on the FET mobility. bR was identify as the main factor leading to the increased transfer, output, and hole mobility in the TiO_2 nanowire compared to the bR-free TiO_2 nanowire FET [53].

Many of the photoactive interactions inside bR remain unknown. This hinders the broad application of bR-based devices. None of the available tools can, so far, predict the bR mutation with the expected properties. Since the branched prototype responsible for the Q state is not standardized, Q-state-based devices are not considered for broad usage yet. Advancements in fields like mutagenesis and directed evolution are changing the way protein investigation is performed [54]. Site-Directed Mutagenesis (SDM) is also a promising approach to understand and create desired features in the bR characters. SDM consists of selectively introducing a specific mutation on the protein sequence inducing a desired behavior of the protein. SDM is, unfortunately, not adapted to large sequence proteins. Mutagenesis in bR focuses on optimizing residues responsible for the M, O and Q state since they have the largest potential. Innate dipole moment, gold binding ability and specificity of ion pumping are bR features that also enhanced via mutagenesis [55, 56].

2.2 Recent methods and techniques

2.2.1 Directed evolution & proteotronics

Directed evolution is with proteotronics (protein-based electronics devices) some of the terms used to describe the use of biological species in the development of new electronic devices. It consists of processes implemented to optimize the functionality of biomolecules outside their native environment. Directed evolution has allowed researchers to enhance the properties of biomolecules and to test them as bio-electronic components [57, 58, 58, 60]. This new research area promotes the understanding of proteins as to use them as reliable materials in bioelectronics devices. Both approaches − directed evolution and proteotronics − are responsible for the development of numerous biologic-based devices. As exceptionally stable ion pumps, bR and hR are excellent candidate for bio-electronic applications [12].

2.2.2 Surface treatment

Electrodes combining nano-particles and nano-fibers properties were developed by R. Mohammadpour et al. [61] to increase light harvesting. The tests showed that surface treatment and bR incorporation are central in manufacturing TiO_2/bR optical devices. The obtained maximum efficiency of 0.3% is the highest ever reported on TiO_2/bR optical devices [61].

2.2.3 Extension of the M state lifetime

D. Ma et al. [13] reported an approach to extend the lifetime of the M state (extended excitation). The idea suggested the incubation of bR in a macromolecular amphiphile called Poly (Ethylene Oxide)-b-Poly (Propylene Oxide)-b-Poly (Ethylene Oxide) (PEO–PPO–PEO). Compared to native bR, the M state duration of incubated bR can be extended while preserving proton pumping. The ability of the pluronic amphiphilic block copolymer to self-assemble (conformal change) is suspected to be responsible for the prolongated decay of the M state. Conformal change of the bR might be hindered by the mutant, which results from the assembly of the copolymer and the purple membrane. This information is important in the usage of bR as a storage material in optoelectronics [13].

2.2.4 Time-resolved current

A time-resolved current can be obtained by irradiating bR with a 540 nm laser and its mutant Asp-85-Glu with a 570 nm laser, both reconstituted in purple membrane and oriented in a polyacrylamide gel in 20 mM potassium chloride at pH = 8.0. In referenced experiments by H.J. Butt et al. [62], intermediate states were identifiable through microsecond time range of the current generated by the bR sample [62].

2.2.5 Simulation of bR activity in membrane

A. Nath et al. [64] studied various zwitterionic lipids. The lipids were mixed in different ratios with bR reconstituted in nano-discs. The goal was to study the relationship between the

type and concentration of lipids, and the bR photoactivity using transient absorption spectroscopy. Results showed that negative charged lipid increases the negative surface charge of nano-discs. It also showed that the bR retinal do not significantly change when changing the lipid composition [63, 64, 65, 66].

2.2.6 Solid Supported Membrane (SSM)

Solid Supported Membrane (SSM) with a surface larger than Black Lipid Membrane (BLM) can maintain high capacitance and low conductance. This was demonstrated by K. Seifert et al. [67]. The main advantage of SSM is the mechanical stability, which implies a higher resistance to external vibration and an extended lifetime of the membranes. This is a decisive benefit when stirring and /or replacement of the electrolyte is required. These types of membranes are appropriate for the investigation of charge transfer in ion pumps [67]. Results showed that despite the large surface, SSMs exhibit comparable characteristics as BLM. The causes leading to high capacitance and low conductance at the electrode potential, as well as the light artifact on SSM, must be investigated to explain the difference with BLM values [67].

2.2.7 Photo-activity enhancement

Silver (Ag) nano-particles were proven by Z. Zhao et al. [68] to be an excellent candidate to speed up proton pumping and enhance the bR photo-activity owing to their physicochemical properties. For this purpose, bR was integrated with Ag nano-particles and used to fabricate efficient nano-bio hybrid systems [68]. Several other investigations (references 68 - 73) used Surface Enhanced Raman Spectroscopy (SERS) to study interactions between bR and silver nano-particles when integrated with each other. Reduced Graphene Oxide (rGO), which enhances the interface between bR and anode nano-particle, was demonstrated by P. Wang et al. [73] to help improve the photo-activity of the bR-based system under white light irradiation.

2.2.8 Photoelectric conversion efficiency

The generated photocurrent can be enhanced using appropriate electrolytes as demonstrated by J. Chellamutu et al. [74]. The investigators found out that the photoelectric conversion efficiency and short-circuit current are twice as high as usual when using triiodide-based electrolyte [74]. It was proven that gel-electrolyte-based BSSCs (TiO_2/bR/AG) experience low electron recombination and, thus, provided the highest photocurrent and efficiency. In general, it was concluded that bR-sensitized BSSCs have a better photovoltaic efficiency. The high BSSC photocurrent derived from the bR reaction with the acetamine- electrolyte [74].

Chapter 3: Photon-activated protein ion pumps bR and hR

In this chapter, the theories, methods, and results presented in the literature are reviewed and used to introduce the concept of photosynthetic proteins. Emphasis is placed on bacteriorhodopsin and halorhodopsin, the proteins used in this work.

3.1 Definition

Although bovine rhodopsin exhibits several similarities with archaeal rhodopsin, it also presents differences in features and in the helices arrangement [75, 76]. The extra cellular region of archaeal rhodopsin exhibits a better organization and is larger than that of bovine rhodopsin. This explains the difference in functionality of these two retinal binding proteins, even if the two proteins have almost the same mass [8].

Numerous studies on these types of proteins have focused on the following issues: how does the photo activation (photo-isomerization and re-isomerization) of the retinal chromophore works? what structural and conformational changes occur in the protein during photocycle? and finally, is there a common mechanism rationalizing the different functions? [77, 78, 79]. Although not central for this research, these questions are discussed in Sections 3.2 and 3.3 to provide a better understanding and judgment of the basic principles underlying ion pumping in proteins.

Besides the known archaeal rhodopsin proteins bR and hR, spiropyrans, a type of organic compound with photochromic properties, also exhibit the ability to pump protons across polymeric membranes. Ultraviolet light induces a conformational change converting spiropyrans into the dye fluorescent merocyanine. Visible light, however, induces the reverse reaction converting merocyanine back into spiropyrans. Photocurrent is observed when a spiropyran containing membrane is irradiated with ultraviolet on one side and with visible light on the other [79].

3.2 Bacteriorhodopsin

Bacteriorhodopsin is a retinal protein found in the membrane of halobacterium salinarum in highly ordered arrays. Bacteriorhodopsin (bR) uses green light (530 nm) to translocate protons across membranes (proton pump) [79 - 83].

Upon illumination and photon absorption, bacteriorhodopsin (bR) isomerizes into specific states identifiable by their absorption maxima (Figure 3-1). These states are labeled in the literature with letters of the alphabet. The K-state being first followed by the L-, M1-, M2-, N-, and O- states. Bacteriorhodopsin returns to its initial state after the O state [84, 85]. M1 and M2 are the states with the highest absorption. The proton pumping increases when the protein is oriented in line with the incident light [84].

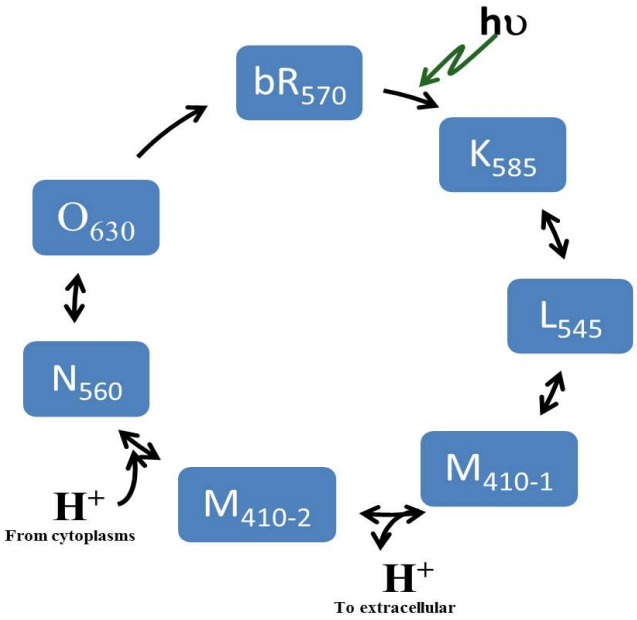

Figure 3-1: bR photocycle (~ 10 ms) and states.

Particularities of the K, L, M, N, and O states were investigated using Visual light Spectroscopy (VIS), Infra-Red (IR), Raman, and Nuclear Magnetic Resonance (NMR) spectroscopy. Each state exhibited clear, distinct spectral properties. The all trans retinal was

found only at the beginning and at the end (bR and O state) of the photocycle [84]. The M state and its substrates (M1 & M2) are the subject of several investigations because of their extended lifetime stability.

The balance and stability optimized between energy storage states, during photocurrent in bR, was first demonstrated by G. Nagel et al. [87]. However, the large conformational change of the structure and the change in voltage-dependent accessibility could not be related to each other [77]. The interaction of green light with bR-layers, and the subsequent photocurrent generation, was central in considering bR a potential material for optoelectronic applications [77]. bR was tested in different types of set-ups including field effect transistor, micro-environment, and more. In all cases, high voltage and light intensity were necessary to increase the induced photocurrent [85]. The voltage dependence of the current (Section 6.5) indicates a structure change during the cycle. The structure change, in return, implies a sequential charge tunneling among the amino acids located close to each other. Beside conformational changes, green light also induces the increase of free energy inside the protein, which changes its degree of connectivity [77]. It was shown that the selectivity of the ion is intrinsic to the transport features but not to the surrounding cytoplasmic and extracellular sites. An innovative model provided new details of the bR photo activity underlying processes [77, 88].

3.2.1 Structure and theory

bR uses light photon energy to induce large conformational changes of the retinal at sub-molecular level. These changes amplify the isomerization of the retinal. This photo-activation of the retinal is controlled by the arrangement around the Schiff base [89]. The bR Schiff base, also called proton donor, and the proton receptor amino acid, Asp85, are connected to each other by a water molecule, Wat402. The Schiff base is connected to the surface by a three-dimensional hydrogen-bonded network. This network is made of seven water molecules and the polar side

chains: Asp85, Asp212, Thr86, Trp86, Tyr83, Tyr57, Tyr185, Arg82, Glu194, Glu204, and Ser193. These side chains were identified by mutagenesis and are assumed to play roles in proton pumping [77, 90, 91].

The first state onto which bacteriorhodopsin isomerizes is called K-state followed by the L-, M1-, M2-, N-, and O- states (Figure 3-1). Bacteriorhodopsin returns to its initial state after the O state [92]. M1 and M2 are the states with the highest absorption. Besides water molecules, several amino acids are involved in the Proton Release Complex (PRC) including aspartic acid 85 (Asp85), aspartic acid 96 (Asp96), arginine 82 (Arg82), and glutamic acid 194 (Glu194) [93, 94]. Following the protonation of the aspartic residues in the M state, the proton is adsorbed in the N-O transition before being released in the transitions from the O-state back to the initial bacteriorhodopsin [95, 96].

Halobacterium salinarum uses high ionic concentrations to enhance the bR activity to survive extreme saline environment. The bR ability to survive in this type of environment is due to the complementary properties of its cellular and cytoplasmic sides**.** The role of tryptophan (Trp) in retinal isomerization was identified using single molecule force spectroscopy at various salt concentrations. Trp appears to be part of several interactions, which control the protein function and mechanical properties. Using Tryptophan (Trp) residues located in the extracellular side, the properties of both regions (EC and CP) adapt to each other to allow cell survival over a wide range of salt concentration. In fact, Trp creates a scaffold that is ultimately responsible for retinal mechanical isomerization, bR structure stabilization, and insertion in the membrane [89]. The scaffold also controls the mechanical parameters of the bR and is responsible for fastening the protein inside the membrane. The Trp-network can bind ions on two sides of the extracellular loops, these two sides are involved in proton transport and release. The cytoplasmic side experiences large modifications during the photocycle. The flexibility of the bond, which

leads to large modifications, is provided by weak interactions.

Rhodopsin's extracellular Trp-based network, which includes the retinal, is used to investigate the protein's efficiency as a bioelectronic component [89]. The closest residues to the Schiff base, which can contribute to its stabilization, are the carboxylate groups, glutamine 113. Approximately 3.5 Å separates the carboxylate and oxygen atoms of Glu113 and the nitrogen in the Schiff base. Around 3.4 Å separates the same Glu113 from the closest OH group of Thr94 which is closer. Other residues such as Thr92 and Thr93 are too far from the Schiff base [8].

Two hydrophobic side chains (Met44 and Leu47) together with a nearby peptide bond between Phe293 and Phe294 support the direction of the side chain of Lys296 along the rhodopsin axis, while the interaction between the two-phenyl ring and other helices stabilizes the region. It is uncertain if water molecules are involved in complex counter-ion making, since it is not clear how the stabilization of the protonated Schiff base occurs in the protein. Enhanced techniques in the future will provide insight details of the protonated region [89]. A water cluster located in the Proton Release Group (PRG) region generates the continuum IR spectrum observed during experiment. The proton release group in bR is a pair of glutamate residues (Glu194/204), which are conserved, and bond to each other by the delocalized proton. P. Phataka et al. [97] verified this theory, using wild type and bR mutant. This fact indicates that not amino acids but water clusters might be responsible for the proton storage. The small space of approximately 3Å between Glu-204 and Glu-194 identified in the ground and L states by High Resolution (HR) x-ray, allows one to think that the protons might get trapped there once released from the water cluster [97].

Fourier Transform Infra-Red (FTIR) is commonly used to characterize the switch which controls the M1 (EC) to M2 (CP) transition. However, IR spectroscopy is better suited to

investigate the role of protein backbone, retinal, amino acid side chains, and internal water molecules during the switch [98]. Contrary to accessibility-based theory, an affinity-based switch is more likely to be the explanation of the (M1-M2) EC-CP switch in bR. Recent studies have shown that coupled proton affinity (known as "subtle switch") can resist bR proton pumping and change without affecting the EC-CP accessibility. Time resolved investigation and identification of the intermediates are central in the detection of the switch mechanism in ion pumps. The unidirectional deprotonation of the Proton Release Group (PRG) leading to the increased attraction of proton by Asp85 provides the affinity switch for the Schiff base [62]. FTIR results show that while Asp-96 is central in the Schiff base re-protonation, Asp-85 is important for the proton release [62]. The absorption spectrum of bR-Asp-85-Glu isolated from halobacterium shows a pH-dependency of the molecule. Changes in pH create two photoactive species, with a maximal absorption at 610 nm for the first and at 550 nm for the second [62]. When bR is rinsed with detergent, the first specie (610 nm) is removed and the absorption maximum is shifted to 550 nm. The decay rate of the M state can also become pH dependent when the C=N double bond is weakened by the bR mutation at the Asp-96 level (Asp-96-Asn) [62].

Solid state NMR, x-ray crystallography, Fourier Transform IR and Raman spectroscopy are the most used methods to characterize the structural and conformational changes in bR following light absorption. The results obtained from investigations allow the definition of theories explaining the conformational change of the retinal, which leads to protons transfer and free energy during the photocycle [84]. X-ray diffraction was use by K. Palczewski [8] to determine the bR structure down to a 2.8 Å resolution. The diffraction data showed that the highly organized and structured extracellular side, which supports the seven trans-membrane helixes around the retinal, includes a disulfide bridge. In the inactive conformation of the

protein, the trans-membrane region is held by the 11-cis-retinal (ground state chromophore). The maximum absorption is defined by interactions between the 11-cis-retinal and a cluster of amino acids residues. The absorption wavelength varies according to the change in the interactions. The set of residues, which regulates the interaction between helices and the cytoplasmic region, was identified through x-ray diffraction and mutagenesis [8].

The presence of pure bR can be evidenced using Raman Spectroscopy (RS) which reveals the bR cis configuration, the bR Schiff base, and the polyene chains. Atomic Force Microscopy (AFM) is frequently used to investigate process underlying photocurrent, such as confirming the presence of trimeric bR patches (10 -12 nm in height) [62].

The FTIR of the bR mutant, Asp-96-Asn, mixed with azide shows a transient signal corresponding to the bond between azide and the protein in the M-N transition. The same signal is seen in wild type bR. This implies that azide can create the IR continuum band in the bR mutant Asp-96-Asn [99]. The mutant, Asp-96-Asn, exhibits a slow M to N transition due to the shortage of Asp-96. In the case involving azide, the M-N transition is accelerated owing to the ability of azide to bind Asp-96 and promote its activity [99]. FTIR results showed that the transition from late 13-cis to all-trans configuration is fast and non-rate limiting during the photo cycle [100].

Isomerization Switch Transfer (IST) and Local Access (LA) are two of the most used models to simulate protein proton pumping. While the IST model assumes that each state is independent from the other, the LA model presumes that each state of the photocycle is the result of the previous one, and will generate the subsequent one [101].

Besides the IST and the LA models, the Impedance Network Protein Analogue (INPA) model is used to simulate the bR photo activity and study underlying processes. The INPA model allows to define interactions radius (Rc) between amino acids and to approach a fit of monolayer

in low voltage [101]. The INPA model assumes that a node represents each bR amino acid and the interaction between amino acids is represented by links. The node/links configuration represents the protein backbone and is used to mimic the bR internal process [102, 104].

The light-induced vectoral proton uptake and release in bR is responsible for the proton balance. It is also responsible for the reduced O_2 consumption under light and acidification in the dark, observed on bR containing species in survival mode. In fact, bR uses its capability to absorb at two wavelengths (570 nm and 415 nm) to provide its host (halobacterium salinarum) with needed proton gradient [99]. The bR structural model developed in recent years contributes to a better description of the retinal conformation, leading to a better interpretation of the retinal functions based on enhanced resolution [77]. Researchers are now investigating the identification and structural localization of all hydrogen networks in the structure; this would allow a better usage of the capabilities of methods such as FTIR, NMR, and Electron Paramagnetic Resonance (EPR) in the analysis of the relationship between function and structure. New crystal forms allow a time resolved x-ray structural analysis to fully deploy owing to the better time and space resolution. This technique is a unique tool that is used to relate conformational change to function [77]. Using photochemical "cyclicity", a process to investigate how many cycles it takes for 37% of the protein to denature, researchers are also exploring new means to optimize the bR stability. It was found that bR with a cyclicity between 10^4 and 10^5 is in an acceptable range for usage in common bioelectronics devices (10^3 to 10^5) [27].

3.3 Halorhodopsin

Initially considered a sodium pump, hR was discovered on the halobacterium salinarum (HS) membrane at a lower concentration than bR**.** The hR retinal was localized between the alpha helical segments [101]. hR is the first photoactive biological anion pump for which an

atomic structure exists in 3D resolution [105, 106]. In nature, hR preferably orients inwardly**.** The chloride and proton pumping are directed toward the cytoplasmic side [106]. Proton pumping can be enhanced using azide (a catalyst that reverses hR deprotonation) [107]. When captured in lipid vesicles, hR absorption maximum does not change with the concentration of the electrolyte in which the protein is dissolved. In an experiment performed by E. Bamberg et al. [107], hR containing membranes generated photocurrent continuously. The pumping stopped when hR was replaced by acetate or sulfate. Acetate or sulfate induced a switch of the maximal absorption to 559 nm. This showed that the light driven hR purified from HS was the species responsible for the observed photo activity [108]. hR photocycle requires one photon for chloride pumping, and two photons for proton pumping. During proton pumping, the first photon is used for the formation of $H_{410.}$ The second one is used for its isomerization and reformation of H_{578}. The reformation of H_{578} induces a proton re-uptake by the Schiff base. This is a particularity of hR, a multi-ion pump, which can be used in diverse applications [109]. It was possible to identify individual photochemical reactions using flash induced spectra and photo cycle kinetics. For the experiments, light- and dark-adapted samples with various hR concentrations were captured in lipid membranes. It was noticed that the change of chloride concentration did not affect the photocycle [110].

After its retina is hit by a photon with approximately 480 nm wavelength, halorhodopsin isomerizes from all-trans to a 13-cis formation called H520. In this new formation, the protein undergoes distinct intermediate states before going back to its original state. The intermediate states can be identified by their absorption maxima. The whole cycle takes 14 milliseconds [111]. Halorhodopsin does not lose protons during this pumping cycle, but its 13-cis byproduct, the H520 mentioned above, does. The deprotonated H520 leads to the second, new byproduct called H410 from which halorhodopsin goes back to its initial state because of thermal effects.

This means that green light (> 500 nm) induces an accumulation of the H410 state, while inhibiting chloride pump [112]. Blue light, however, accelerates the halorhodopsin thermal transition from H410 back to the all trans configuration. In order to generate an optimal chloride ion stationary current, it is necessary to irradiate the protein-lipid membrane with white light (or with blue and green light) laser [112]. Laser intensity should preferably be stable and located at a defined distance from the membrane. Chemicals like azide accelerate the deprotonation of the H520 and, thus, the accumulation of H410. As a result, the chloride ion transport is drastically reduced or even stopped under green light irradiance. Additional blue/purple light reactivates chloride transport across the membrane [113, 114].

3.3.1 Structure and theory

The role of hR on the surface of halobacterium salinarum (HS) is not only to regulate the chloride concentration, but also to regulate the cell volume through the osmotic pressure during cell growths. The hR balances the chloride concentration by replacing the lost chloride ion via selective extrusion using different processes [110]. This is achieved by using the hR photochromic pigments as a photoactive energy source. hR is completely deactivated under yellow light [105, 106, 115]. The hR transfer mechanism starts with the chloride once the cis part of the retinal has been activated. First, the chloride deforms the surrounding proteins and opens a lumen. The helices C and G must collectively be in motion for the lumen near the Schiff base to open on the Ser115 attached to the retinal. A hook present in helix C facilitates up to 10 Å deformation of the proteins around the Schiff base. This deformation cannot be seen in the hR ground state. The protein deformation continues behind the chloride. The force deployed to open the lumen is also used to selectively prevent the chloride from flowing back in the now resting area (back isomerization). The active-to-resting cycle creates a kinetic valve. hR is ordered so as to optimize pumping while hindering ion leakage. The physiological timescale of the cell

allows a differentiation of the ion in pumping and resting states of the cycle [116].

Charge delocalization is a technique which can be used to increase the high of the barrier preventing back isomerization. Following charge delocalization, 25% of the positive charges are moved out of the Schiff base and the interaction between Schiff base, nearby chloride and Asp238 anion are weakened. The weakened interaction deteriorates the pumping rate. Since the absent positive charge (counter ions) is no longer contributing to it, the barrier of the 13-cis to all-trans is lower than in the normal K state, and the return is faster [100].

The hR photocycle includes light absorption of hR_{578} leading to the hR' state which converts into hR_{600} after a time interval k_1. After another time interval k_2, hR_{600} transitions into hR_{520}. Chloride is released to the hR^{1}_{410} after k_3, during the hR_{520} to hR_{640} transition. After k_4, hR_{640} converts into hR_{565}. hR_{565} subsequently converts into hR_{578} by "stealing" a chloride ion from the hR^{0}_{410} solution and the cycle can start again (Figure 3-2) [115].

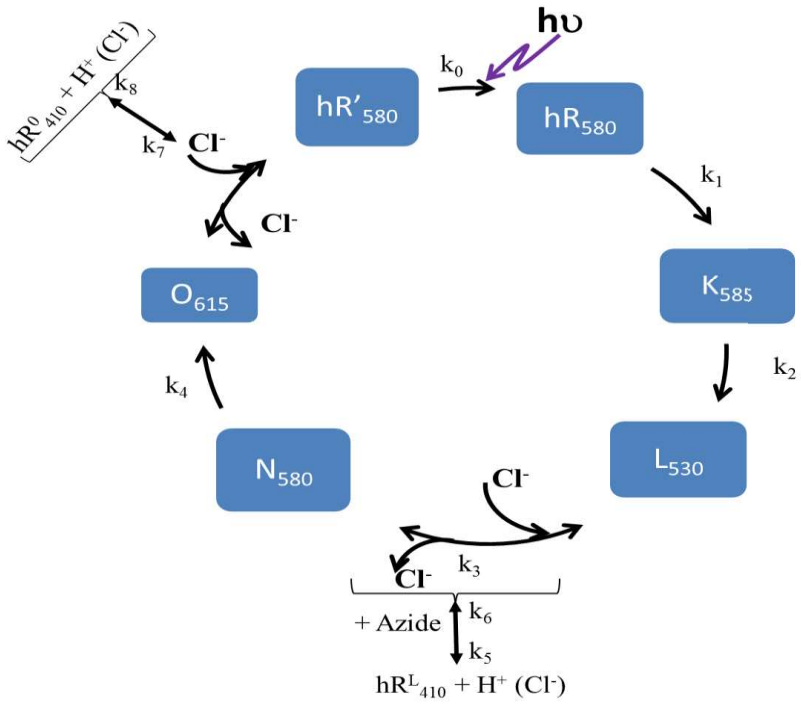

Figure 3-2: Halorhodopsin (hR) photocycle steps with ion release and reuptake.

3.3.2 hR transport mechanism

hR exhibits two steps during chloride pumping. The first pumping is instigated by the isomerization of the retinal, which involves the Schiff base. The second pumping step is carried by the rearrangement of the Arginine residues, leading to protein conformation change [116]. Within approx. 100 ms, the two intermediates hR_{520} and hR_{640}, accumulate in the photo-steady state. The third species, hR^{l}_{410}, formed from chromophore deprotonation, also accumulates. When flashing stops, hR^{l}_{410} thermally transitions into hR_{578}. This process takes several minutes. Azide, an inorganic base, is used to catalyze the deprotonation of the hR_{520}/hR_{640} complex and the re-protonation of the hR^{l}_{410} while maintaining the concentration of the hR^{l}_{410}.

The hR^{l}_{410} from hR and the M state of the bR are both the maximum absorption and protonation of their chromophore. Both states thermally relax into their respective ground state [118]. The quantum yield of hR_{578} was identified to be $\Phi_{(green)} = 0.344 \pm 0.02$, while that of the hR^{l}_{410} to hR_{578} transition was around $\Phi_{(blue)} = 0.01 \pm 0.004$ [115]. A quantitative description of the hR photocycle based on the formation and the decay of hR^{l}_{410} in light-adapted hR was proposed. The results obtained using flash photolysis and steady-state illumination confirmed the hR characteristic properties such as the photochromic behavior [115].

After relaxing into the electronic ground state, the protein exhibits a high-energy configuration, from which a photocycle is started. During the photocycle, the energy that is gradually released is used to transfer chloride ions along different sites. It results in the translocation of exactly one chloride from the extracellular to the cytoplasmic side of the membrane [119, 120]. Histidine, a single amino acid not present in bR, is suspected to be central in chloride pumping [101].

Upon illumination, protons start flowing. The flow slows down with increasing proton concentration and decreasing proton motive force (created by the proton flow). The proton flow

stops when the motive force approaches zero. The incident light drives the uptake of NaCl leading to a volume increase [116]. In its dark- and light-adapted forms, hR can exhibit chloride binding and chloride resisting behavior [110]. In the dark-adapted hR, the retinal is 45% all-trans and 55% 13 Cis. When constantly illuminated, the retinal moves to 75% all-trans and 25% 13 Cis. This implies that only 75% of the retinal will ever be active [121]. When excited in NaS (sodium sulfate), the retinal remains at 67% for both the dark- and the light-adapted forms. In some mutant (phR), the all trans configuration has a constant of 85% [101]. The change in the hR spectrum depends upon the chloride concentration. Increasing chloride will cause the spectrum to shift toward blue, while reducing chloride will push the spectrum toward red. Retinal light adaption occurs through evolving cycles with negligible quantum efficiency. The dark adaptation takes several hours to set. During light adaptation, a minimum of 25% of the retinal is always in 13-cis configuration. It is suspected that part of the all-trans retinal moves into 13-cis at the same time 13-cis converts to all-trans [122].

When captured in lipid vesicles, hR absorption maximum does not change with the concentration of the electrolyte in which the protein is dissolved. In an experiment performed by E. Bamberg et al. [107], the structure of wild type hR was resolved using x-ray spectrometry down to a 1.8 Å resolution. hR assembled to trimmers and surrounded a palmitic acid patch. A single chloride ion sits at the transport site next to the Schiff base and between the retinal and the Lys242. In order to stabilize the anion below the membrane surface, hR exhibits a combination of ion-ion and ion-dipole interactions. The fact that ions can be dragged across the Schiff base is suspected to be the reason why chloride and proton transport is possible with the same photoactive pump [76]. Wild type hR does not exhibit any purple membrane. It's mutated strains, however, overproduces 2D crystalline purple patches, which appear in the strain cell membrane [77]. A major difference between bR and hR is the volume of the wall chain on the

cytoplasmic side, which is smaller in hR. Furthermore, the space between the B, C, F, and G helices is larger in hR. These facts justify that chloride, and not proton ions, are pumped since chloride ions are larger than protons [101]. Additional investigation of the hR states would provide helpful information on the protein after excitation [122].

hR translocates chloride ions across the membrane by using the energy of the absorbed photon. The photon energy is stored through isomerization of the retinal chromophore from all-trans to 13-cis configurations. Quantum mechanical and molecular mechanical processes were combined to confirm that the energy is primarily stored via charge separation. The observed large fluctuation in retinal distortion makes twisting an improbable means of storage. However, only one fifth of the photon energy comes from the energy stored in the K state. This is probably because storing more energy in the K-state would also give rise to unproductive decay through the decrease of the energy barriers. This would lead to early back isomerization from the cis to trans configuration. The protein mastered the K state charge storage so that the decay rate always remains shorter (1/100ms) than the rest of the photocycle (1/20ms). hR acts as a light driven pump in which the photon energy is captured, stabilized, and stored until it can be used in photocycle steps [123]. As mentioned above, hR uses charge delocalization, and retinal twisting, to raise the barrier of the K state early and to lower the same barrier after the chloride has been transferred to allow back isomerization [123]. In order to be able to overcome successive energy barriers during the photocycle, hR stores up to 11 kcal/mol in the meta-stable K state and uses only 5 kcal/mol per barrier. hR could thus pump faster if less energy was stored. Halobacterium salinarum, the mother cell, uses the additional stored energy to limit the number of synthesized hR molecules needed to keep the pressure stable [124]. The hR evolution has maximized its potential by optimizing its capacity to store the energy needed to overcome the barrier, and by optimizing its capability to limit the storage capacity, which hinder unproductive decays and

premature back-isomerization [125].

3.4 Influence of biological agent

3.4.1 Azide

In the presence of azide and under a 410 nm flash illumination, the hR absorption tends to rise to a maximum and stabilize at a plateau value within the first 100 ms of the experiment [107]. Under 490 nm, in the presence of azide after the flash, hR absorption decreases slowly to zero within the first 100 ms of the experiment. Under a 610 nm flash illumination, the absorption slowly goes up to 578 nm (hR_{578}) within the first 200 ms of the experiment [115]. While stable current is possible under white irradiation, the absence of blue light inactivates the pump, azide was shown to accelerate this inactivation. Blue light is responsible for the formation of H_{410} requiring one photon, while white light is responsible for preventing H_{410} accumulation [107]. In the absence of chloride ions and ionophore, green light causes hR to pump protons in the same direction than chloride ions. After accumulating H_{410}, hR transfers a proton from the cytoplasm to the extracellular side of the membrane. Adding azide can enhance this capacitive current. An undershot will be noticed since azide favors H_{410} formation, which does not contribute to the generated current [107].

Acid pH can be used to neutralize the bR proton receptor (Asp85), the bR spectrum is then red shifted (acid blue form). By adding chloride, the spectrum shifts back to purple (acid-purple). The acid purple form can perform charge transport across the membrane upon continuous illuminations. bR can thus transport chloride in acid purple form. In hR, without proton donors or acceptors, chloride and azide compete to bind to the same site. Adding azide and upon illumination, a proton transfer is induced such as in bR. It is suggested that azide binds on the extracellular and cytoplasm and acts as a proton donor and /or acceptor [126, 127].

Azide can also be used to monitor protonation reactions in bR and hR [128, 129]. Azide

can bind with the donor side of the sulfate treated PSII. Azide has the particularity that the bands of its anti-symmetric infrared absorption cofactor are outside the bands expected from peptides [130]. To use hR as a continuous proton pump, azide is mixed with an hR containing solution and green light is used to irradiate the hR containing membrane. The first observed transient current indicates H_{410} formation. Adding the protonophore 1799 and blue light induces a large stationary current. Since gluconate and buffer anions cannot pass through the membrane, protons must be the only ion responsible for the current [107].

3.4.2 Triphenyltin and protonophore 1799

Triphenyltin, a charge carrier exchanger, and 1799, a protonophore, are added to stabilize the generated current. Triphenyltin and 1799 activate the porosity of lipid membrane for chloride ions and for protons. Since triphenyltin provides stationary current and the protonophore 1799 is not photoactive, chloride can be considered the unique charge carrier in the system. hR is reconstituted in lipids and adsorbed as planar lipid membranes. In practice, after forming the lipid membrane in a chamber system filled with electrolyte, and connected to an electrical system via Ag/AgCl electrodes for example, aliquots of the hR solution are added while stirring the solution and the hR photosensitivity develops within 40 min. Irradiating the membrane with a 100 W xenon lamp passing through filters to allow green and white light irradiation generates the photocurrent. hR reacts to purple/blue light by pumping chloride; adding green light causes hR to start pumping protons [107].

The fact that the negative charges are transported toward the protein containing chamber (negative current) demonstrates that the charges are adsorbed from the extracellular through the cytoplasmic side of the hR. Enhanced sample preparation is responsible for the improved current generation [107]. To demonstrate proton transport in the presence of Cl^- ions, the membrane lipid is permeabilized with triphenyltin and the protonophore 1799.

Under green light, protons are released following H_{410} formation. Only a capacitive current can be observed. Adding blue light initiates a balance between H_{578} and H_{410}. This is a stationary current with a large overshoot of the current. This time, however, the current is opposite to the current generated with chloride ion only. It shows that protons and chloride ions are pumped in the same direction [107].

3.4.3 Carbonyl Cyanide M-Chlorophenyl hydrazone (CCCP) and sodium chloride

R. A. Bogomolni [108] reported that, when irradiating an hR containing vesicle in the absence of chloride, the vesicle shows a positive large transient at 640 nm while showing a small negative one at 500 nm. 15 min after adding a 1.25 M NaCl solution, the transient observed at 640 nm is smaller than the peak observed without. The peak is still positive and larger than the now positive peak at 500 nm. Six hours after adding the 1.25 M NaCl, the photoactivity reversed completely. The transient observed at 640 nm is now negative and smaller than all the peaks observed with and without chloride and smaller than the positive peak at 500 nm. It was observed that light does not significantly affect the pH in the absence of the proton ionophore. After adding the protonophore, CCCP (Carbonyl cyanide m-chlorophenyl-hydrazine), the pH significantly changed and photoactivity was recorded. Adding triphenyltin to the solution completely inhibited the CCCP effect. The pH returned to normal and no photoactivity was observed [108].

3.4.4 Change of physicochemical conditions

Change of physicochemical conditions and point mutations are among the methods that contributed to discovering the change in ion specificity and retinal vectorality in the hR cycle. The approaches can be resumed in a three-stage cyclic event which organizes into four to six individual steps [77]. M. Kolbe [76] reported the 7 Å resolution of an hR specimen, which gives an idea on the structure of the rest of the rhodopsin family, including bR. The mechanism of the

ion transport observed in the mutant shR could so far not be definitively explained. None of the obtained results could accurately explain the signal transport from the photoactive receptor to the transducing part, nor the signal path inside the photoreceptor itself. Future work includes: the study of the molecules in their catalytic cycle and dark state, investigating the correlation between structural data, and functional data; and implementing them as a function of time [77].

3.5 bR - hR correlation

3.5.1 Ions transfer / cycle states

Bacteriorhodopsin and halorhodopsin are retinal proteins found in the membrane of halobacterium salinarum in highly ordered arrays [131, 87]. Owing to their fast photochemical reaction time, stability against photochemical degradation and sustained biological activity, bacteriorhodopsin and halorhodopsin are the most promising biomaterials used for light energy conversion, nonlinear optics, optical storage, and more [132, 133].

Bacteriorhodopsin and halorhodopsin (Figure 3-3) exhibit the same tertiary structure and share 30% amino acid sequence identity. This includes a circular arrangement of their helices, which constitute the trans-membrane pore, when incorporated in lipid membrane [134, 135]. While bacteriorhodopsin was found to be a proton pump, halorhodopsin was identified as a chloride ion pump primarily, and a reversed (inward) proton pump under specific conditions [136, 137].

In both proteins, the cytoplasmic and the extracellular side are separated by a Schiff base located in the center of the helices [135, 138]. It was found that halorhodopsin lacks the acid residues called aspartic acid 85 and aspartic acid 96 existing in bacteriorhodopsin. Both residues appear to be central in proton translocation [139, 140]. The ion transfer can be characterized using transient capacitive current, which is induced after the protein ion pump is activated with a laser light. Elaborated systems including amplifier, digitizer, and electrophysiology patch-clamp

instruments are used to capture and evaluate capacitance, resistance, and generated photocurrent.

While photon absorption of specific states in bacteriorhodopsin induces the proton translocation from the extracellular side, azide, a commercially available chemical, facilitates proton equilibrium at the Schiff base level through the cytoplasmic side in halorhodopsin [114, 141].

A two-photon driven proton transport results from blue light absorption by the H_{410}. H_{410} is the second state onto which halorhodopsin isomerizes (see Figure 3-1 and Section 3.3) [142].

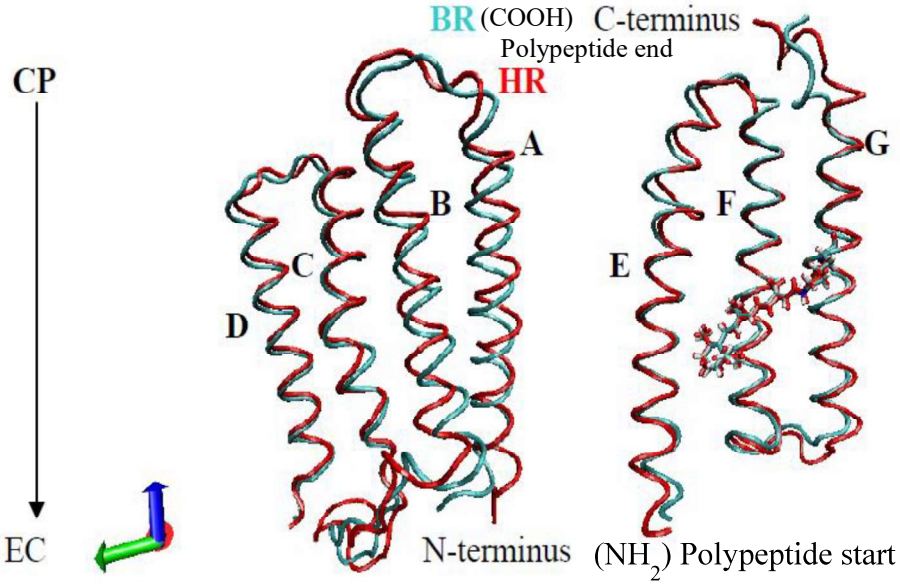

Figure 3-3: bR and hR structures.

In bR, the photo cycle starts with the L state. The changes in the pKa value of the Asp-85 (proton acceptor) induces the proton transfer toward the extracellular (EC) side and creates the M state. M_1 (EC side) and M_2 (CP side) are subsequently created. From M_2, where the proton is hosted by Asp-96 (proton donor), the proton is transferred to the Schiff base where the N state is generated. The M_1-M_2 transfer induces an increase in volume, which implies that the CP conformation has a larger volume than the EC. After the N state, the retinal relaxes into the O states followed by the bR and ground states with the host protein [101]. The L to M transition

in bR is the transfer of the proton from the Schiff base to the proton acceptor Asp-85. The most popular transition within a state (silent transition) is the M_1 to M_2 transition. Here the retinal switches from extracellular to cytoplasmic following the Schiff base deprotonation [143]. The proton donor, Asp-96, then refills the Schiff base on the ([100]) cytoplasmic side. This induces the immediate formation of the N state. The N state then hands over the proton to the surrounding medium. The retinal relaxes back to the all trans, giving rise to the O state and the initial ground state.

In hR, however, Thr replaces the proton acceptor. The cycle starts with a long L state, which goes into the N, the O, the silent hR', and the ground state hR [62, 144, 145]. During the cycle, the free energy stays almost constant. At a pH above 6 and very low proton concentration, the M_2 free energy is smaller than that of M_1. The M_1 to M_2 transition becomes unidirectional. In hR, the states are more ordered because enthalpy provides the energy for all reactions [120]. This means that none of all amino acids involved in proton transport is titrate (modified), and the charge transfer occurs inside the protein [101]. Except the K state, all states in both proteins have a positive electrogenicity. However, the bR L states can also have a negative electrogenicity, which defines the direction of the charge transport in general [146].

The cycle of both proteins can be described in three steps Isomerization, Switch, and Transfer (IST) [79]. In hR, the retinal relaxes into a 13-Cis form during the K to L transition following excitation. The protein is between two configurations until the N state is reached in the CP conformation. Between the two configurations, the site bonds become low and the chloride can be released. The volume decreases from the L to the N transition. This indicates that the CP has now a smaller volume than the EC [147].

The role of the hR^{l}_{410} present in hR is completely different from the role of the M state in bR. Blue light regulates the hR^{l}_{410} conversion in hR_{578} efficiently, while the M state

automatically goes into the O and the bR ground state [115].

3.5.2 Spectrum / structure

bR and hR exhibit very similar spectra (measured using time resolved spectroscopy). However, hR does not exhibit an M intermediate. This is the indication for an empty Schiff base. Instead, the L state is longer in hR than in bR. While the bR photocycle is driven by entropy, the hR photocycle is enthalpy driven [101].

Measuring the light dependent volume change of bR and hR containing vesicles shows that sodium and passive chloride extrusion cause an energized volume decrease of bR containing vesicles. hR containing vesicles, however, exhibited a volume increase during illumination, assumingly induced by chloride transport and cation (Na^+ or K^+) uptake. Chloride is transported against the ion and electrical flow. Without chloride on the external part of the vesicle, no light related potential, pH change, or swelling could be observed. This is in line with the assumption that hR is an inward chloride pump and reversed proton pump [105].

B. Schobert et al. [105] investigated the primary structure of hR and bR by gene sequencing. The study revealed around 25% homology between bR and hR, with up to 36% similarities in the trans-membrane part, and only 19% in the loop [105]. The similarities in sequence identity were identified to be close to 66%. bR hosts protons, the acceptor (Asp-85) and donor (Asp-96) group on helices C. Both groups (Asp-85 and Asp-96) are replaced in hR by natural residues. The extracellular sides of both proteins (hR & bR) are characterized by the existence of a proton release complex including Arg-82, Glu-194, Glu-204 (Thr in hR), and several water molecules. The protonated Schiff bases are stabilized by highly conserved amino acids such as Asp-212 and Arg-82 in bR, and position 238 and position 108 in hR. These positions also serve as counter ion complex. Arg plays an important role in the hR chloride transport process [148, 149].

3.5.3 Protein extraction

According to S. Dutta et al. [9], bR and hR extraction methods can be based on detergent combination. The researchers used batho-Phenanthroline-10 and 8 (Phen-C10 or Phen-C8) combined with one of the following five specific non-ionic detergents: octyl β-D-glucoside (OG), octyl β-D--1-thioglucoside (OTG), nonyl- β-D-glucoside (NG), decyl- β-D-maltoside (DM), and dodecyl- β-D-maltoside (DDM). These detergents are frequently used in membrane protein purification. The combination tested on bR showed that, up to 86% of the bR was extracted while preserving the bR native conformation and excluding up to 90% of artificial contamination agent. The second method designed for engineered membrane included the conjugation of the same hydrophobic complexes while keeping the membrane protein in the bilayer environment. This method was tested on hR and showed up to 89% extraction and over 85% removal of artificial contaminants while keeping the hR functionality [9].

Chapter 4: Lipid membrane

4.1 Definition

The lipid membrane role in nature is to provide cells with a frame, and to protect the cells inside. The diverse type of proteins encrusted in lipid bilayers serves as communication agents with the outside. Lipid membranes are thus the backbone for most of the cells properties. The biomedical industry uses mock systems, mostly vesicles but also solid supported bilayers, to test the interaction of medication with body cells and to evaluate the efficiency of developed drugs [56]. A detailed diagram of a cell lipid membrane is shown in Figure 4-1 [94].

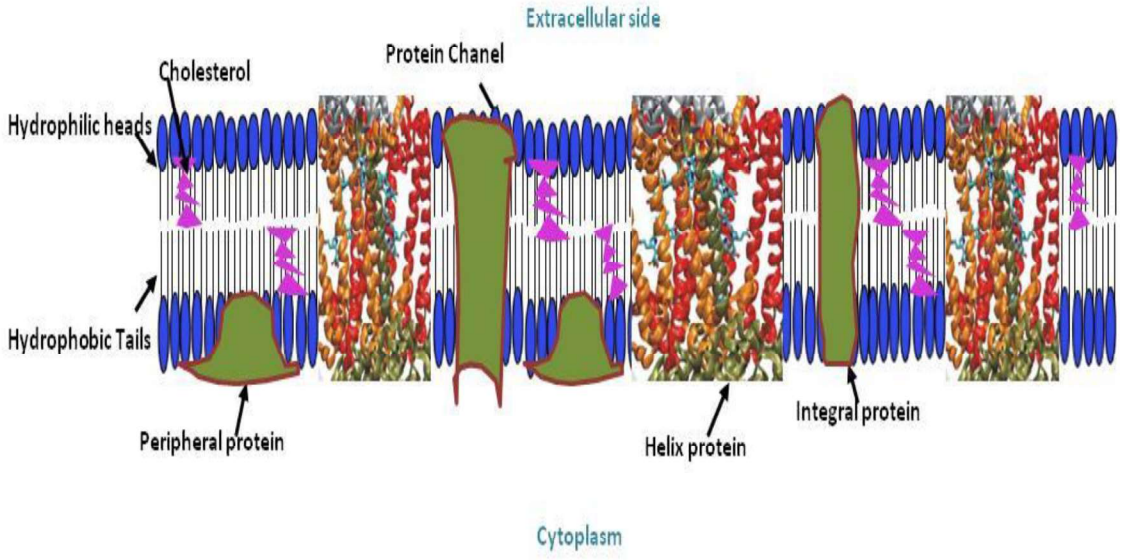

Figure 4-1: Diagram of a typical cell lipid membrane.

Artificial bilayers were initially developed to understand complex systems such as two-dimensional fluid plasma membranes [94]. Mueller et al. [95] developed the Black Lipid Membrane (BLM), the first reliable artificial lipid membrane system. The researchers used an extract of brain lipid to form membranes by painting the phospholipids solution across a 1 mm septum separating two chambers filled with aqueous solution.

The possibility to form and transport membrane on a solid substrate was later developed

by Tamm and McConnell [96]. This was followed by the development of lithographically patterned corals from lipid bilayers by Boxer et al. [150]. Using these results and advances in the field, Spinke and Yang [151] were able to couple lipid bilayers with several substrate types: metals, oxides, and semiconductor electrodes using a thin film approach.

4.2 Di-Phytanoyl (3,7,11,15-tetramethylhexadecanoic) Phosphatidyl-Choline (DPhyPC)

4.2.1 Structure

The structure of this artificial lipid is shown in Figure 4-2. The structure includes archaebacterial, and non-mammal carbon chains connected to each other with phosphate and glycerol groups. The carbon chains are specific to archaebacterial and non-mammalian membranes. The robustness of this lipid compared to other lipids leans on the saturation of its hydrocarbon chains. The robustness of the lipids conveys to the DPhyPC a very low transition temperature (< 120°C), an exceptional stability in most biological fluids, and the largest area / lipid rate among commonly used lipids. Beta-bodipy asolectin, agarose type 7, alamethicin, and gramicidin D are some other lipids used in the formation of artificial lipid bilayers [132].

4.2.2 Characteristics

DPhyPC is a useful lipid that can be tailored to an artificial system to support investigations of processes such as: electrophysiological measurements, model ion channels, basic lipid mixtures, peptide-lipid interactions, and the relationship between the membranes intrinsic curvature and its packing structure [151]. DPhyPC cannot be used to investigate water related processes accurately when the lipid interacts with other entities. The permeability of water in DPhyPC was proven by Tristram-Nagle and Kim [151, 152] to be more related to the membrane area than to the membrane thickness. The group described DPhyPC as a temperature dependent structure with a central hydrocarbon core layer surrounded by two interfacial headgroup layers.

This result was used by Shinoda et al. [153] to demonstrate that the water permeability in saturated hydrocarbon is mostly controlled by the small diffusion rate compared to unsaturated chains. For this reason, unsaturated hydrocarbon membranes are less water permeable in the hydrocarbon region.

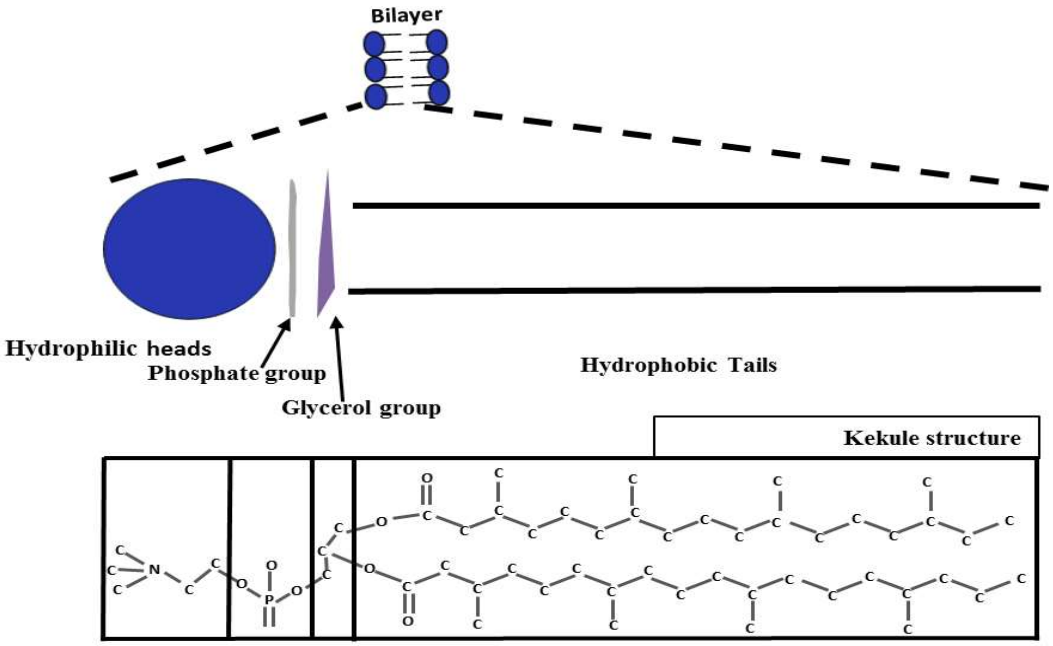

Figure 4-2: Structure of the used DPhyPC lipid.

Mammalian cell membranes, for example, exhibit an unsaturated carbon chain and cannot be simulated accurately using DPhyPC membranes, unless the permeability has been adjusted. The permeability of DPhyPCcan be adjusted by changing the concentration of water which influences the structure of the lipid. In fact, under a ratio of 16 water molecules per each DPhyPC molecule, the orientation of the headgroup is changed and so is the ground structure of the lipid: a cubic like structure is observed. When the water/lipid ration is around 6, DPhyPC exhibits a hexagonal structure [152].

Chapter 5: Description of the experiment

5.1 Definition

The equipment and set-ups used in this research are presented in this chapter. Various methods used in the lipid-protein environment to conduct experiments will be presented. A Faraday cage was fabricated around the final set-up to shield the experiments from surrounding noises.

5.2 Membrane formation

Forming membranes is a natural protection mechanism to shield sensitive systems from surrounding harsh environments. Nature uses membranes as “walls” to protect and keep internal structures safe from outside influence. Similar to walls, artificial and natural membranes include “windows” and “doors” through which separated environments can communicate and exchange. While lipids can be seen as walls allowing two environments to sense and adapt to each other but not to communicate, proteins can, most of the time, be considered as “doors or windows” through which two environments can exchange. Membranes are thus the main target when it comes to establishing a communication between environments that should not be mixed together. Several techniques have already been developed in the past. The first reliable artificial system that was used to investigate bilayers was developed by Mueller et al. [91]. This method, known as Black Lipid Membrane (BLM), consists of painting phospholipid made of brain lipid extracts across a 1 mm septum. The septum is used as a channel connecting two chambers filled with conductive aqueous solution. The advantage of the Black Lipid Membrane (BLM) is the decay of th intrusion present inside the membrane, which leads to thin robust membranes. Boxer et al. [150] developed a lithographic procedure to fabricate patterned corals out of such lipid bilayers.

In 1984, Tamm and McConnell [96] developed the solid substrate membrane. This method consists of the formation and deposition of membranes on solid substrate. Spinke and

Yang [151] found out that lipid bilayers could be coupled with different substrate materials such as metals, oxides, and semiconductor electrodes using thin polymer films. All these methods pioneered the artificial formation of polymer lipid bilayers. The folding and the painting methods used in this work are derived from the above-described techniques. Both procedures are among the most used membrane formation techniques.

5.2.1 The folding method

The folding method resulted from the bilayer formation technique developed by Montal and Mueller in 1971 [154]. The principles of the method are depicted in Figure 5-1. The folding method is the method closest to natural processes, since the membranes are formed without external interferences. After filling up the two compartments until under the septum with an electrolyte solution Figure 5-1 (C), the membranes solutions are injected on top of the electrolyte Figure 5-1(D). The membrane solutions are expected to float atop the electrolyte solution since they are partly made of hydrophobic lipid. Next, the solution level in both compartments is raised by sequentially injecting more electrolytes in each of the compartment Figure 5-1(E). A monolayer is formed in each compartment at the passage of the membrane solution over the septum. Since the septum is an opening, both monolayers fall into each other forming a bilayer Figure 5-1(F) & (G).

5.2.2 The painting method

Painting a membrane is the method of choice to create new membrane types. This method offers the advantage for the operator to physically craft monolayer or multilayer, and thus to define the membrane's exact location, thickness, physical, and electrical characteristics.

Figure 5-2 cartoons the steps of the painting method: in Figure 5-2 (A) and Figure 5-2 (B) the window on the cup-chamber is pre-painted with the lipid solution to facilitate the membrane adherence. In Figure 5-2 (C), both compartments are filled with the same electrolyte solution

above the septum level. After submerging a functionalized brush (reduced number of bristles) or a syringe tip into the electrolyte solution, the membrane is painted across the pre-painted septum.

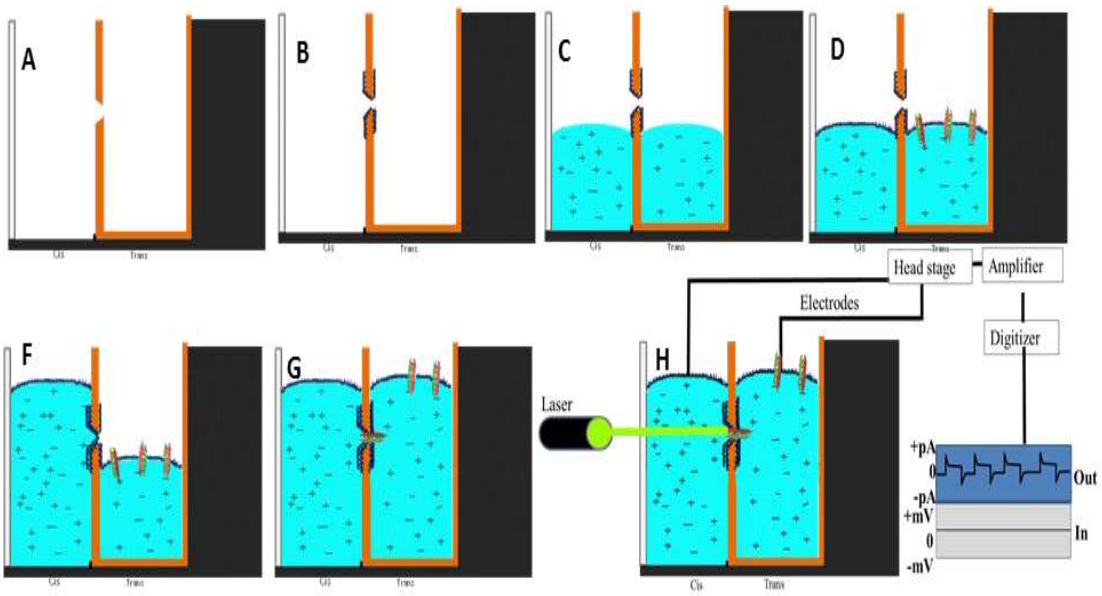

Figure 5-1: Steps of the folding method used to form membranes.

Using a syringe with its tip submerged into the electrolyte, a bubble is blown and popped on the pre-painted septum as shown in Figure 5-2 (D). The bubble layer is expected to stick to the pre-painted wall around the septum. In the case of a functionalized brush, closing the septum by crossing it with the brush forms the membrane. Painted membranes are usually thicker and, thus, more robust.

5.3 Characterization

The results presented later in Chapter 6 were obtained by characterizing the signals from the formed membrane. To obtain accurate results, calibrating the system was a fundamental part of the research. For this purpose, tests were designed and carried out for each part of the system. Protein absorption, membrane capacitance, and resistance were used as core parameters and obtained mostly through calculation using values from experimental results.

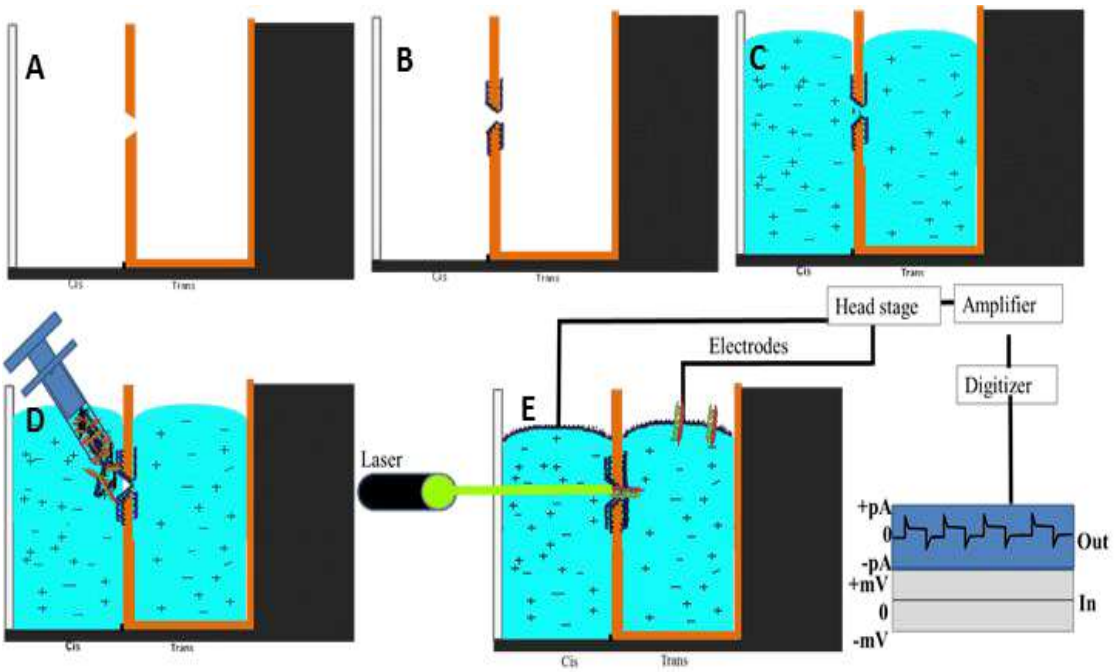

Figure 5-2: Painting methods.

5.3.1 System

The system used to perform the experiment is presented in Figure 5-3. Silver chloride (AgCl) electrodes were used to connect the bath (experiments area) to the headstage.

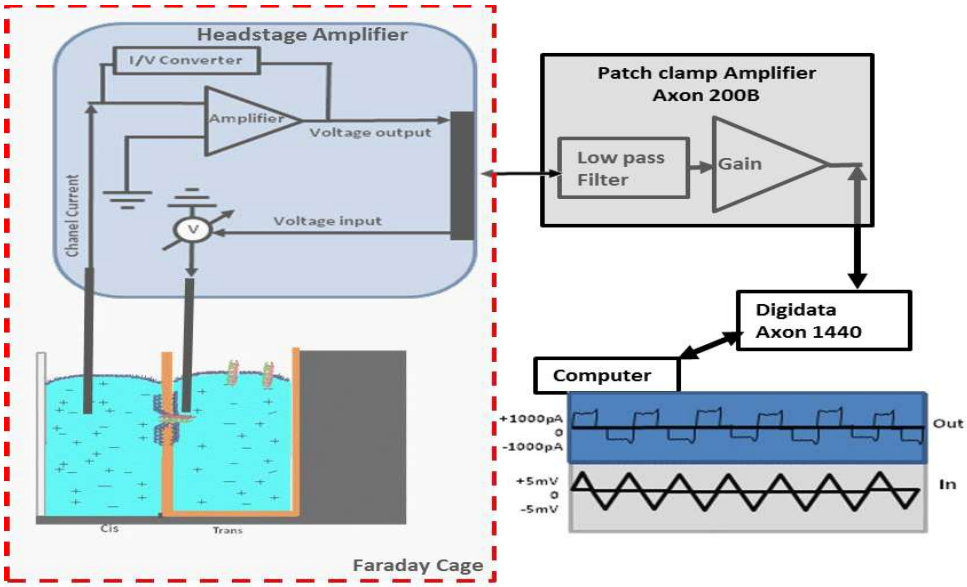

Figure 5-3: Experimental set-up.

The headstage was the unique contact between the experiment stage and the control unit, which consisted of computer, digitizer, amplifier and function generator. Most connections between the digitizer and the amplifier allowed the operator to control several signals via the computer, while the signal from the function generator was controlled manually.

Figure 5-4 shows the detailed connection of the system. The headstage was connected to the bath (C1) and to the amplifier. This allowed the applied voltage from the generator to be sent to the membrane via the amplifier, the headstage, and the electrodes. The voltage applied to form and test the membranes was generated by the voltage generator and sent to the computer over the digitizer and to the membrane via the amplifier and electrodes. For this purpose, a "T-joint" was used to connect the function generator to the channel 3 (C3) of the digitizer and to the external command rear switch located in the back of the amplifier (line C2). The digitizer was connected to the computer via a USB2 port (C2). The scale output of the amplifier was connected to the channel 0 of the digitizer to conduct the signal generated by the amplifier for the measurement of the resistance (C3). The 10 mV output of the amplifier was connected to channel 1 of the digitizer (C4); this connection allowed the amplified response signal from the membrane to be displayed on the computer. The channel 2 of the digitizer was connected with the 10 kHz (I) output of the amplifier for the generated current (C5) to be displayed on the computer screen. The second external command of the amplifier and the analog output of the digitizer were connected to each other. The connection aimed at transmitting the voltage signal used to measure the membrane resistance to the cell (C6). A direct measurement and display of the membrane characteristic was achieved by connecting the gain, the frequency, and the cell capacitance of the amplifier to the channels 0, 1, and 3 of the digitizer telegraph input (C7, C8, C9), respectively. All connections were tested using Clampex and pClamp.

5.3.2 Chamber

The membranes were mainly formed in a two-chamber system. The chambers were manufactured by Warner Instruments [a Harvard Apparatus Company, Hamden, Connecticut (warneronline.com)] under the product BCH-M13 and BCH-M22. As depicted in Figure 5-5, the Warner chamber system is made of two compartments and a cup.

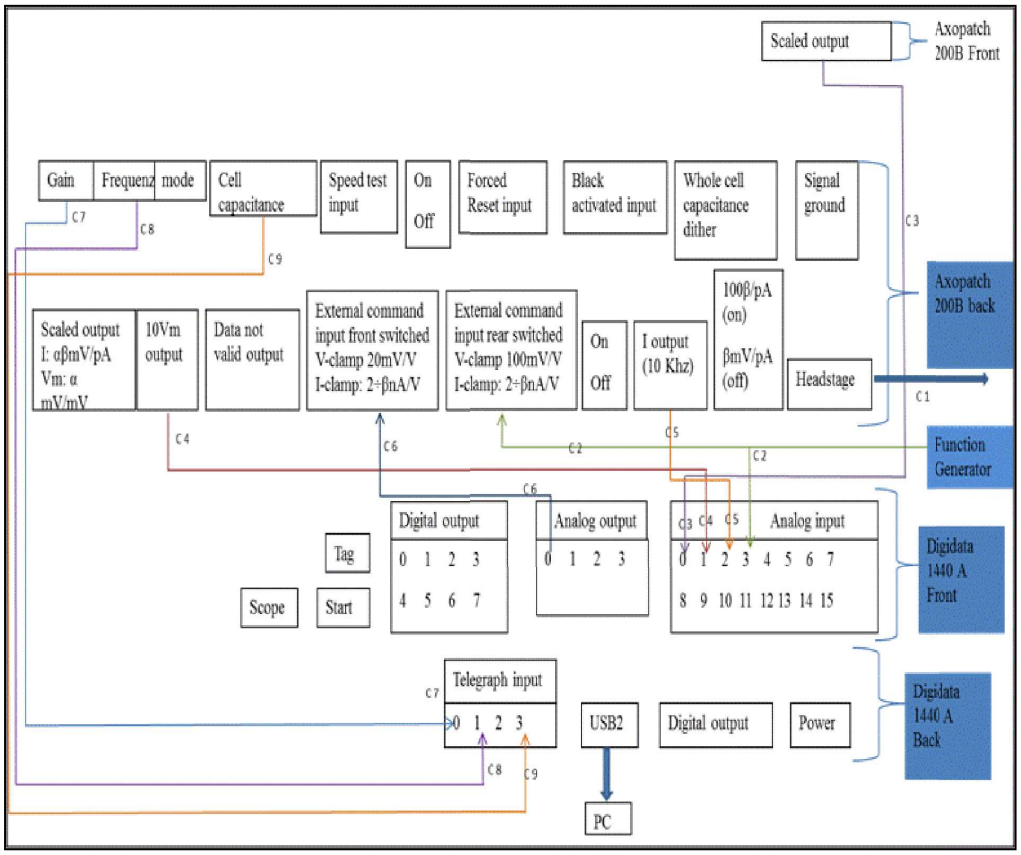

Figure 5-4: System electrical connection.

For the experiment, the cup was inserted in the back compartment. A Plexiglas window at the front of the Cis-chamber allowed the operator to monitor the events. A screw in the back of the system allowed fastening the cup in the desired position (Figure 5-5 (2)). A rubber plug was inserted between the screw and the cup to avoid over tightening and cracking the cup (Figure 5-5 (2)). The system was made of polyoxymethylene (POM). POM is a suitable

material for the presented work. Its high dimensional stability, excellent stiffness, and low friction fulfilled the precision required for the used parts.

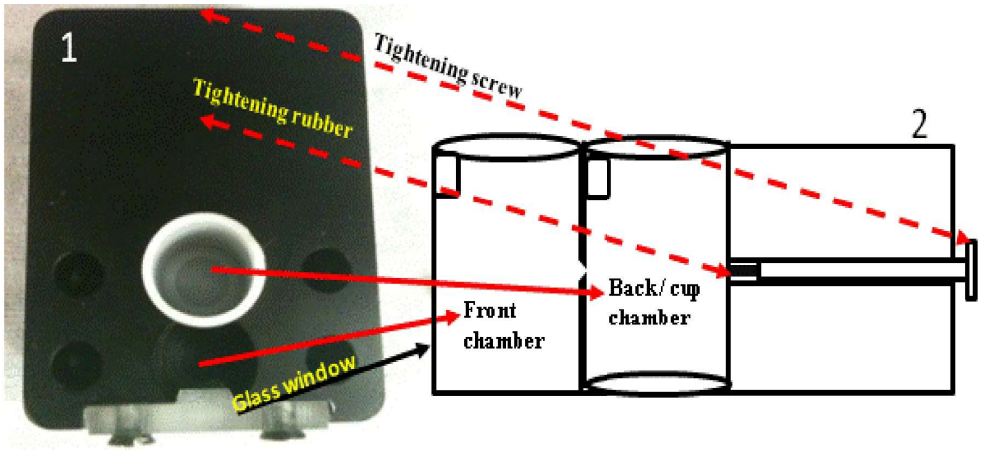

Figure 5-5: Warner chamber system.

5.3.3 Electrodes

Silver chloride electrodes were used in this investigation. Since silver is sensitive to laser light, chloride was deposited atop the silver surface to obtain silver chloride electrodes (not photoactive). For this purpose, silver wires were dipped into commercially available Clorox for 10 to 15 seconds. The electrodes were then rinsed, dried and connected to the head-stage on one end, and to the bath on the other end.

5.3.4 Laser

Two types of commercially available lasers were used in this work: a 532 nm (green) battery powered laser (CL20-0004) manufactured by Guangzhou Haike Outdoor Sport Co., Ltd. Guangzhou, China, and a 405 nm (purple) battery powered laser sold by Gearbest.com under the type, laser pointer, and the model number, 301. The green light laser was used to activate the proton pumping activity of bacteriorhodopsin while the purple laser was used to activate halorhodopsin pumping. Laser light is best suited for this type of experiment. In fact, the light

energy of a laser can be adjusted to the power level required to start and maintain ion translocation depending on the used species.

5.3.5 Power meter

The power meter used to calibrate the laser was manufactured under the model number 843-R by Newport, Tel Aviv, Israel. The power meter was borrowed from Dr. Yong Wang's group (University of Arkansas, Physics Department) to calibrate the lasers and identify the power decay. The power meter presented the advantage of easy handling and set-up for this type of experiment.

5.3.6 Amplifier

The amplifier, Axon Axopatch 200B (AA200B) (Figure 5-6), from Molecular Devices Sunnyvale, California, is a signal enhancer that is indicated for basic investigations of ion channels. The amplifier was used to generate voltage for resistance measurement. The amplifier was also used to increase the output signal from the electrodes and adjust the signal from the function generator to the electrode during membrane testing. This amplifier is best suited to record ultra-low-noise and to capture capacitor feedback [155].

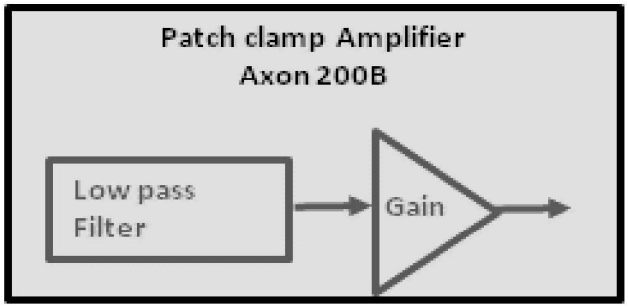

Figure 5-6: Diagram of the used amplifier.

5.3.7 Digitizer

The digitizer used in this work was manufactured by Molecular Devices under the model

number Digidata 1440A. Digidata 1440 A is a low-noise data acquisition system best suited for continuous data acquisition from working systems while performing multiple tasks. The digitizer was used to convert input and output into signals suitable for interpretation by the computer. The digitizer was connected to the amplifier and to the computer via a USB 2.0 interface. The Digidata 1440A is easy to install and has an exceptionally rapid signal transmission owing its 16-bit. Another advantage of using the Digidata 1440 is the low inherent digitizer and channel noises [156].

5.3.8 Software

5.3.8.1 pClamp 10

The Digidata 1440A was used in combination with the pClamp 10 software from Molecular Devices, Sunnyvale, California. This software was designed for electrophysiology under Microsoft Windows as a data acquisition and analysis tools in microanalysis. pClamp 10 was used to record emitted and acquired signals. The software is best suited for the recording of "clamp" experiments. The pClamp 10 can also be used to detect events, to synchronize simulation, and to perform analysis online. After installation, the Digidata 1440A is ready to perform and gather data immediately. No extra programming is required [157].

5.3.8.2 Clampfit 10

The Clampfit 10 from Molecular Devices was the main software used in this work. Clampfit 10 allows data filtering and routine fittings after recording. Under template, and single-channel mode, it also permits the detection and analysis of events. Clampfit 10 is most appropriate for the investigation of layouts and graphs from Clampex, including I-V curve and voltage spectrum. This helps establish links between analysis observation and data acquisition [157].

5.3.9 Head-stage

The pre-amplifier Model CV 203BU from Axon Instruments Inc. (acquired by Molecular Devices) is the head-stage used in this work [155]. The head-stage (Figure 5-7) served as the pre-amplifier to adjust the signal from the bath and to protect it from high voltage. The head-stage role was to supply the voltage electrode with power, then to collect the membrane potential and forward the signal to the main amplifier. The transmitted voltage was defined by the operator, and applied to the head-stage via the main amplifier. The head-stage was the single connection between the stage and the control units. The head-stage was connected to the ground and to the cathode on one end and to the anode on the other end. Figure 5-7 (B) shows the internal circuit of the head-stage used.

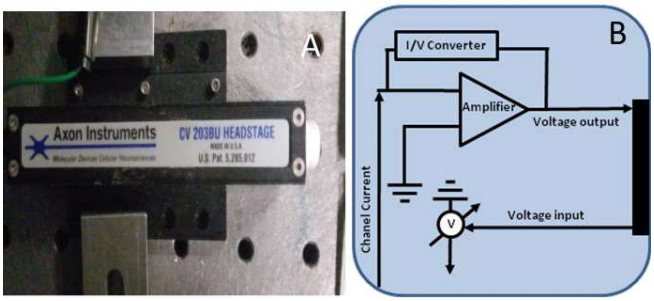

Figure 5-7: Photo (A) and diagram (B) of the used head-stage amplifier.

5.3.10 Function generator

The function generator in Figure 5-8 was manufactured by Agilent Technology, Santa Clara, California under the model name 33250A 80 MHz function/Arbitrary waveform Generator [158]. The generator was used to provide the system with a -5 mV to +5 mV amplitude (10 mV peak-to-peak) at a 100 Hz frequency. The generator also produced the voltage used to align the proteins inside the membrane. This device offered the possibility to characterize the parameters of the voltage desired for the experiment, such as triangular or square waves, DC and AC voltage, and more. The supplied voltage was adapted to the bath condition

inside the amplifier [158].

The photos of the set-up inside the fabricated Faraday cage are compiled in Figure 5-8. The Faraday cage was used to shield the experiments from surrounding noise. This set-up was used to form and characterize several membrane types and to generate photocurrent.

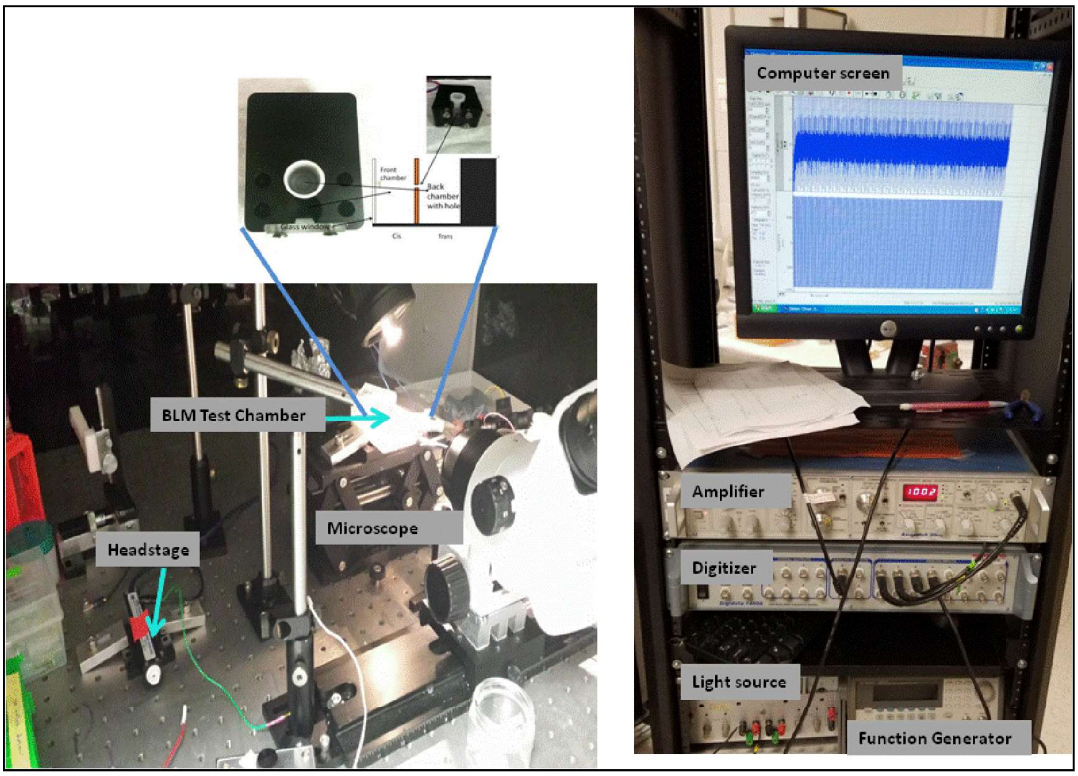

Figure 5-8: Photos of the complete system with parts.

Chapter 6: Results

The most significant results of this investigation are presented in this chapter. The membranes were formed using the painting or the folding methods described in Sections 5.2.1 and 5.2.2. The experiments included the identification and characterization of features caused by the variation of lipid concentration, protein concentration, and applied voltage. The absence of a laser with variable power prevented the assessment of the impact due to change in light intensity. The photocurrent was generated using a green (~100 mW, 532 nm) laser for the bR-protein and a purple (~ 5 mW, 405 nm) for the hR-protein.

6.1 Laser calibration

The laser calibration was performed to identify the decay rate of the laser beam. The goal of this experiment was to ensure that the intensity of the laser beam, at the membrane level, was high enough to convert the proteins into ion pumps. For this experiment, the laser was fixed at a specific position and a power meter (Section 5.3.5) was used to measure the change of the laser intensity at different positions.

Figure 6-1 shows that between ~ 1 cm and 245 cm away from the laser, the beam intensity decreased slowly (~ -0.3% rate) from 69.3 mW to ~ 61.3 mW. Beyond 245 cm (red dotted line), the laser intensity abruptly went down to 45.7 mW (-1.5%). This result indicated that the 12 mV, battery-powered 532 nm laser would not be suitable for experiments in which targets are located farther than 250 cm from the laser. The 532 nm laser would be suited for study where the distance between laser and target (membranes) was less than 50 cm. In this work, the distance between the laser and the membranes, indicated in Figure 6-1 (orange dotted line) was 23 cm. The laser calibration experiment was performed with a Plexiglas cup, filled with electrolyte and placed in front of the detector.

The beam intensity of the 405 nm purple laser (Figure 6-2), experienced a constant decrease

of approximately -2.6% between 1 cm and 182 cm. Beyond 182 cm (red dotted line), the intensity of the purple laser went down to ~ 2 mW.

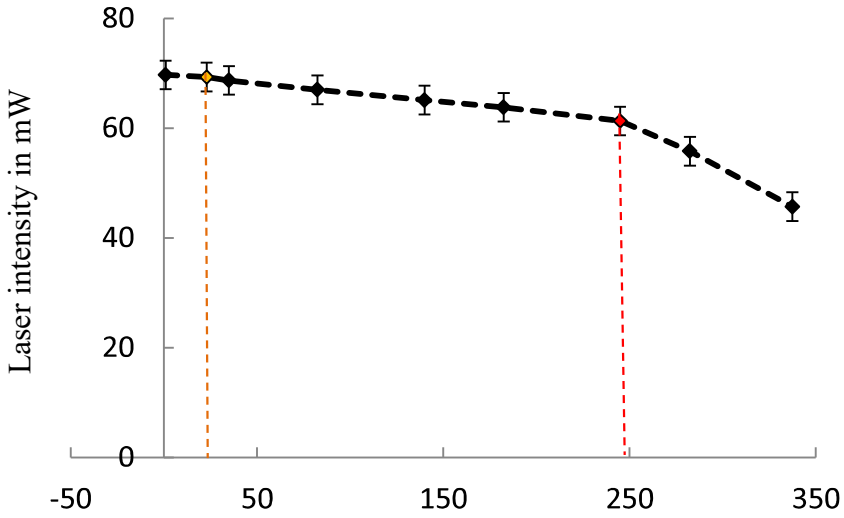

Figure 6-1 Calibration diagram of the green (532nm) laser.

The results confirmed that the beam power of both lasers (69.3 mW for the green and 3.5 mW for the purple laser) was appropriate to activate the ion pumping of the lipid-protein membrane located 23 cm (orange dotted line) away from the laser heads.

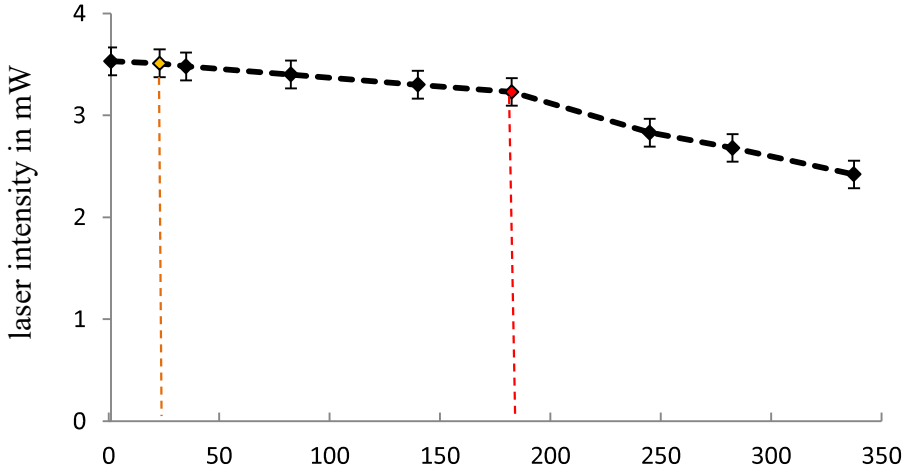

Figure 6-2: Calibration of the purple (405 nm) laser.

6.2 Absorption spectrum

Absorption spectra of both proteins were taken prior to the experiments. This step was a control of the activity of the proteins. In fact, active proteins have specific wavelengths at which their absorbance is maximal. For the experiment, 20 µl of the protein solution was dissolved in 180 µl of a 0.1 M NaCl in a cuvette. 200 µl of the 0.1 M NaCl solution was injected in a second, reference cuvette. The spectrum was run from 200 nm to 800 nm, and then from 400 nm to 750 nm, to expand the interesting areas. The absorption maximum of both proteins was predicted through calculations presented in 0.

6.2.1 bR absorption

The absorption spectrum of bacteriorhodopsin in Figure 6-3 shows that the protein was most active around 560 nm. The absorption dropped a little from 400 nm to 457 nm, before going up and culminating at 558 nm. The wavelength of the maximum absorption coincided with reference values from Hamp et al. [30, 107]. A small dimple at 545 nm indicated the presence of impurities floating in the solution. The absorption decreased after 558 nm down to a minimal value (0.15 counts) at 700 nm. It was noticed that the intensity (counts) differed from the values estimated through calculation in 0. Impurities and a dilution factor were suspected to be responsible for this difference. Figure 6-3 implies that the tested bacteriorhodopsin was most active between 457 nm and 650 nm with maximum activity at 558 nm. This information was used in the experiment to confirm that the used wavelength (532 nm) was appropriate to excite the lipid-protein membrane and to produce photocurrent.

6.2.2 hR absorption

The absorption spectrum of halorhodopsin in Figure 6-4 shows that the protein was most active at 576 nm. The absorption dropped from 400 nm to 450 nm and then rose up to 576 nm. The maximum absorption (576 nm) coincided with reference values [107].

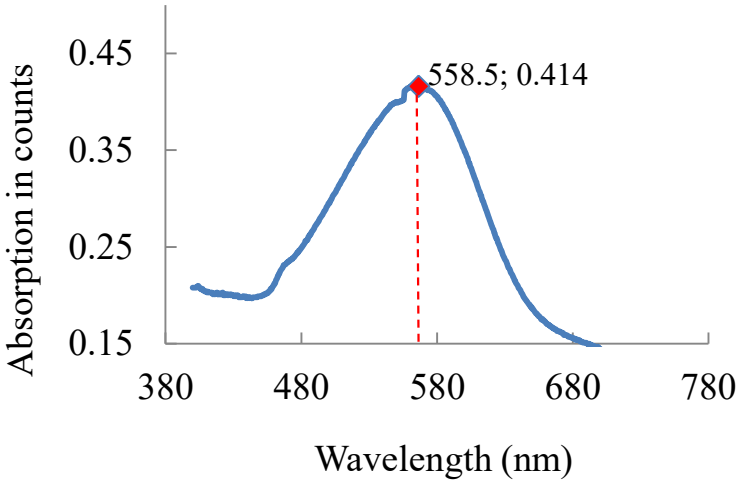

Figure 6-3: bR absorption spectrum.

The absorption decreased after 576 nm down to a minimal value (0.0071 counts) at 676 nm. Figure 6-4 implies that halorhodopsin was most active between 450 nm and 650 nm with maximum activity at 576 nm. The aim of the experiment was to activate the chloride pump, which occurred between 350 and 455 nm as shown in the hR window in Figure 6-4. The used 405 nm laser was, thus, appropriate to trigger the hR chloride pumping activity and produce electricity.

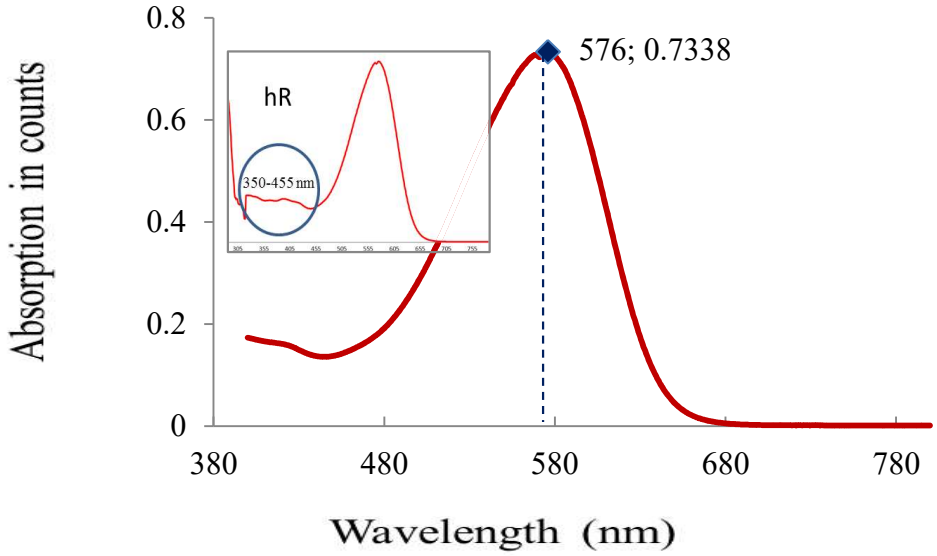

Figure 6-4: Halorhodopsin absorption spectrum.

6.3 Membrane resistance

The membranes characterized in this work were mostly formed with the folding method described in Section 5.2.1. The membrane resistances were obtained from I-V curves such as the one presented in Figure 6-5. A voltage of ± 100 mV was applied to the membranes via electrodes. The output current signal was plotted against the applied ± 100 mV (I-V curve). According to Ohm's law (Equation 6-1), the membrane resistances were equivalent to the calculated slopes of the membranes. Ohm's law (Equation 6-1) includes: the resistance, R, the applied voltage, ΔV, the measured current, ΔI, the membrane thickness, d, the membrane area, A, and the membrane conductivity, σ.

$$R = \frac{\Delta V}{\Delta I} = \frac{d}{\sigma A} \qquad \text{(Equation 6-1)}$$

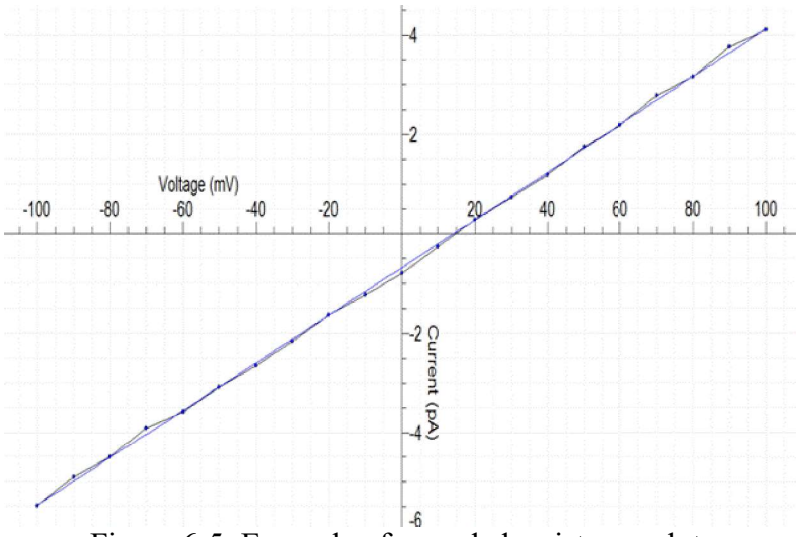

Figure 6-5: Example of recorded resistance plot.

The plot of the resistance against the concentration in Figure 6-6 was an effort to investigate the relationship between lipid concentration and membrane characteristics. This experiment was performed to find the best lipid concentration for photocurrent generation. For this experiment, the resistances of solutions with different lipid concentrations were used. The

resistance values varied between 22 GΩ and 58 GΩ. Figure 6-6 shows that the correlation between resistance and concentration is not linear but tends to be exponential above 5 mM lipid concentration. Between 1 x 10^{-3} M and 5 x 10^{-3} M, the resistance did not remarkably change, since the lipid density in the membrane did not significantly change either. In fact, the number of lipid molecules participating to the formation of the membrane is proportional to the area of the septum across which the membrane is formed. Because the septum diameter did not change, and can only host a limited number of lipid molecules, the lipid density of the membrane, and thus, the membrane resistance, also change slightly with increasing lipid concentration. Above 5 x 10^{-3} M, the resistance increased exponentially. 5 x 10^{-3} M seemed to be the turning point above which the membrane was probably made of more than two layers, or excess lipid assembled into vesicles. This type of membrane exhibited a higher resistance due to its increased thickness. The membranes in that lipid concentration range, however, were not appropriate for this work. In fact, proteins would not be able to translocate ions, if incorporated in membranes with thickness greater than the protein length.

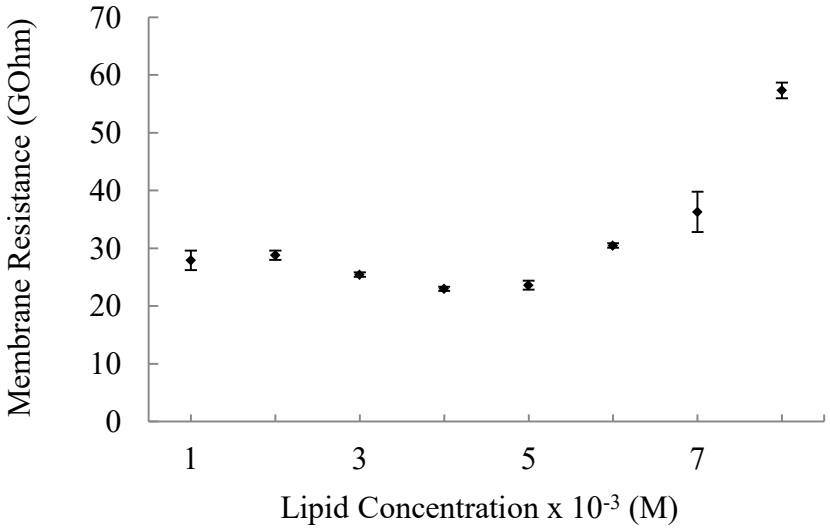

Figure 6-6: Relationship between lipid concentration and resistance of membrane.

6.4 Membrane capacitance

The capacitances of the membranes were calculated using the capacitance law (Equation 6-2). The capacitance is calculated based on the charge, ΔQ, the applied voltage, ΔV, the measured current (event), I, and the event duration, t, as follow:

$$C = \frac{\Delta Q}{\Delta V} = I \times \frac{\Delta t}{\Delta V} = \frac{\varepsilon_0 \, \varepsilon_r \, A}{d} \qquad \text{(Equation 6-2)}$$

The capacitance can also be calculated using the membrane area, A, the membrane thickness, d, the dielectric constant of the membrane material, ε_r= 8.85 x 10^{-14} F/cm, and the dielectric constant of the vacuum, ε_0 = 1. In this investigation, the capacitance was used to evaluate the membrane thickness around 10 to 15 nm. The folding method (Section 5.2.1) was used to form the membranes described in this section. A function generator (Section 5.3.10) was used to apply ± 5 mV triangular wave voltages to the membranes. Figure 6-7 presents an example of raw data including the frequency, the amplitude of the output current, and the applied voltage, used to calculate the membrane capacitance, according to the capacitance law (Equation 6-2).

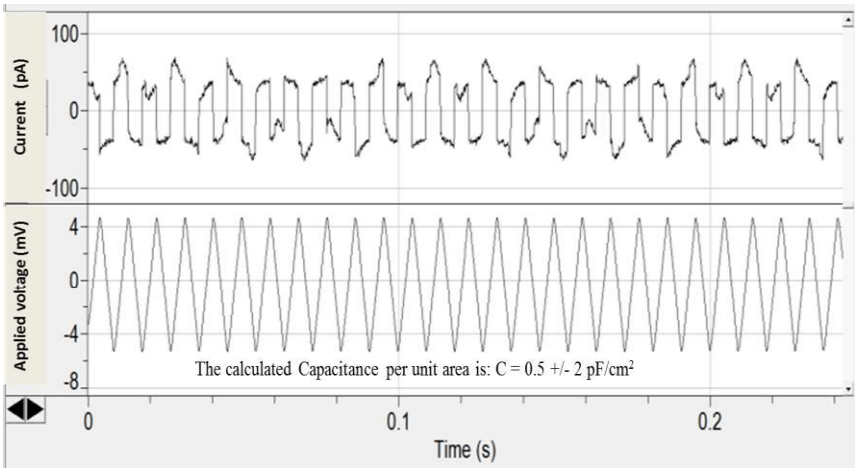

Figure 6-7: Example of signal recorded and used to calculate the membrane capacitance.

The capacitances of the membranes used in Figure 6-6 were calculated and used to find a

relationship between capacitance and lipid concentration. Figure 6-8 presents the plot of a series of capacitance values calculated using raw data as presented in Figure 6-7. Similar to the resistance plot in Figure 6-6, Figure 6-8 showed that the capacitance did not linearly increase with increasing lipid concentration. The stable capacitance from 1 x 10^{-3} M to 5 x 10^{-3} M was, similar to the stable resistance in the same range, due to the fact that the number of lipid molecules participating to the membrane formation did not change significantly (see Section 6.3).

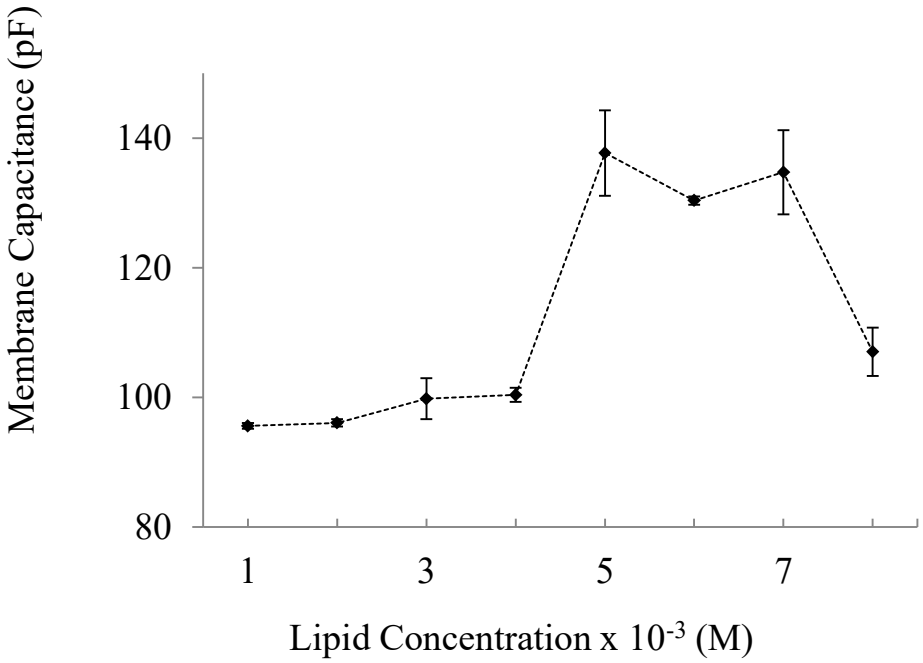

Figure 6-8: Relationship between lipid concentration and membrane capacitance.

Figure 6-8 shows a jump of the capacitance above 5 x 10^{-3} M, which indicated the formation of membranes with more than two layers. Subsequently, the capacitance tended to stabilize between 5 x 10^{-3} M and 7 x 10^{-3} M, and then decreased to 100 pF at 8 x 10^{-3} M. This behavior indicated that, at first, the contribution of excess layers on the membrane capacitance was dominant, which explained the jump of the capacitance values for 5 x 10^{-3} M to 7 x 10^{-3} M.

The impact of the membrane thickness, however, became dominant above 7 x 10^{-3} M and, according to (Equation 6-2), the capacitance fell to a much lower value. This work did not investigate the capacitance behavior beyond 8 x 10^{-3} M lipid concentration. Additional data in higher concentration range could provide more explanation about the behavior beyond 8 x 10^{-3} M lipid concentration. It should be noted, in Figure 6-8, that the capacitances stayed between 94 pF and 138 pF (~ 0.5 and 0.8 μF/cm^2) for all lipid concentration values, which was in line with consulted literature [9, 64, 67].

6.5 Photocurrent

The photocurrent was generated by flashing laser light on and off on the lipid-protein membranes as cartooned in Figure 4-1. It was important for the laser beam to hit the membrane without losing much energy. The laser calibration described in Section 6.1, showed that the intensity of the laser experienced negligible decrease within the distance (23 cm) between laser and membrane used in this work.

Further optical parameters, such as the refractive index of the Plexiglas and refractive index of the electrolyte solution were considered. It was found that the influence of the used electrolyte solution and the Plexiglas was negligible.

6.5.1 Bacteriorhodopsin (bR) generated photocurrent.

As shown in Figure 6-9, the bR-free membrane did not exhibit a current variation upon laser flash. This meant that the lipid membrane and the system were totally photo-inactive. Figure 6-10 displays the laser flash on a bR containing membrane. The figure shows clear variations in the current signal following the laser on and off cycles. No voltage was applied to the membrane. Since Figure 6-9 already showed that protein-free membranes did not generate current upon laser light illumination, this result indicated that the output current was solely due to the presence of the bR in the membrane.

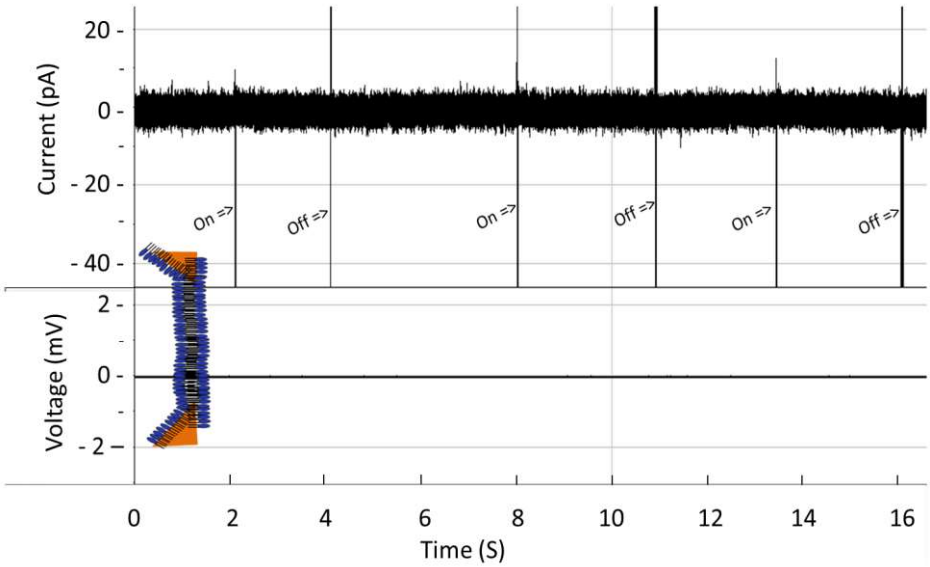

Figure 6-9: Control experiment showing the light inactivity of the protein free membrane.

In Figure 6-10, when the laser was flashed on the membrane, the current signal went up to 40 pA, before dropping around 10 to 20 pA within 4 to 5 seconds. The longer the laser was on, the lower the amplitude at which the current stabilized. However, the current never went back to zero during illumination. When the laser was turned off, the signal decreased abruptly to -30 pA and slowly increased to stabilize at near 0 pA.

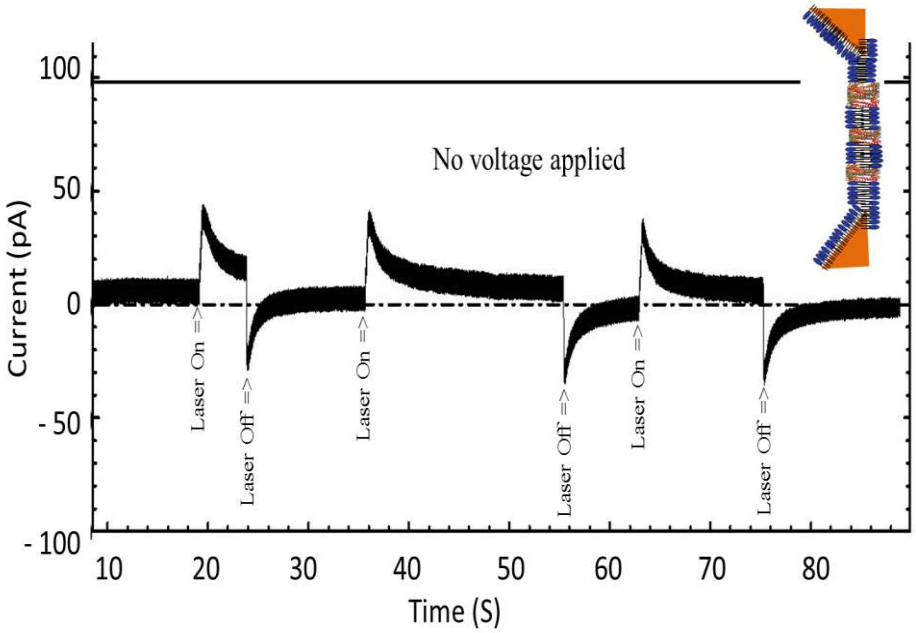

Figure 6-10: Photocurrent generated with bR- containing membrane.

6.5.1.1 Voltage dependency of the bR generated current

A voltage dependency of the generated current was obtained by supplying the lipid-protein membranes with an increasing voltage and measuring the generated current for each voltage level. Figure 6-11 recapitulates the complete voltage dependency of the bR-generated current. A closer look displayed in Figure 6-12 shows the individual current peaks and the amplitude difference of the current with increasing voltage. Figure 6-13 showed an increase of the generated current with increasing voltage. As displayed in Figure 6-11, increasing voltage led to higher generated current. A plateau was not expected, as the voltage just facilitated the protein orientation and the proton agglomeration around the membranes. The generated current was, thus, expected to be continuously rising with increasing voltage. Ultimately, the membrane would break at the expected overvoltage (~150 mV), which was lower than the voltage corresponding to the maximum expected current.

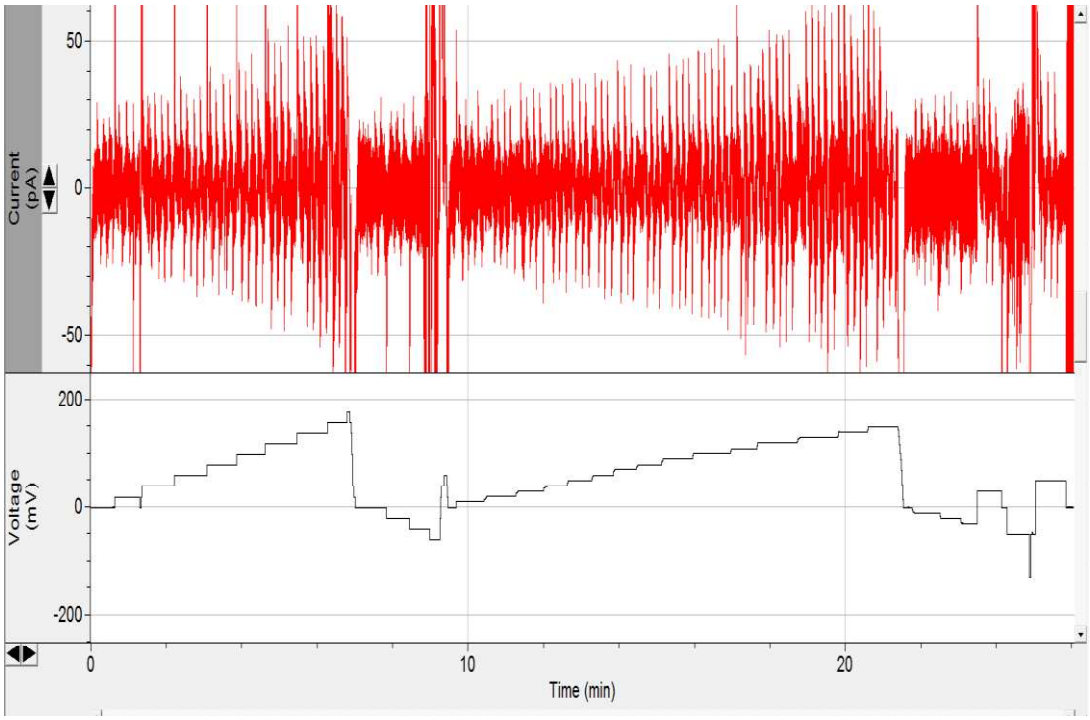

Figure 6-11: Overall photocurrent-voltage dependency.

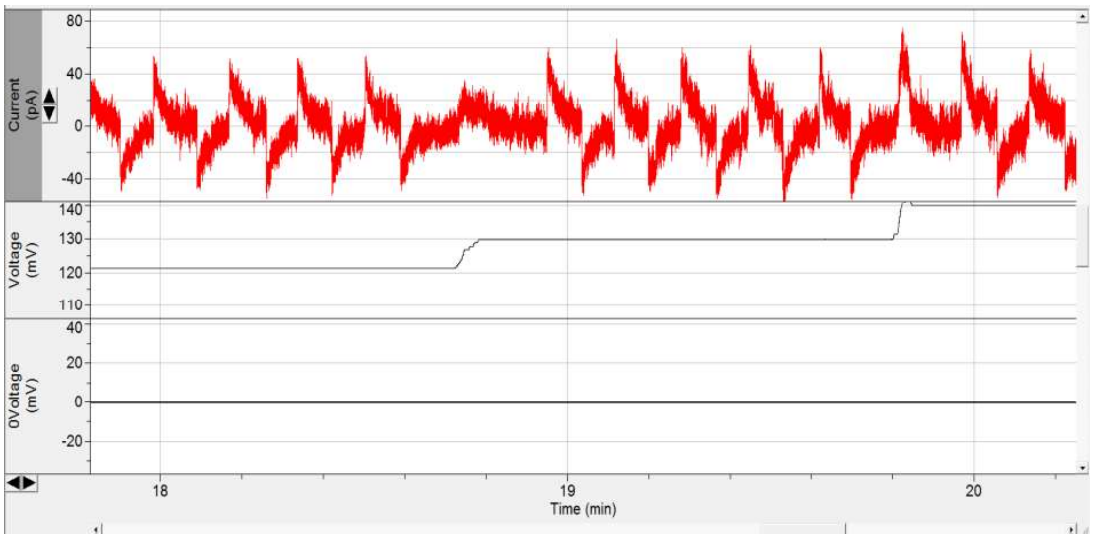

Figure 6-12: Individual photocurrent peaks.

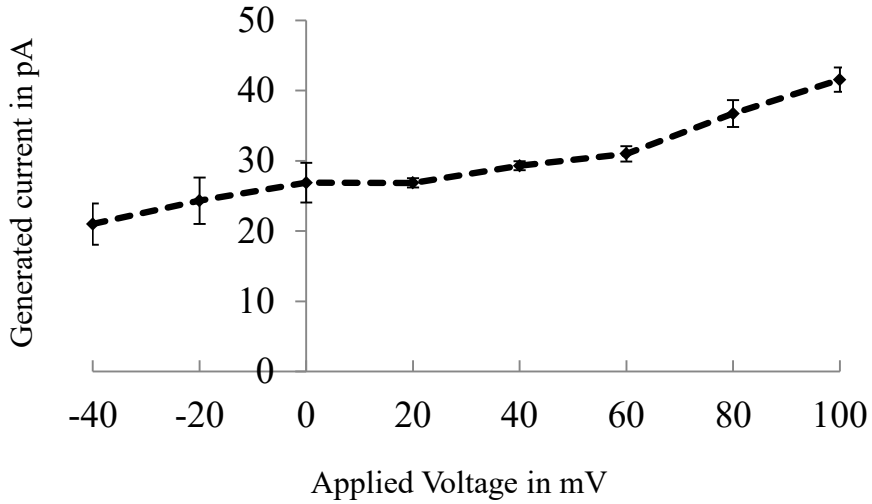

Figure 6-13: Voltage dependency of bR generated current.

6.5.2 Halorhodopsin (hR) generated photocurrent.

Figure 6-14 presents the photocurrent generated with hR. Upon illumination, the current signal abruptly went down to -20 pA. Within 7 to 12 seconds, the signal increased back and stabilized around 0 pA after the laser was turned off. The amplitude of the current drop was constant and did not depend upon the duration of the illumination. Since it was shown, with

identical calibration as in Figure 6-9, that a protein-free membrane is not photoactive, the variations in current amplitude (photocurrent) observed in Figure 6-14 were most probably due to the presence of hR in the system.

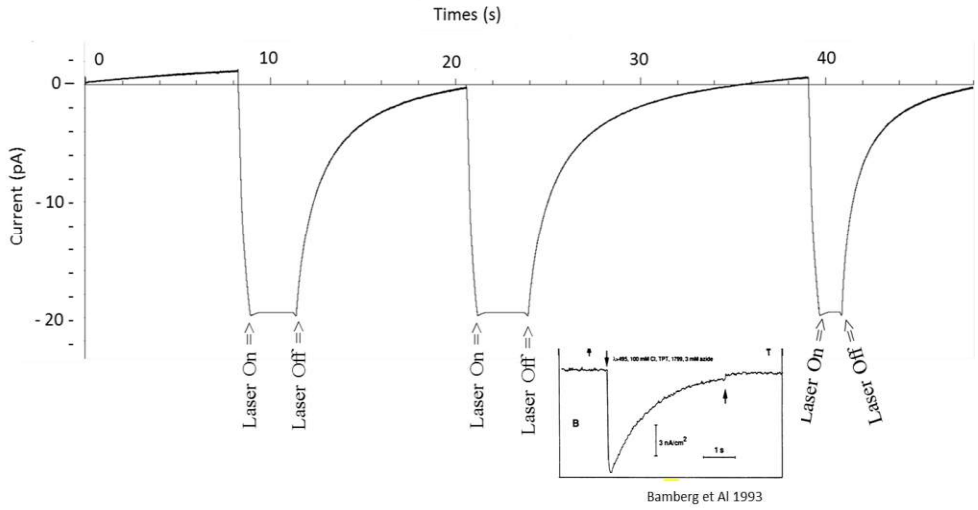

Figure 6-14: hR generated photocurrent.

The surprisingly low noise level was, as shown in the window (Bamberg et Al 1993 [107]), not unusual for hR-generated photocurrent. This result proved that hR photoactivity could be studied using the fabricated set-up.

6.5.2.1 Voltage dependency of the hR generated Photocurrent

Similarly, to bR, the influence of applied voltage on the hR-generated current was investigated. For this purpose, an hR containing lipid membrane was formed and used to generate photocurrent. Next, an increasing voltage was applied to the membrane. The applied voltage went from 0 to 100 mV and from 0 to -100 mV in 20 mV increments. The generated photocurrent was recorded each time and then plotted against the increasing voltage. Figure 6-15 showed that the change in the photocurrent amplitude was minimal. The generated current did not remarkably change with increasing voltage except at 40 mV (orange dotted line). Since the whole experiment was performed with the same membrane, the current value observed at 40

mV was most probably impacted by error of the system.

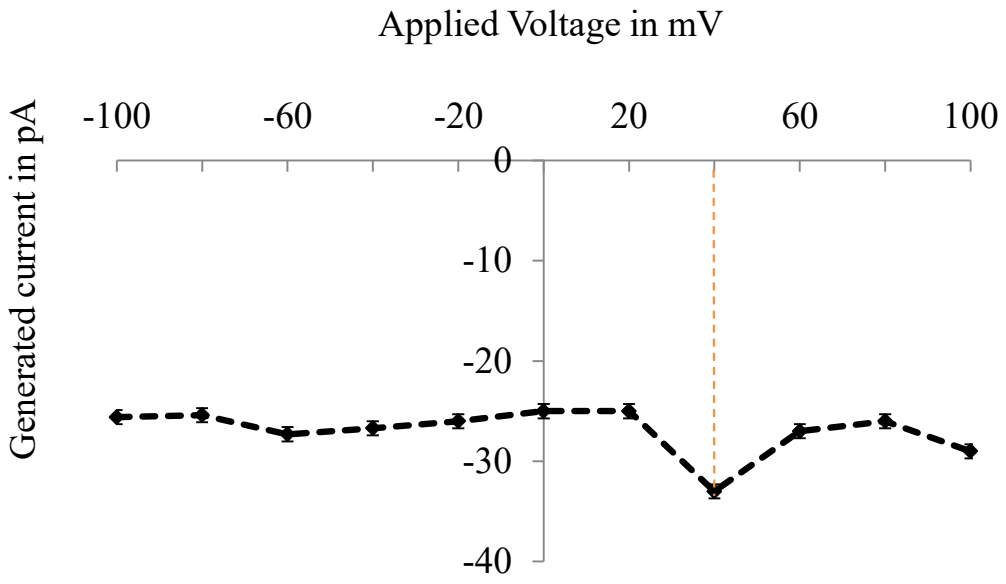

Figure 6-15 Voltage dependency of hR generated photocurrent.

Contrary to bR, where increasing the voltage forced the protons toward the protein channel, and increased the efficiency of the bR pump, the hR pump did not experience any significant current increase. Increasing the voltage should drag chloride ions toward the hR containing membrane and increase the output current, which was not verified here. The overshoot observed once the light was turned off was expected. However, the overshoot signals were almost the same amplitude as the generated current, which was not expected. Although this effect was observed only when the hR was part of the membrane, the high overshoot implied a release of a positive charge upon turning the laser off. Even if the response of the protein-free membrane was captured in an experiment such as in Figure 6-9, the possibility that this whole hR behavior could be an artifact generated by the system could not be excluded.

6.6 Image characterization

One of the goals of this investigation was to image the structure of lipid-proteins membrane solutions. This step was in line with future work aimed at establishing a correlation between the structure of lipid-proteins membrane solutions and their capability to generate photocurrent. A Transmission Electron Microscope (TEM) was used to capture the structure of the membrane solutions. Two types of solutions were used for this experiment: first, images of a protein-only solution were realized at different magnifications (Figure 6-16 (A), and (B)), then image of a mixture containing 7 µl bR and 3 µl lipid were taken (Figure 6-17(A), and (B)). Comparing both sets of images allowed an evaluation of the interaction between lipid and protein. Since the lipid was a completely transparent solution, no images were taken from lipid only solutions. The first set of images Figure 6-16 (A) and (B) are the image of a 5 µl bR sample. The images showed that the protein tended to aggregate in long patches of more than 500 nm long and 100 nm wide as selectively indicated, in green, in Figure 6-16 (A) and (B). The patches had a longitudinal form and appeared to be somewhat transparent. The higher magnification of Figure 6-16 (B) allowed the identification of small components (around 7 nm, cyan dots in in Figure 6-16 (B)), which can be attributed to single protein in the sample.

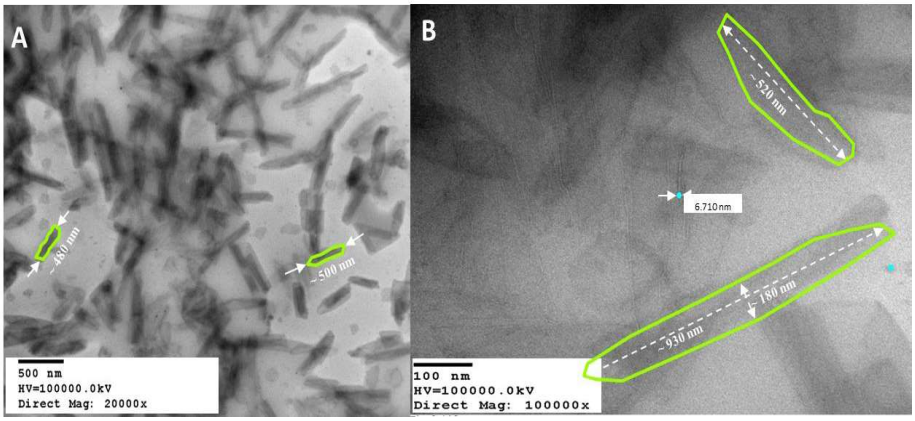

Figure 6-16 bR solutions at 20,000x magnification (A) and 100,000x magnification (B).

In Figure 6-17 (A), and (B), the solution contained 7 µl bR and 3 µl lipid. The picture shows that the lipid tended to agglomerate in large islands of approximately 100 nm in diameter. This behavior was expected, since proteins must be suspended within the lipid island in order for the formed lipid-protein membranes to be photoactive. From these images, it could not be stated with accuracy that the protein was captured inside or in between the lipid particles.

However, the absence of the patches observed in Figure 6-17 (A), and (B) was an indication that the sonication process was successful in dispersing the bR and the lipid. The observed lipid agglomeration was, thus, highly suspected to contain some bR in it. The tiny nature of the bR patches (7-10 nm) made it impossible to identify them in these images.

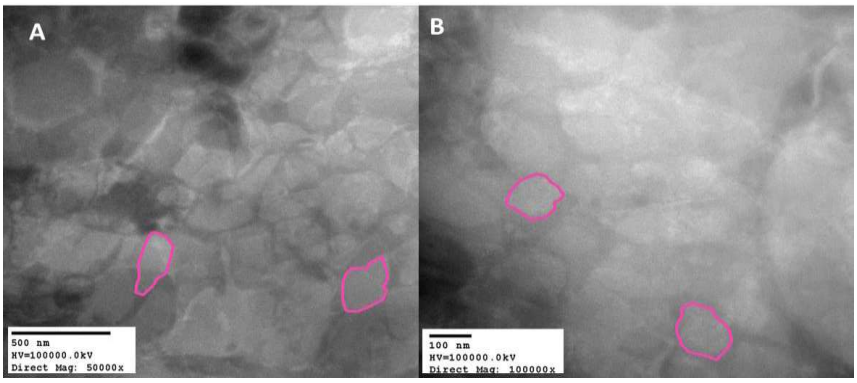

Figure 6-17: Lipid-bR solutions at 50,000x (A) and 100,000x magnification (B)

Figure 6-18 and Figure 6-19 show the structure of the membrane mixtures used to produce the hR photocurrent. In Figure 6-18 and Figure 6-19, the solution contained 5 µl hR and 5 µl lipid. Unlike the bR sample, Figure 6-18 (A) showed that the hR sample tended to form small (grey dots) agglomerates dispersed across the field. This difference in behavior was probably due to the fact that both proteins were suspended in different electrolytes.

Figure 6-18 (B) at 100,000x magnification, exhibited the lipid islands inside which the hR was expected to be suspended. The dark spot on the image was suspected to be an aggregation

of the protein sample. The spot was used to compare the two images at the same location.

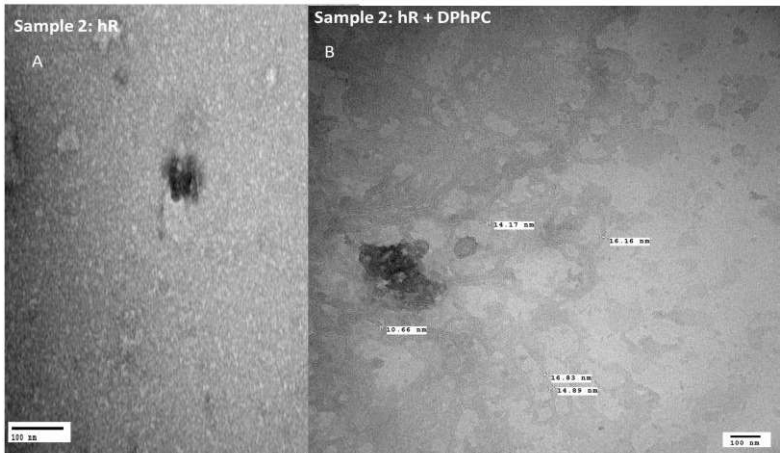

Figure 6-18: Lipid-free (A), and lipid containing (B) hR membrane solution.

In Figure 6-19 (A), the image showed at 50,000x and 100,000x magnification, that the protein agglomerated in the same type of transparent patches observed in Figure 6-17 with bR. A closer look of the structure presented in Figure 6-19 (B) confirmed this fact. Although the presence of the patches indicated the presence of the hR, it also exhibited the unsuccessful sonication of the hR-lipid mix at those locations.

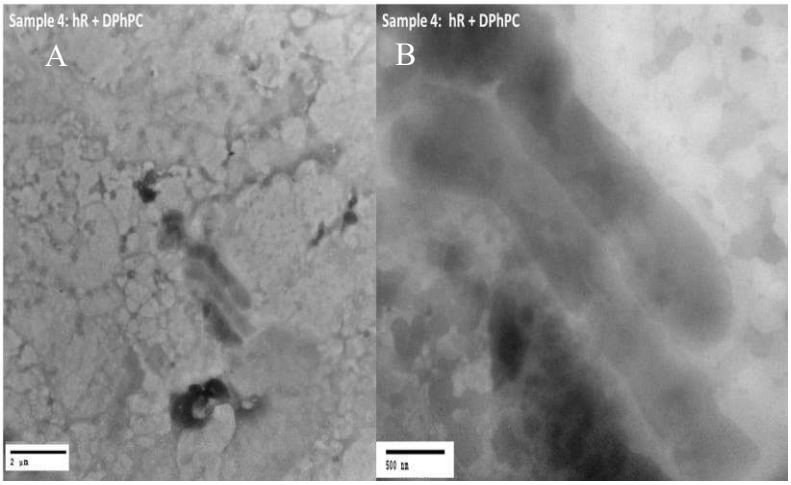

Figure 6-19: Lipid-hR solutions at (A) 10,000x and at (B) 50,000x magnification.

Similar results were published by M. Kolbe and D. Oesterhelt [76]. The researchers identified that hR assembled to trimmers and surrounded a palmitic patch. The hR structure determination was obtained using x-ray diffraction at 1.8 Å resolution.

The images above served as reference to identify the bR and hR in current generating membrane solutions. Images of real membranes were not taken, but were expected to exhibit similar features. A direct correlation between the membrane structure and the generated current could not be established based on these images. Subsequent works on this subject will use the system described in 0 to capture the structure of a membrane.

6.7 Concentration dependence of generated photocurrent

Photocurrent was generated several times using membrane solutions with different protein concentrations. This experiment was performed to capture the relationship between protein concentration and generated current in a defined concentration range. The goal of this experiment was to be able to predict the generated photocurrent based on the concentration of the used proteins. The bR concentration was slowly decreased, by adding more lipids into the primary solution, used to generate the initial photocurrent.

This experiment was performed for several protein concentrations, however, only eight solutions could form membranes that generated considerable photocurrent. Examples of raw data of the generated photocurrent are presented in Figure 6-20.

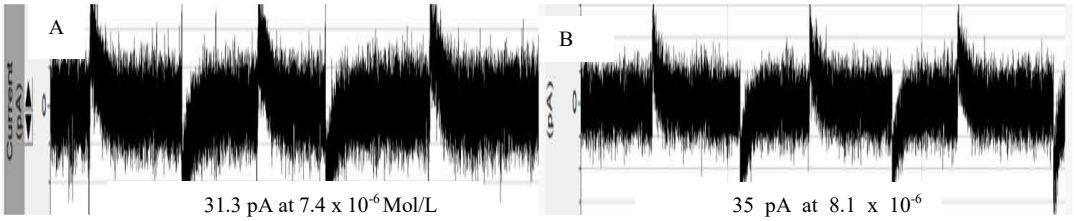

Figure 6-20: bR photocurrent at 5.9 x 10^{-6} Mol/L (A) and at 8.1 x 10^{-6} Mol/L (B).

The values obtained from the raw data were plotted against the concentration in Figure 6-21. As expected, Figure 6-21 showed a near linear relationship between protein concentration and generated current. The higher the protein concentration, the higher the generated current up to 8.9 x 10^{-6} M, which might be the turning point at which the generated current do no longer experience significant increase.

This behavior was expected, since the current generating membrane can host active protein molecules up to a limited number (saturation level), above which there is just no more space on the membrane for additional proteins, if the membrane is to maintain its stability. This assumption must be confirmed with more data > 8.9 x 10^{-6} M in protein concentration. In fact, several of the non-conclusive experiments were in that range.

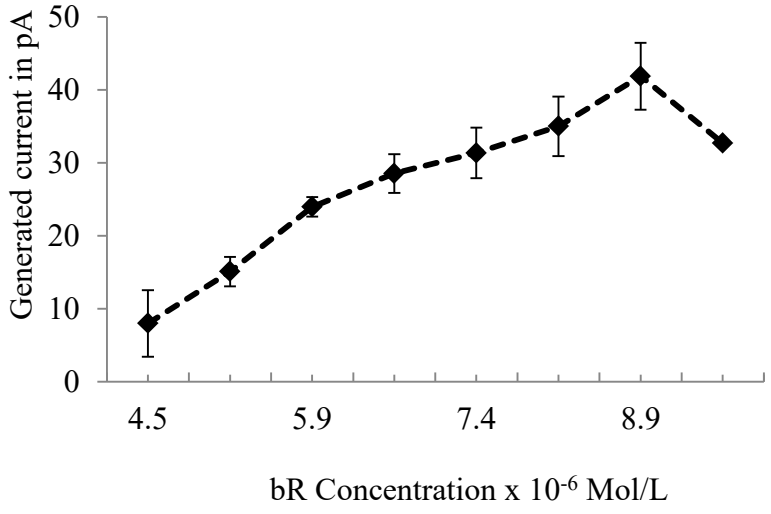

Figure 6-21: Plot of the concentration dependence of the bR generated photocurrent.

Figure 6-22 shows an example of the current generated with hR. For the concentration dependency, a total of 10 µl DPhyPC was mixed with an increasing amount of hR. The volume of the protein was increased from 5 to 10 µl in 1 µl increment, to change the hR concentration.

The five solutions formed were sonicated for 6 to 10 minutes each. Each solution was used to form a membrane and an attempt to generate a photocurrent was made.

The ~18 pA generated (dotted blue line in Figure 6-22) are close to the hR current generated with 5 µl hR + 5 µl DPhyPC presented in Figure 6-14. This was in line with the hR current voltage dependence described in Section 6.5.2.1. Figure 6-23 shows the plot of the generated current with increasing hR concentration. Similar to the voltage dependency, increasing the hR concentration did not significantly increase the presence of hR in the membrane as expected.

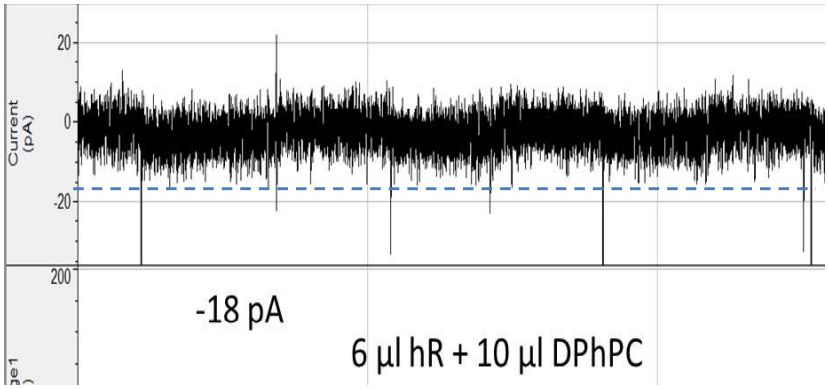

Figure 6-22: Example of the hR generated current with changing hR concentration.

Experiments with lower hR concentrations exhibited either no or too small current. G. Varo, and J. K. Lanyi [110] also showed in their work on hR photocycle, that the change of chloride concentration does not affect the photocycle. Using an hR mutant, a different electrolyte, or a specific reagent might be better alternative ways to stabilize and increase the hR current generation.

6.7.1 Governing equation

In this section, only the bR results will be considered. The hR-results did not provide enough distinction in the generated current to be used here.

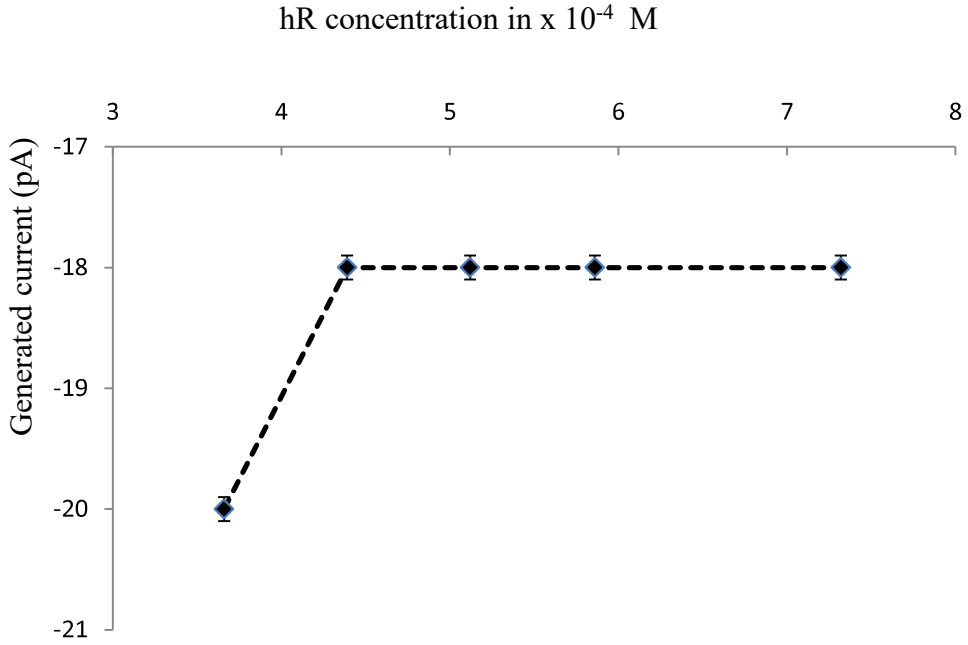

Figure 6-23: Dependence of hR generated current from hR concentration.

It was suggested by W. Stoeckenius [3] that each bR generates approximately 100 protons per second when suspended in a lipid bilayer membrane. J.K Lanyi et al. [2] reported that the bR-cycle duration is around 10 ms.

According to O. Berthoumieu [55], a proton bears the absolute value of the charge of an electron $Q_0 = 1.6 \times 10^{-19}$ C. If I_0 is defined as the current generated by one bR, then

$$I_0 = \frac{100 \text{ protons x } 1.6 \text{ x } 10^{-19}\,C}{10^{-2}\,s} = 1.5 \text{ x } 10^{-15}A \qquad \text{(Equation 6-3)}$$

The number of cycles, and thus the number of bR, N'_{bR}, that contributed to the generation of the generated current, I, is obtained by dividing I by the current generated by one retinal, I_0.

$$N'_{bR} = \frac{I}{100 \text{ x } I_0} \qquad \text{(Equation 6-4)}$$

N_{bR} is defined as the number of bR-molecule inside the membrane that are expected to generate photocurrent. Since the membrane is exclusively made of lipid and proteins, the total

membrane area ($A_m = 1.77 \times 10^{+4}\ \mu m^2$) is proportional to the total area of lipids plus the total area of proteins. The lipid and protein area are obtained by multiplying the number (concentration) of lipid by their respective molecule areas. The lipid $a_{Lipid} = 1.96 \times 10^{-12}\ \mu m^2$ and protein $a_{protein} = 1.96 \times 10^{-7} \mu m^2$ area were derived from calculations by R. Peters et al. [169]. The value R was defined as the lipid/protein ratio obtained by dividing the lipid concentration, C_L, by the bR concentration, C_P. R could be revised by adjusting C_L, and C_P. These defined parameters were used to determine N_{bR} as follow:

$$N_{bR} = \frac{A_m}{R * a_{Lipid} + a_{Protein}} \qquad \text{(Equation 6-5)}$$

Figure 6-24 presents the plot N'_{bR} against N_{bR}. The plot described the relationship between N'_{bR} and N_{bR}, and was used to determine the participation or activity constant, K, which indicates the probability of proteins to be active during the performed experiments. This constant was calculated as the slope of the plot.

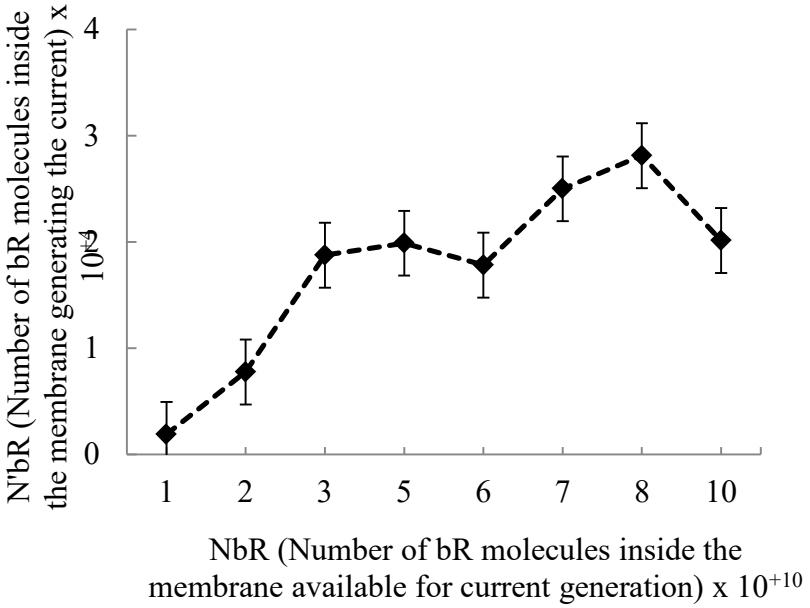

Figure 6-24: Determination of the activity constant, K.

The slope, K, was determined to be around ~ 2.26 x 10^{-5} (Figure 6-24). The proportionality, $\frac{\Delta N'_{bR}}{\Delta N_{bR}} \approx K \approx 2.3 \times 10^{-5}$, leads to the relationship:

$$I = K * N_{bR} * I_0 \qquad \text{(Equation 6-6)}$$

Equation 6-6 was plotted in Figure 6-25 alongside the results obtained in this work. In Figure 6-25, the black dotted line represents the values of the generated current against the available total charges. The red dotted line represents the plot of Equation 6-6.

As expected, both plots fit with each other. Parameters such as electrolytes, type of electrodes, and light intensity were not considered in this equation. Equation 6-6, was intended to provide a basis from which lipid/protein ratio, and thus, concentration, could be defined prior to experiments. Further investigations with a significantly higher number of data, in and outside the concentration range considered in this work, will be required to adjust Equation 6-6 to more accurately fit the reality.

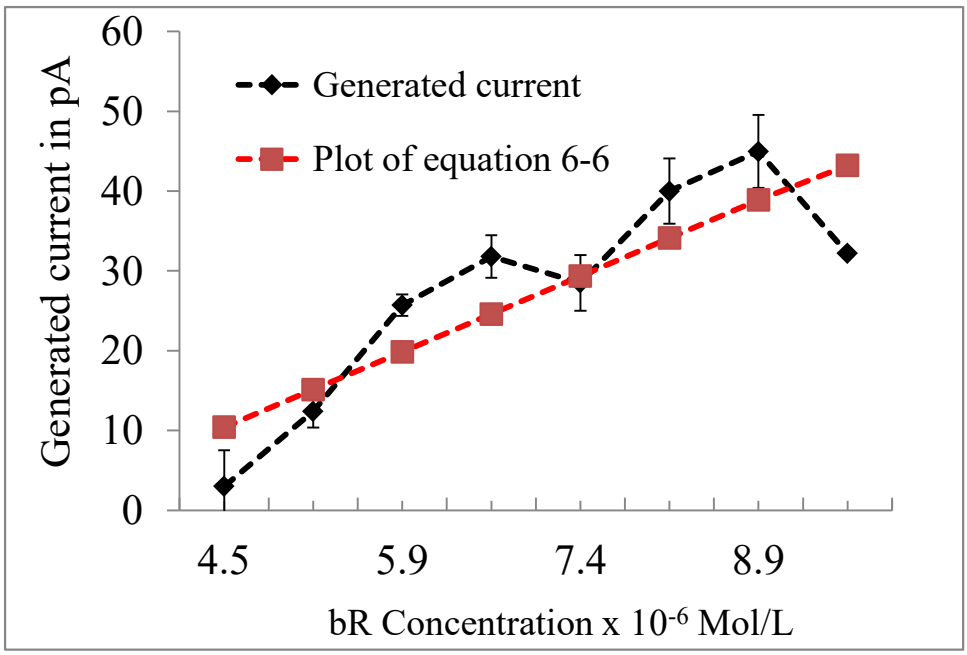

Figure 6-25: Plot of Equation 6-6 (in red) compared to measured data (in black).

Figure 6-25 was generated using bR results only. As presented in Figure 6-22, the change in hR concentration did not significantly chang the hR current generation. It will be necessary to perform additional experiments within a wider concentration range, to capture changes due to modification of the hR concentration.

Equation 6-6 could be used as source to estimate the photocurrent prior to experiments. More data will be required to fit the equation to other type of proteins and lipids, and to determine if the value of K is valid outside the concentration range considered here.

Chapter 7: Discussion

This work showed that the fabricated set-up could be used to characterize current generating lipid-protein membrane. It was shown that bacteriorhodopsin and halorhodopsin are photoactive ion pumps. The ratio between the used lipid (DPhyPC) and the protein needed to be accurately calculated. P. Hegemann et al. [118], and J.K Lanyi et al. [144] reported on the concentration of the sodium chloride (NaCl) solution (0.1 M), used as electrolyte. Several control experiments allowed confirming that this concentration was appropriate for the intended experiment.

The photocurrent generated with bR and hR presented in Figure 6-10 and Figure 6-14 confirmed the conclusion from P. Hegemann and D. Oesterhelt [118]. The researchers suggested that, in the bR experiment, the proton base at the retinal level, is emptied and refilled in a millisecond time frame. As a result, the proton pumping is regulated while initial peaks decay rapidly and settle down at a steady value. A proton was repossessed to fill up the Schiff base, and a negative undershot was observed as the laser was switched off (Figure 6-10). In the hR experiment, one photon was needed to capture and translocate one chloride anion under blue/purple light illumination, while two photons were needed to capture and translocate one proton under white light illumination. The transient peak represented the translocated ion. As the laser was switched off, the current went back to zero, with a small overshot, since the pumped chloride anion was not replaced but surrounding charge suddenly stopped converging.

Control experiments were conducted on protein-free lipid membrane to test the accuracy of the fabricated set-up, and to collect reference data against which the electrical properties of protein pumping membrane could be compared. Bamberg et al. [107] reported that after recording the capacitance and resistance of protein-free membranes, protein molecules were injected close to the membrane. After approximately 40 minutes, a photocurrent was observed

upon illumination. This evidenced the fact that the used proteins (bR) could penetrate lipid membranes. The main evidence of the ion pumping and current generation of the system was based on the use of the same electrolyte at the same concentration in both chambers. In addition, Figure 6-9 showed that excitation of protein-free membranes did not induce any photocurrent. Thus, the variation observed in the output current, using protein-containing membranes, could only be attributable to the presence of proteins. TEM images, Figure 6-16 trough Figure 6-19, of the protein alone and the lipid-protein membrane solutions, exhibited features that could be traced back to the behavior of the protein inside the lipid. However, the obtained images did not show a clear identifiable structure that explained the observed photocurrent. Using Atomic Force Microscopy (AFM) could provide a topographic image that might offer better details of the proton pumping structure.

Chapter 8: Summary

Lipid membranes were characterized using capacitance and resistance values from membranes with different lipid concentration. The resistance seemed to increase exponentially with increasing lipid concentration beyond 5 x 10^{-3} M. In this concentration range the membranes exhibited a higher resistance due to their increased thickness. Below 5 x 10^{-3} M, since the septum could only host a limited number of lipid molecules, the lipid density of the membrane, and thus, the membrane resistance, could only experience minimal changes with increasing lipid concentration.

As expected, it was observed that the membrane capacitance did not show significant change in the low concentration range, below 5 x 10^{-3} M, however, above this concentration the capacitance increased indicating the formation of more-than-two-layer membranes during which, the contribution of excess layers on the membrane capacitance was dominant. The capacitance dropped close to 100 pF at 8 x 10^{-3} M where the impact of the membrane thickness became dominant according to Equation 6-2.

The lasers were characterized by plotting their intensity against the distance separating the laser head from the detector. A Plexiglas cup, filled with the experimental electrolyte, similar to the used chamber, was inserted between laser and detector for the experiments. It was found that the laser intensity slowly decreased with increasing distance from the objects with an abrupt drop beyond 250 cm for the green laser and 240 cm for the purple laser. Those results were used to set appropriate conditions to successfully generate photocurrent using both proteins successively.

TEM imaging did not allow a definite conclusion on the state of the structure of protein containing membrane solutions. However, the TEM image exhibited features that were most likely compatible with the behavior of the used proteins. In fact, the protein patches subsequently

mixed with the lipid and were no longer to be seen, which indicated a successful sonication process in the bR experiment. The absence of the patches in the hR images was surprising but traceable back to the solution in which the hR was suspended. This was confirmed by the appearance of the patches in the hR-lipid images, which also indicated little success of the sonication process. In order to establish a clear relationship between structure and recorded photocurrent of the membranes, it will be necessary to gather numerous images with different lipid-proteins ratios. It might also be judicious to use more appropriate equipment such as Atomic Force Microscopy (AFM), which can provide better detail of the interaction between protein and lipid.

A least squares linear fit (Equation 6-6) was drawn out of the results from this work to describe the relationship between the protein concentration and the generated current. The hR experiments did not provide enough significant data to accurately relate the hR concentration with the generated chloride current. Equation 6-6 could be used as basis in other experiments, upon adjustment of critical parameter such as number of ion translocated by cycle, membrane diameter, and used lipid to predict photocurrent amplitude. Equation 6-6 would be most appropriate for pre-experiment work to provide estimation of expected photocurrent, assuming the parameters described in this work are used.

Chapter 9: Conclusion and future work

This investigation included the fabrication of a Faraday cage, and the set-up of an electrophysiology system capable of accurately recording signals in the picoampere range. The set-up was used to form and characterize nano-lipid bilayers, and nano-lipid-protein bilayers. The bilayers were formed using the painting, and mostly the folding method.

The formed bilayers were characterized based on their resistance and capacitance. For this purpose, numerous membranes were tested to calibrate the set-up and to understand the membrane behavior. Relationships between capacitance and lipid concentration and between resistance and lipid concentration were measured. The lipid-protein bilayers were used to generate photocurrent. Here also, the relationship between the concentration of the proteins and the generated current was evaluated.

Although the obtained TEM images could not be used to describe the generated current, the observed features helped understand the protein behavior when mixed with the lipid. The obtained results proved that the fabricated set-up can be used to generate photocurrent. The results presented here are intended to further the understanding of bR and hR photoactivity. The set-up and the suggestion made in this work will support a large-scale application of both proteins in bio-solar cell, bioelectronics, and more.

These results could also support biomedical application of the used proteins. In fact, the retinal contained in both proteins can mimic mammalian retinal and can be prospected as prosthesis. Further, since the formed membranes resemble animal cell membranes, and the membrane is the target of most developed drugs, the results presented in this work could support specific tests of new developed drugs. For example, in vivo ion channels and transport systems can be mimicked via the double layer. Especially, the conception of drug delivery systems with the capability to sense, transmit signal, and target specifics tissues, could benefit from the

presented work.

The present work opens possibilities to look deeply into the hR photocurrent generation. Although the current generated using Lipid-hR membrane was in line with expectations and reference literature, the voltage dependence of the hR current was not determined in this work. It was also not possible, so far, to evaluate the change of the photocurrent upon change of hR concentration. Using a different sample type (powder) might help stabilizing the hR photocurrent generation.

The TEM image acquired in this work provided a starting point for future investigation of the structural properties of current generating lipid-protein membranes. It will be required to transport the current generating membrane into a TEM device for imaging. The PDMS chamber described in 0 could be further developed and used for this purpose.

Extensive collaboration with research groups involved in membranes, and / or protein characterization could open unforeseen opportunities to deploy the potential of the fabricated system and acquired knowledge.

References

1. B. Alberts, D. Bray, K. Hopkin, J. Lewis. “Essential Cell Biology, 3rd Edition” Reproduced with permission of Garland Science/Taylor & Francis LLC Copyright 2009 pp. 629-650.

2. J.K Lanyi “Proton Translocation Mechanism and Energetics in The Light-Driven Pump Bacteriorhodopsin” Biochem. Biophysics. Acta Vol. 1183, 1993, pp. 241-261.

3. W. Stoeckenius, “Bacterial rhodopsin: Evolution of a mechanistic model for the ion pumps” Protein Science Vol. 8, 1999, pp. 447–459.

4. V. Drachev and N. Frolov, “Reconstitution of Biological Molecular Generators of Electric Current” The Journal of Biological Chemistry Vol. 251, 1976, pp. 7059-7065.

5. W. Kühlbrandt, “Bacteriorhodopsin — The Movie” Nature Vol. 406, 2000, pp. 569-570.

6. T.R. Herrmann, G. W. Rayfield, “The Electrical Response to Light of Bacteriorhodopsin in Planar Membranes”, Biophysical Journal Vol. 21, 1978, pp.111-125.

7. B. Yao, D. Xu, “Analyze and Proof of Multiexponential Process of Bacteriorhodopsin Photoelectric Response” Journal of Applied Physics Vol. 89, 2001, pp. 795-797.

8. K. Palczewski, T. Kumasaka, A. Behnke, “Crystal Structure of Rhodopsin: A G Protein–Coupled Receptor” Science Vol. 289, 2000, pp. 739 - 745.

9. S. Dutta, G. Patchornik “Engineered-Membranes and Engineered-Micelles as Efficient Tools for Purification of Halorhodopsin And Bacteriorhodopsin” The Analyst, Vol. 140.1, 2015, pp. 204-212.

10. N. L. Wagner, R.R Birge “Visual Restoration Using Microbial Rhodopsin. In Bio Nanotechnology: Biological Self-Assembly and Its Applications” Rehm, ed. Caister Academic Press, Norfolk, United Kingdom, 2013, pp. 205-240.

11. J. A. He, S.K Tripathy “Photoelectric Properties of Oriented Bacteriorhodopsin /Polycation Multilayers by Electrostatic Layer by Layer Assembly” J. Phys. Chem. B Vol. 102, 1998, pp.7067–7072.

12. S. Tőkés, T. Roska “Bacteriorhodopsin as An Analog Holographic Memory for Joint Fourier Implementation of CNN Computers” Research Report DNS-3-2000.

13. D. Ma, J. Ding, “Amphiphilic Block Copolymers Significantly Influence Functions of Bacteriorhodopsin in Water” Soft Matter (The Royal Society of Chemistry), Vol. 6, 2010, pp. 4920–4930.

14. S. Subramaniam, D.A. Greenhalgh, “Aspartic Acid 85 In Bacteriorhodopsin Functions Both as Proton Acceptor and Negative Counterion To the Schiff Base” J. Biol. Chem. Vol. 25, 1992, pp.730–733.

15. K. J. Wise, R. R. Birge, “Optimization of Bacteriorhodopsin for Bioelectronic Devices” Trends Biotechnol. Vol. 20, 2002, pp. 387–394.

16. J.R Hillebrecht, R.R Birge. “Optimization of Protein based Volumetric Optical Memories and Associative Processors by Using Directed Evolution” Nanobiotechnology Vol.1, 2005, pp. 141–152.

17. S. Geibel, T. Friedrich, “Voltage Dependence of Proton Pumping by Bacteriorhodopsin Mutants with Altered Lifetime of the M Intermediate” PLoS One., Vol. 8.9, 2013, pp. 1-11.

18. Z. Lu, C. M. Li, Nanoscale, “Controllable Stationary Photocurrents Generated from A Bacteriorhodopsin/Up conversion Nanoparticle-Based Bionanosystem Under NIR Illumination” Vol.8, 2016, pp. 18524–18530.

19. V. Thavasi, A. Kumar, “Study on The Feasibility of Bacteriorhodopsin as Bio-Photosensitizer in Excitonic Solar Cell: A First Report” J Nanosci Nanotechnology Vol. 9, 2009, pp. 1679-1687.

20. R. Mohammadpour, S. Janfaza “Efficient Nanostructured Bio Photovoltaic Cell Based on Bacteriorhodopsin as Bio photosensitizer” ACS Sustainable Chem Eng. Vol. 3, 2015, pp.809-813.

21. A. Molaeirad, B. Mahyad “Photocurrent Generation by Adsorption of Two Main Pigments of Halobacterium Salinarum On Tio2 Nanostructured Electrode” Biotechnol Appl Biochem Vol. 62, 2015, pp. 121–125.

22. S. Janfaza, J. Mehrvand “Efficient Bio-Nano Hybrid Solar Cells Via Purple Membrane as Sensitizer” BioNanoSci Vol. 4, 2014, pp.71–7.

23. B. Mahyad, E. S. Hosseini, “Bio-Nano Hybrid Materials Based on Bacteriorhodopsin: Potential Applications and Future Strategies” Advances in Colloid and Interface Science Vol. 225, 2015, pp.194–202.

24. M.H. Griep, C.R. Friedrich “Quantum Dot Enhancement of Bacteriorhodopsin-Based Electrodes” Biosensor Bioelectronics Vol. 25, 2010, pp.1493-1497.

25. I.R. Nabiev, G.D. Chumanov “The Chromophore-Binding Site of Bacteriorhodopsin. Resonance Raman And Surface-Enhanced Resonance Raman Spectroscopy and Quantum Chemical Study” J Biosci Vol.8, 1985, pp. 363-374.

26. Z. Zhao, Y. Jin “Bacteriorhodopsin/Ag Nanoparticle-Based Hybrid Nano-Bio Electro catalyst for Efficient and Robust H_2 Evolution from Water” Journal of the American Chemical Society, Vol. 137.8, 2015 pp. 2840–2843.

27. M.J. Ranaghan, R.R. Birge, “Photochemical and Thermal Stability of Green and Blue Proteo-rhodopsin: Implications for Protein based Bioelectronic Devices” J. Phys. Chem. B Vol.114,

2010, pp. 14064 - 14070.

28. A. Rakovich, M. Artemyev, A. Sukhanova, N. Bouchonville, E. Lukashev, V. Oleinikov, M. Artemyev, V. Lesnyak, N. Gaponik, M. Molinari, M. Troyon, Y. P. Rakovich, J. F. Donegan, I. Nabiev "Resonance Energy Transfer Improves the Biological Function of Bacteriorhodopsin within a Hybrid Material Built from Purple Membranes and Semiconductor Quantum Dots" Nano Lett., Vol.10.7, 2010, pp 2640–2648.

29. L.G. Reijmers, M. Mayford "Localization of A Stable Neural Correlate of Associative Memory" Science Vol. 317, 2007, pp.1230–1233.

30. N. Hampp, D. Oesterhelt "Diffraction Efficiency of Bacteriorhodopsin Films for Holography Containing Bacteriorhodopsin Wildtype BRWT And Its Variants BRD85E And BRD96N" J. Phys. Chem. Vol. 96, 1992, pp. 4679–4685.

31. Y.S. Abu-Mostafa, D. Psaltis "Optical Neural Computers" Sci. Am. Vol. 256, 1987, pp. 88–95.

32. F.V. Bunkin, T.B. Shevchenko "Diffraction Efficiency of Bacteriorhodopsin and Its Analogs" Sov. Tech. Phys. Lett. Vol. 7, 1981, pp. 630–631.

33. T. Pavlovic, A. Ignatiev, "Optical and Microstructural Properties of Anodically Oxidized Aluminum" Thin Solid Films Vol. 138, 1986, pp. 97-109.

34. D. H. Bradhurst, J. S. L. Leach, "The Mechanical Properties of Thin Anodic Films on Aluminum" J. Electrochemical. Soc. Vol. 113, 1966, pp.1245-1249.

35. R.R. Birge, N. B. Gillespie. "Biomolecular Electronics: Protein-Based Associative Processors and Volumetric Memories" J. Phys. Chem. B Vol.103.10, 1999, pp.746–10 766.

36. J.A. Greco, R.R. Birge, "Fourier Transform Holographic Associative Processors Based on Bacteriorhodopsin" Int. J. Unconventional Comput. Vol. 8, 2012, pp. 433–457.

37. O. Jessensky, U. Goesele, "Self-Organized Formation of Hexagonal Pore Arrays in Anodic Alumina" Applied Physics Letters Vol. 72.10, 1998. pp. 959-965.

38. A. P. Li, U. Goesele, "Fabrication and Micro-structuring of Hexagonally Ordered Two-Dimensional Nanopore Arrays in Anodic Alumina" Adv. Mater. Vol. 11.6, 1999, pp. 483-487

39. A. P. Li, U. Goesele "Hexagonal Pore Arrays with A 50–420 Nm Interpore Distance Formed by Self-Organization in Anodic Alumina" Journal of Applied Physics Vol. 84.11, 1998, pp. 6023 - 6026

40. J.A. Stuart, R.R Birge "Protein-Based Volumetric Memory" Proc. IEEE Nonvol. Mem. Tech. (INVMTC) 6, 2002, pp. 45–51.

41. J. A. Stuart, R. R. Birge “Volumetric Optical Memory Based on Bacteriorhodopsin” Synth. Met. Vol.127, 2002, pp. 3–15.

42. R.R. Birge, N. B. Gillespie. “Biomolecular Electronics: Protein-Based Associative Processors and Volumetric Memories” J. Phys. Chem. B Vol. 103.10,1999 pp. 746–766.

43. N. K. Allam, M.A. El-Sayed “Bacteriorhodopsin/TiO_2 Nanotube Arrays Hybrid System for Enhanced Photo Electrochemical Water Splitting” Energy Environ Sci, Vol. 4, 2011, pp.2909-2914.

44. N. Naseri, R. Irani. “Visible Light Switchable Br/TiO_2 Nanostructured Photoanodes For Bio-Inspired Solar Energy Conversion” RSC Adv. Vol.5, 2015, pp.18642-18646.

45. S. Balasubramanian. E. A. Rozhkova “High-Performance Bio-assisted Nano-photo catalyst for Hydrogen Production” Nano Lett., Vol.13, 2013, pp.3365−3371.

46. S. Iijima “Helical Microtubules of Graphitic Carbon” Nature Vol. 354,1991, pp.56–8.

47. K. Bradley, G. Grüner “Integration of Cell Membranes and Nanotube Transistors” Nano Lett Vol. 5, 2005, pp. 841-845.

48. P. Bertoncini, O. Chauvet “Conformational Structural Changes of Bacteriorhodopsin Adsorbed onto Single-Walled Carbon Nanotubes” J Phys Chem B Vol. 114, 2010, pp.4345-4350.

49. Y. Jin, D. Cahen, “Bacteriorhodopsin as An Electronic Conduction Medium for Biomolecular Electronics” Chem. Soc. Rev., Vol. 37, 2008, pp. 2422–2432.

50. B. Javidi, J.L. “Horner, Single SLM Joint Transform Optical Correlator”, Vol 28(5), Appl. Opt. 1989, pp. 1027-1032.

51. K. Kodate, R. Thapliya, “Binary Zone-Plate Array for A Parallel Joint Transform Correlator Applied to Face Recognition” Appl. Opt. Vol. 38(14), 1999, pp. 3060-3067.

52. VanderLugt, “Signal Detection by Complex Spatial Filtering” IEEE Trans. Inf. Theory IT Vol. 10,1964, pp.139-145.

53. R. Li, H. Yang, “Bidirectional Mediation of Tio2 Nanowires Field Effect Transistor by Dipole Moment from Purple Membrane” Nanoscale Vol. 2, 2010, pp.1474-1479.

54. P.E. Carrigan, S. Tuzmen “Site-Directed Mutagenesis” Methods Mol. Biol. Vol. 700, 2011, pp.107–124.

55. O. Berthoumieu, A. Watts “Molecular Scale Conductance Photo Switching in Engineered Bacteriorhodopsin” Nano Lett. Vol. 12, 2012, pp. 899–903.

56. A. Patil, J. Davis “Enhanced Photocurrent in Engineered Bacteriorhodopsin Monolayer

Films" J. Phys. Chem. B Vol. 116, 2012, pp. 683–689.

57. D. Umeno, F.H. Arnold, "Diversifying Carotenoid Biosynthetic Pathways by Directed Evolution" Microbiol. Mol. Biol. Rev. 69, 2005, pp. 51–58.

58. C. Jaeckel, D. Hilvert "Protein Design by Directed Evolution" Annu. Rev. Biophysics. Vol. 37, 2008, pp. 153–173.

59. K. Miyazaki, F.H. Arnold "Exploring Non-natural Evolutionary Pathways by Saturation Mutagenesis: Rapid Improvement of Protein Function" J. Mol. Evol. Vol. 49, 1999, pp. 716–720.

60. U.T. Bornscheuer, S.H. Krishna "Optimizing Lipases and Related Enzymes for Efficient Application" Trends Biotechnol. Vol. 20, 2002, pp. 433–437.

61. R. R. Mohammadpour, S. Janfaza "Efficient Nanostructured Bio Photovoltaic Cell Based on Bacteriorhodopsin as Bio photosensitizer" ACS Sustainable Chem. Eng., Vol. 3, 2015, pp. 809−813.

62. H.J. Butt, E. Bamberg, D. Oesterhelt "Aspartic Acids 96 And 85 Play A Central Role in The Function of Bacteriorhodopsin as A Proton Pump" The EMBO Journal Vol.8 no.6, 1989, pp.1 657 – 1663

63. Tsung-Yen Lee, Tsyr-Yan Yu "Tuning the Photocycle Kinetics of Bacteriorhodopsin in Lipid Nanodiscs" Biophysical Journal Volume 109, 2015, pp. 1899–1906.

64. A. Nath, S. G. Sligar. "Applications of Phospholipid Bilayer Nanodiscs In the Study of Membranes and Membrane Proteins" Biochemistry Vol. 46, 2007, pp. 2059–2069.

65. T.H. Bayburt, S. G. Sligar. "Self-Assembly of Discoidal Phospholipid Bilayer Nanoparticles with Membrane Scaffold Proteins" Nano Lett. Vol. 2, 2002, pp.853–856.

66. V.M. Hernandez-Rocamora, M. Vicente. "Dynamic Interaction of The Escherichia Coli Cell Division Zipa And Ftsz Proteins Evidenced in Nanodiscs" J. Biol. Chem. Vol. 287, 2002, pp. 30097–30104.

67. K. Seifert, E. Bamberg "Charge Transport by Ion Translocating Membrane Proteins on Solid Supported Membranes" Biophysical Society Vol. 64,1993, pp. 384-391.

68. Z. Zhao, Y. Jin, "Bacteriorhodopsin/Ag Nanoparticle-Based Hybrid Nano-Bio Electrocatalyst For Efficient and Robust H_2 Evolution from Water" J Am Chem Soc Vol. 137, 2015, pp.2840-2843.

69. D. Cialla, A. Maerz, R. Boehne, F. Theil, K. Weber, M. Schmitt, J. Popp, "Surface-Enhanced Raman Spectroscopy (SERS): Progress and Trends" Anal Bioanal. Chem Vol. 403, 2012, pp. 27-54.

70. X. Zhang, R.P. Van Duyne “Sensitive and Selective Chem/Bio Sensing Based on Surface-Enhanced Raman Spectroscopy (SERS)” Vib Spectrosc Vol. 42,2006, pp. 2-88.

71. I.R. Nabiev, R.G. Efremov “Surface-Enhanced Raman Spectroscopy of Biomolecules. Part II. Application of Short- And Long-Range Components of SERS to The Study of The Structure and Function of Membrane Proteins” J Raman Spectrosc Vol. 21, 1990, pp. 43-48.

72. V. Polovinkin, T. Balandin, O. Volkov, E. Round, V. Borshchevskiy, P. Utrobin, D. von Stetten, A. Royant, D. Willbold, G. Arzumanyan, V. Chupin, J.-L. Popot, V. Gordeliy “Nanoparticle Surface-Enhanced Raman Scattering of Bacteriorhodopsin Stabilized by Amphipol A8-35” J Membr Biol Vol. 247, 2014, pp. 971-980.

73. P. Wang, N. M. Dimitrijevic, A. Y. Chang, R. D. Schaller, Y. Liu, T. Rajh, E. A. Rozhkova “Photoinduced Electron Transfer Pathways in Hydrogen-Evolving Reduced Graphene Oxide-Boosted Hybrid Nano-Bio Catalyst” ACS Nano Vol. 8, 2014, pp.7995-8002.

74. J. Chellamuthu, A. Sambandamb “Enhanced Photocurrent Generation in Bacteriorhodopsin Based Bio-Sensitized Solar Cells Using Gel Electrolyte” Journal of photochemistry and photobiology, 2016, pp.1011-1344.

75. H. Luecke, J.-P. Cartailler, J. K. Lanyi, “Structure of Bacteriorhodopsin At 1.55 Å Resolutions.” J. Mol. Biol. Vol. 291, 1999, pp. 899-911.

76. M. Kolbe, D. Oesterhelt, “Structure of The Light-Driven Chloride Pump Halorhodopsin at 1.8 A Resolution” Science Vol. 288, 2000, pp.1390-1396.

77. D. Oesterhelt “The Structure and Mechanism of The Family of Retinal Proteins from Halophilic Archaea” Current Opinion in Structural Biology 1998, Vol.8 pp.489-500.

78. J.K. Lanyi “Mechanism of Ion Transport Across Membranes” J Biol Chem, Vol. 272, 1997, pp. 31209-31212

79. U. Haupts, J. Tittor J, D. Oesterhelt “General Concept for Ion Translocation by Halobacterial Retinal Proteins: The Isomerization/ Switch/ Transfer (IST) Model” Biochemistry, Vol. 36, 1997, pp. 2-7.

80. X. Xie, A. Gaston, E. Bakker, “Photocurrent Generation Based on A Light-Driven Proton Pump in An Artificial Liquid Membrane” Nature Chemistry, Vol. 6, 2014, pp. 202-206.

81. E. Alfinito, C. Pennetta, L. Reggiani, “A Network Model to Correlate Conformational Change and The Impedance Spectrum of Single Proteins” Nanotechnology, Vol.19, 065202, 2008, pp.1-13.

82. R. Birge, M.B. Gillespie, K.J. Wise, “Biomolecular Electronics: Protein-Based Associative Processors and Volumetric Memories” J. Phys. Chem. B, Vol.103, 1999, pp. 746-766.

83. H. Imam, L.R. Lindvold, P.S. Ramanujam “Photo anisotropic Incoherent-To-Coherent

Converter Using a Bacteriorhodopsin Thin Film" Optics Letters, Vol. 20(2), 1995, pp. 225-227

84. Janos K. Lanyi, "Bacteriorhodopsin" Annu. Rev. Physiol. Vol. 66, 2004, pp. 665–88.

85. F. Zhou, A. Windemuth, K. Schulten "Molecular Dynamics Study of The Proton Pump Cycle of Bacteriorhodopsin" Biochemistry Vol.32, 1993, pp. 2291–2306.

86. J. Yongdong, S. Mordechai, D. Cahen "Bacteriorhodopsin as An Electronic Conduction Medium for Biomolecular Electronics" Chem. Soc. Rev. Vol.37, 2008, pp. 2422–2432.

87. G. Nagel, E. Bamberg "Voltage Dependence of Proton Pumping by Bacteriorhodopsin Is Regulated by the Voltage-Sensitive Ratio of M1 to M2" Biophysical Journal Vol. 74, 1998, pp. 403–412.

88. R. Dutzler, B. Campbell, R. MacKinnon "X-Ray Structure of a Clc Chloride Channel At 3.0 Å Reveals the Molecular Basis of Anion Selectivity" Nature Vol. 415, 2002, pp. 287-294.

89. K. Voıtchovsky, J. F. Ryan "Electrostatic and Steric Interactions Determine Bacteriorhodopsin Single-Molecule Biomechanics" Biophysical Journal Vol. 93, 2007, pp. 2024–2037.

90. B. Roux, M. Nina, "Thermodynamic Stability of Water Molecules in The Bacteriorhodopsin Proton Channel: A Molecular Dynamics Free Energy Perturbation Study" Biophysics. J. Vol. 71, 1996, pp. 670–81.

91. Y. Gat, M. Sheves "A Mechanism for Controlling The pKa Of the Retinal Protonated Schiff Base in Retinal Proteins. A Study with Model Compounds". J. Am. Chem. Soc. Vol. 115, 1993, pp. 3772–73.

92. W. W. Wang, A. S. Bassi "Toward Mimicking Biological Vision with Protein-Based Flexible Imaging Arrays" SPIE Newsroom 2006, pp. 1-3

93. H. Bayley, A. Heron, "Droplet Interface Bilayers: The Two-Droplet System" Molecular Biosystem, Vol.4, 2008, pp. 1191–120.

94. E. T. Castellana, P. S. Cremer "Solid Supported Lipid Bilayers: From Biophysical Studies to Sensor Design" Surface Science Reports Vol. 61, 2006, pp. 429–444.

95. P. Muller, H. Ti Tien, W.C. Wescott, "Methods for Formation of Single Bimolecular Lipid Membranes in Aqueous Solution" Journal of Physical Chemistry Vol.6, 1963 7, pp. 534-535.

96. L .K. Tamm and H.M. McConnell, "Supported Phospholipid Bilayers" Biophysics Journal Vol. 47, 1985, pp. 105-113.

97. P. Phataka, M. Elstnera "Amino Acids with An Intermolecular Proton Bond as Proton Storage Site in Bacteriorhodopsin" PNAS vol. 105.50, 2008 pp. 19672–19677.

98. A. Victor, Lorenz-Fonfrıa “Spectroscopic and Kinetic Evidence on How Bacteriorhodopsin Accomplishes Vectorial Proton Transport Under Functional Conditions” Jour. Am. Chem. Soc. Vol.131, 2009, pp. 5891–5901.

99. J. Le Coutre, D. Oesterheltt, “Experimental Evidence for Hydrogen-Bonded Network Proton Transfer in Bacteriorhodopsin Shown by Fourier-Transform Infrared Spectroscopy Using Azide As Catalyst” Proc. Natl. Acad. Sci. USA Vol. 92, 1995, pp. 4962-4966.

100. J. Guijarro, M. Engelhard, F. Siebert, “Anion Uptake in Halorhodopsin From Natronomonas Pharaonis Studied by FTIR Spectroscopy: Consequences for The Anion Transport Mechanism” Biochemistry Vol. 45, 2006, pp. 11578–11588.

101. G. Varo “Analogies Between Halorhodopsin And Bacteriorhodopsin” Biochemical et Biophysical Acta (BBA) - Bioenergetics Vol.1460. 1, 2000, pp. 220-229.

102. E. Alfinito, G. Gomila, “Thermal Fluctuations of A GPCR: A Two Force Constant Model” AIP Conference Proceedings Vol. 800, 2005, pp.38.

103. V. Akimov, E. Alfinito, C. Pennetta, L. Reggiani, J. Minic, T. Gorojankina, E. Pajot-Augy, R. Salesse Akimov “An impedance network model for the electrical properties of a single protein nanodevice” in “Nonequilibrium Carrier Dynamics in Semiconductors” Springer Proceedings in Physics Vol. 110 7, 2006, pp. 229-232.

104. E. Alfinito, C. Pennetta, and L. Reggiani, “A Network Model to Correlate Conformational Change and The Impedance Spectrum of Single Proteins” Nanotechnology Vol.19, 2008, pp. 1-13.

105. B. Schobert, J.K. Lanyi, “Halorhodopsin Is a Light-Driven Chloride Pump” J. Biol. Chem. Vol. 257.17, 1982, pp. 10306-10313.

106. D. Oesterhelt, “Structure and Function of Halorhodopsin” Isr. J. Chem. Vol. 35, 1995, pp. 475-494.

107. E. Bamberg, J. Tirtort, D. Oesterhelt “Light-Driven Proton or Chloride Pumping by Halorhodopsin” Proc. Natl. Acad. Sci. USA Vol. 90, 1993, pp. 639-643.

108. R. A. Bogomolni, W. Stoeckenius “Reconstitution of Purified Halorhodopsin” Proc. Natl. Acad. Sci. USA Biophysics Vol. 81, 1984, pp. 5408-5411.

109. G. Varo, J. K. Lanyi “Photocycle Of Halorhodopsin From Halobacterium Salinarium” Biophysical Journal Vol. 68, 1995, pp. 2062-2072.

110. J. K. Lanyi, “Light Energy Conversion in Halobacterium Halobium” Microbiol. Rev. Vol. 42, 1978, pp. 682-706.

111. H.T. Tien, “Light-Induced Phenomena in Black Lipid Membranes Constituted from

Photosynthetic Pigments" Nature Vol 219, 2010, pp. 272-274.

112. Felix T. Hong, "Erratum Molecular Sensors Based on The Photovoltaic Effect of Bacteriorhodopsin: Origin of Differential Responsivity", Materials Science and Engineering, Vol 5 1997, pp. 267-285.

113. Y. Okada-Shudo, K. Tanaka "Robot Vision Using Biological Pigments" SPIE Newsroom. 2012. pp. 201-2012.

114. L. Zimányi, J.K. Lanyi, "Pathways of Proton Release in The Bacteriorhodopsin Photocycle". Biochemistry Vol.31, 1992, pp. 8535–8543.

115. D. Oesterhelt, J. Tittor "The Photocycle of The Chloride Pump Halorhodopsin.II: Quantum Yields and A Kinetic Model" The EMBO Journal Vol.4.9, 1985, pp. 2351-2356.

116. A. D. Gruia1, S. Fischer "Mechanism of a Molecular Valve in The Halorhodopsin Chloride Pump" Structure Vol. 13, 2005, pp. 617-627.

117. L. Zimanyib, J.K. Lanyi, "Halorhodopsin: A Light-Driven Active Chloride Transport System" Annals of the New York Academy of Sciences, Vol. 574, 1989, p. 11-19.

118. P. Hegemann, D. Oesterhelt "The Photocycle of The Chloride Pump Halorhodopsin. I: Azide cartelized Deprotonation of The Chromophore Is a Side Reaction of Photocycle Intermediates Inactivating the Pump" The EMBO Journal Vol. 4.9, 1985, pp. 2347-2350.

119. A. Losi, A. Wegener, "Thermodynamics of The Early Steps in The Photocycle of Natronobacterium Pharaonis Halorhodopsin. Influence of the Medium and of Anion Substitution" Photochemistry and Photobiology, Vol. 74.3, 2001, pp. 495–503.

120. G. Váró, J.K. Lanyi, "Lightdriven Chloride Ion Transport by Halorhodopsin from Natronobacterium Pharaonis. 2. Chloride Release and Uptake, Protein Conformation Change and Thermodynamics" Biochemistry Vol. 34, 1995, pp. 14500-14507.

121. G. Váró, J.K Lanyi, "Photocycle of Halorhodopsin From Halobacterium Salinarium" Biophysics. J. 68, 1995, pp. 2062-2072.

122. A.D Kaulen, L.A Drachev, "Proton Transport and M-Type Intermediate Formation by 13-Cis-Bacteriorhodopsin" Biochemical. Biophysics. Acta, Vol.1018, 1990, pp. 103-113.

123. C. Pfisterer, S. Fischer "The Mechanism of Photo-energy Storage in the Halorhodopsin Chloride Pump" Journal of Biological Chemistry, Vol. 284.20, 2009, pp. 13562–13569.

124. A. Seki, N. Kamo, "Heterologous Expression of Pharaonis Halorhodopsin in Xenopus Laevis Oocytes and Electrophysiological Characterization of Its Light-Driven Cl- Pump Activity" Biophysics J. Vol. 92, 2007, pp. 2559–2569.

125. N. Bondar, S. Fischer, J. Smith, "Tuning of Retinal Twisting in Bacteriorhodopsin Controls

the Directionality of the Early Photocycle Steps" J. Phys. Chem. Vol. 109, 2005, pp. 14786–14788.

126. A. Dér, L. Keszthelyi "Bacteriorhodopsin as a Possible Chloride Pump" FEBS Lett., Vol. 259, 1989, pp. 24-26.

127. A. Dér, W. Stoeckenius "Alternative Translocation of Protons and Halide Ions by Bacteriorhodopsin" Proc. Natl. Acad. Sci. USA, Vol. 88, 1991, pp. 4751-4755.

128. J. Le Coutre, K. Gerwert. "Experimental Evidence for Hydrogen-Bonded Network Proton Transfer in Bacteriorhodopsin Shown by Fourier-Transform Infrared Spectroscopy Using Azide as Catalyst" Proc. Natl. Acad. Sci. USA. Vol. 92, 1995, pp. 4962– 4966.

129. J. Guijarro, F. Siebert "Binding of Anions to Halorhodopsin from Natronobacterium Pharaonis Studied by Static and Time-Resolved FTIR Spectroscopy" Biophysics. J. 2003 vol. 84, 2003, pp. 270A.

130. I. B. Cooper, B.A. Barry "Azide as a Probe of Proton Transfer Reactions in Photosynthetic Oxygen Evolution" Biophysical Journal Vol. 95, 2008, pp. 5843–5850.

131. H. Michel, D. Oesterhelt, "Light-Induced Changes of the Ph Gradient and the Membrane Potential in Halobacterium Halobium" FEBS Lett. 65, 1976, pp. 175–178.

132. L. P. Hromada, Jr. "Bilayer Lipid Membrane (BLM) Integration into Microfluidic Platforms with Application Toward BLM-based Biosensors" University of Maryland, College Park, 2007.

133. M. Sheves, M. Ottolenghi "Controlling the pKa of the Bacteriorhodopsin Schiff Base by Use of Artificial Retinal Analogues" Proc. Natl. Acad. Sci. USA. Vol. 83, 1986, pp. 3262–3266.

134. D. Oesterhelt, B. Hess, "Reversible Photolysis of the Purple Complex in the Purple Membrane of Halobacterium Halobium" Eur. J. Biochem. Vol. 37, 1973, pp. 316 –326.

135. H. J. Sass, M. H. Koch, G. Bueldt, "The Tertiary Structural Changes in Bacteriorhodopsin Occur Between M States: X-Ray Diffraction and Fourier Transform Infrared Spectroscopy" EMBO J. 16, 1997, pp. 1484 –149.

136. F. T. Dubrovskii, F. F. Litvin, "Photoinduced Changes in the Quantum Yields of the Photochemical Cycle of Conversions of Bacteriorhodopsin and Transmembrane Transport of Protons in Halobacterium Halobium Cells" Biokhimiya Vol. 47, 1982, pp. 1230 –1240.

137. H. Luecke, J.K. Lanyi "Structural Changes in Bacteriorhodopsin During Ion Transport at 2 Angstrom Resolution" Science Vol. 286, 1999, pp. 255–261.

138. K. Edman, E. Pebay-Peyroula, "High-Resolution X-Ray Structure of an Early Intermediate in The Bacteriorhodopsin Photocycle" Nature Vol. 401, 1999, pp. 822–826.

139. Pebay-Peyroula, J.P. Landau, “X-ray Structure of Bacteriorhodopsin at 2.5 Angstroms from Microcrystals Grown in Lipidic Cubic Phases” Science Vol. 277, 1997, pp. 1676–1681.

140. V.A. Lórenz -Fonfría, H. Kandori, “Spectroscopic and Kinetic Evidence on How Bacteriorhodopsin Accomplishes Vectorial Proton Transport Under Functional Conditions” J. Am. Chem. Soc. 131, 2009, pp. 5891–5901.

141. C. Li-Kang, M.A. El-Sayed, “Bacteriorhodopsin-Based Photo-Electrochemical Cell” Biosensors and Bioelectronics Vol. 26, 2010, pp. 620–626.

142. N.N. Vsevolodov, T.V. Dyukova “Retinal—Protein Complexes as Optoelectronic Components” Trend. Biotechnol. Vol. 12 8i, 1994, pp. 81-88

143. C. Rödig, F. Siebert “Time-Resolved Step-Scan Fourier Transform Infrared Spectroscopy Reveals Differences Between Early and Late M Intermediates of Bacteriorhodopsin” Biophysics. J., Vol. 76, 1999, pp. 2687-2701.

144. G. Váró, J.K Lanyi “Light-Driven Chloride Ion Transport by Halorhodopsin from Natronobacterium pharaonis. I. The Photochemical Cycle” Biochemistry, Vol. 34, 1995, pp. 14490-14499.

145. A. Blanck, D. Oesterhelt “The Halo-Opsin Gene. II. Sequence, Primary Structure of Halorhodopsin and Comparison with Bacteriorhodopsin” EMBO J., Vol. 6, 1987, pp. 265-273.

146. K. Ludmann, G. Váró “Charge Motions During the Photocycle of Pharaonis Halorhodopsin” Biophysics. J, Vol. 78, 2000, pp. 959-966.

147. T.J. Walter, M.S Braiman “Anion-Protein Interactions During Halorhodopsin Pumping: Halide Binding at the Protonated Schiff Base” Biochemistry Vol. 33, 1994, pp. 1724-1733.

148. M. Rüdiger, D. Oesterhelt “Specific Arginine and Threonine Residues Control Anion Binding and Transport in the Light-Driven Chloride Pump Halorhodopsin” EMBO J., Vol.16, 1997, pp. 3813-3821.

149. M. Ariki, J.K Lanyi “Effects of Arginine Modification on the Photocycle of Halorhodopsin” Arch. Biochem. Biophysics., Vol. 248, 1986, pp. 532-539.

150. S.G. Boxer, J.T. Groves, N. Ulman, “Micropatterning Fluid Lipid Bilayers on Solid Supports”, Science Vol. 651, 1997, pp. 651-653.

151. J. Spinke, J. Yang, “Polymer-Supported Bilayer on a Solid Substrate” Biophysics Journal, Vol. 63, 1992, pp. 1667-1671.

152. S. Tristram-Nagle, D. J. Kim “Structure and Water Permeability of Fully Hydrated Phytanoyl” Chemistry and Physics of Lipids, Vol.163, 2010, pp. 630–637.

153. W. Shinoda, S. Mikami, M. Baba, T. Hato, “Molecular Dynamics Study on the Effects of Chain Branching on the Physical Properties of Lipid Bilayers” J. Phys. Chem. B Vol.108, 2004, pp. 9346–9356.

154. M. Montal and P. Mueller “Formation of Bimolecular Membranes from Lipid Monolayers and a Study of Their Electrical Properties” Proc. Nat. Acad. Sci. USA, Vol. 69, 1972, pp. 3561-3566.

155. Molecular Device Axopatch 200B Microelectrode Amplifier Part Number: Axopatch 200B-2 axon-axopatch-200b-datasheet-rev-b. https://www.autom8.com/wp-content/uploads/ 2016 /07/Axopatch-200B.pdf (Accessed on 07/25/2018)

156. The Axon™ Guide A guide to Electrophysiology and Biophysics Laboratory Techniques 1-2 500-0102D. https://mdc.custhelp.com/euf/assets/content/Axon%20Guide%203rd%20 edition.pdf (Accessed on 07/25/2018)

157. pCLAMP 10 Data Acquisition and Analysis for Comprehensive Electrophysiology User Guide1-2500-0180Rev. A. https://moleculardevices.app.box.com/s/l8h8odzbdikalbje1iw j85x8800 4f588. (Accessed on 07/25/2018)

158. User’s Guide, Agilent 33250A 80 MHz Function / Arbitrary Waveform Generator Publication Number 33250-90001 April 2000 Copyright Agilent Technologies 2000 All Rights Reserved.

159. E. Alfinito, L. Reggiani “On the Mechanisms Responsible of Photocurrent in Bacteriorhodopsin” Physical Review Vol. 91, 2015, pp. 1-7

160. L.O. Essen “Halorhodopsin: Light-Driven Ion Pumping Made Simple” Current Opinion in Structural Biology Vol. 12, 2002, pp. 516–522.

161. A. F. L. Creemers, R Kelle, “Solid State 15N NMR Evidence for a Complex Schiff Base Counterion in the Visual G-Protein-Coupled Receptor Rhodopsin” Biochemistry Vol. 38, 1999, pp. 7195-7199.

162. W.A Havelka, D. Oesterhelt “Projection Structure of Halorhodopsin from Halobacterium Halobium” J. Mol. Biol., Vol. 234, 1993, pp. 837-846.

163. G. Váró, J.K. Lanyi, “Light-Driven Chloride Ion Transport by Halorhodopsin from Natronobacterium Pharaonis. 2. Chloride Release and Uptake, Protein Conformation Change, and Thermodynamics”, Biochemistry Vol. 34, 1995, pp. 14500-14507.

164. N. L. Wagner1, M. J. Ranaghan “Directed Evolution of Bacteriorhodopsin for Applications in Bioelectronics” J R Soc Interface Vol.10, 2013, pp. 1-15.

165. J. R. Hillebrecht, R. R. Birge “Directed Evolution of Bacteriorhodopsin for Device Applications” Method Enzymol. Vol. 388, 2004, pp. 333–347.

166. V. Cutsuridis, T. Wennekers “Hippocampus, Microcircuits and Associative Memory” Neural Networks Vol. 22. 8, 2009, pp. 1120–1128.

167. G. Karp “Cell and Molecular Biology: Concepts and Experiments” 7th Edition, 2017, Chapter 4, pp. 121-181.

168. C. H. Hsieh and S. C. Sue, “Membrane Packing Geometry of Di-phytanoyl-phosphatidyl-choline is Highly Sensitive to Hydration: Phospholipid Polymorphism Induced by Molecular Rearrangement in the Headgroup Region”, Biophysical Journal, Vol. 73, 1997, pp. 870-877.

169. R. Peters, R.J. Cherry. “Lateral and Rotational Diffusion of Bacteriorhodopsin in Lipid Bilayers: Experimental Test of the Saffman-Delbrück Equations” Proc Natl Acad Sci U S A. 1982 Jul79(14): pp4317-21.

Appendix A. Estimation of Protein Absorption

The bR protein used in this work was obtained from collaborating with Dr. Oliver P. Ernst group (Department of Biochemistry and Department of Molecular Genetics, University of Toronto, Canada). The protein was suspended in a sucrose solution. Upon reception, the bR was pelted using ultracentrifuge and Milli-Q water from Dr. Feng Wang (Department of Chemistry and Bio Chemistry University of Arkansas, Fayetteville). The final bR sample was re-suspended and stored in a 100 mL 10 mM Tris-HCl solution (pH7). The calculations were adapted to the bR sample bought from Sigma Aldrich.

According to W. Stoeckenius, and R. Bogomolni [1, 2], The bR Mol mass is around 26 kDa = 26 kg/mol (1Da = 1g/mol). 10 mg bR were acquired and ~1 mg (1 mL) was used

$$\frac{10^{-6}\text{kg}*1\text{ Mol}}{26\text{ kg}} = 2.85 * 10^{-8}\text{ Mol} \qquad \text{(Equation A-1)}$$

In final $2.85 * 10^{-8}$ Mol were available.

=> The bR concentration was calculated to be:

$$\frac{3.85*10^{-8}\text{ Mol kg}}{1*10^{-3}L} = 2.85 * 10^{-5}\text{ Mol/L} \qquad \text{(Equation A-2)}$$

The hR protein was obtained from collaborating with Prof. John Golbeck (Pennsylvania State University). The hR was received in a 1.5 mL Eppendorf tubes suspended in a ~ 1 mL natronomonas pharaonis-halorhodopsin (pHR LEHIS). The sample had been expressed and purified from E. coli by Ni affinity chromatography. hR was expressed in around 0.5 mL of a buffer made of: 50 mM MES pH 6.0, 300 mM NaCl, 0.1% DM (decyl maltoside), and 10% glycerol. With a given concentration of 1.83 mg/mL, the molar concentration of hR was calculated to be:

$$\frac{31.83\text{ mg}}{25 * 10^{\mp 6}\text{ mg}} = 7.32 * 10^{-8}\text{ Mol in 1 mL} => 7.32 * 10^{-5}\text{M} \qquad \text{(Equation A-3)}$$

Both absorption spectra (hR and bR) were calculated as follows.

- bR concentration 3.85 x 10^{-5} Mol/L,
- Cuvette length L = 1 cm,
- Absorption coefficient ε = 63000 L/Mol cm at 570 nm (and 75000 at 280 nm).

the maximum predictable absorption for the bR sample was:

$$A = C * L * \varepsilon = 2.9 \text{ at } 570 \text{ nm and } 3.5 \text{ at } 280 \text{ nm} \quad \text{(Equation A-4)}$$

Similarly, the concentration of hR was 7.32 x 10^{-5} Mol/L, with the same cuvette length L = 1 cm and same absorption coefficient ε = 63000 L/Mol cm at 570 nm (and 75000 at 280 nm).

the maximum predictable hR absorption was: 3.0 at 570 nm and 3.6 at 280 nm.

Note: The calculations were made assuming a high-end saturation (concentration of 1mg /mL); reducing the saturation to 0.3 mg/mL, the maximum predictable absorption would be 0.87 at 570 nm and 1.04 at 280 nm. Both absorption spectra (hR and bR) are shown in Section 0.

References:

1. G. Varo, J. K. Lanyi "Photocycle Of Halorhodopsin From Halobacterium Salinarium" Biophysical Journal Vol. 68, 1995, pp. 2062-2072.
2. W. Stoeckenius, "Bacterial rhodopsin: Evolution of a mechanistic model for the ion pumps" Protein Science Vol. 8, pp 447–459, 1999.

Appendix B. Polydimethylsiloxane PDMS Chamber

The PDMS chamber presented in Figure B.1 was designed especially for this investigation. The chamber system is made of two identical components "Walls" #1. The Polydimethylsiloxane is a transparent material made of a mix of a soft and a hardening material. The mixture is poured into designed forms and let to rest for at least 10 hours. As pictured in Figure B.1 each wall (#1) includes a cave-chamber on its large surface (#2). A smaller cave (#3) is imprinted in each chamber to host the silicon chip (#4). Injection channels # 6 & #7 are used to fill the chambers with electrolyte, buffer, and to empty the chambers when necessary. The #7 channels are mostly used to inject the membrane solutions atop the electrolytes (Figure. A 1 (C). The principle of the system is depicted in Figure B.1 (A –D). The silicon chip #4 is inserted between the two "walls" and a metal frame is used to seal the system from leakage. The silicon chip is equipped with a micro-sized window at its center. The hole (window) serves as connection between both chambers #5. The electrolyte and buffer are pumped (channel #6) on both sides of the chip, up to under the window, Figure B.1 (B.). Next, the lipid solution is injected in the front (cis) chamber, while the lipid-protein solution is injected in the back (trans) chamber Figure B.1(C.). The electrolyte-buffer solution is then raised in both chamber (back chamber first) and a bilayer is formed at the window, Figure B.1 (D). Silver chloride electrodes incorporated in the walls (#8) are used to detect changes of potential in the system. Once illuminated the lipid-protein bilayer starts translocating ions and a photocurrent current can be measured.

The system was designed to allow the transportation of a photocurrent generating membrane. One of the goals of the investigation was to capture the image of a photocurrent generating membrane with a Transmission Electron Microscope (TEM). The folding method (Section 5.2.1) is the only method that can be used with this system. This confers the system a

high accuracy in forming natural membranes.

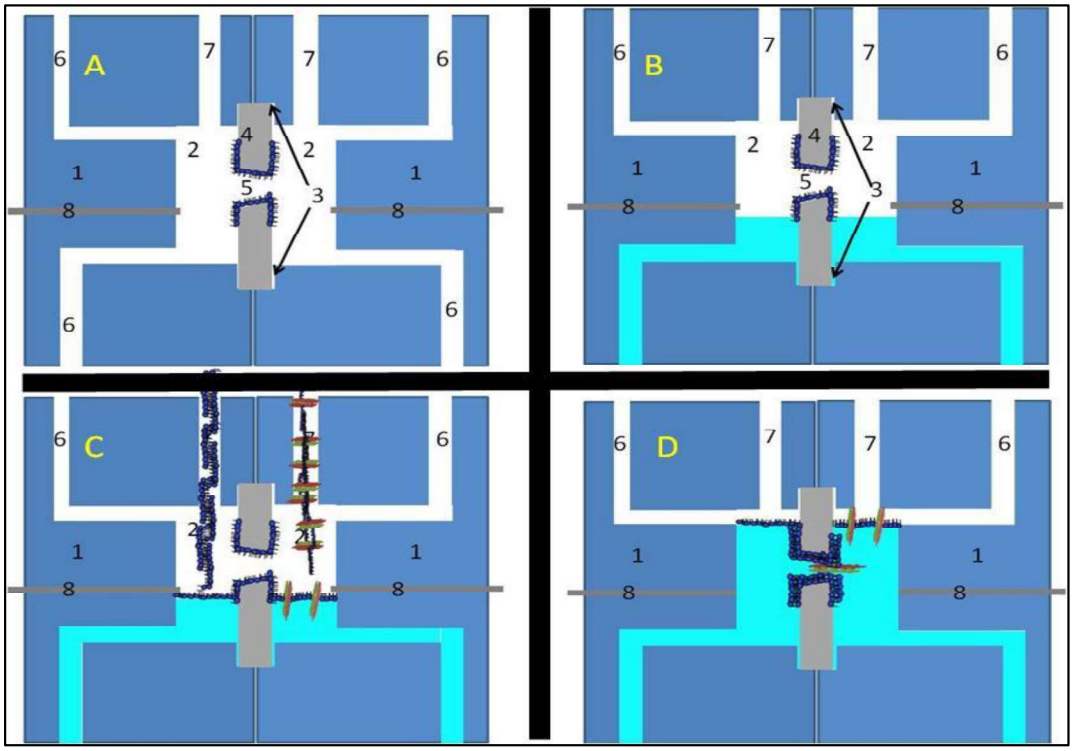

Figure B.1: Polydimethylsiloxane PDMS chamber.

Unfortunately, early in the experimental phase, the membranes were not strong enough to stand firm against the vibrations caused by the removal of the chip. It was, thus, not possible to capture the image of a photocurrent generating membrane. However, the image of a photocurrent generation membrane solution was captured and discussed in Section 6.6. Additional research on this system should address the chip removal procedure, which appears to weaken the membrane stability.

Appendix C. Conception of Membrane Solution

Since one of the goals of this work was to relate the generated current with the concentration of proteins used, mixtures were prepared according to the chemical properties of used species (bR, hR, DPhyPC, etc...). A total of three main solutions were mixed. A molecular ratio of 1/200 bR /DPhyPC was targeted and calculated as follows. The bR protein considered here was purchased from Sigma Aldrich. The calculation was adapted to the sample obtained from collaborating with Dr. Oliver P. Ernst group (Department of Biochemistry and Department of Molecular Genetics, University of Toronto, Canada).

1- bR Mol mass: 26 kDa = 26 kg/mol (1Da = 1 g/mol) [1].

2- 1 mg bR was purchased from Sigma Aldrich => 1 x 10^{-6} kg x 1 Mol / 26 kg = 3.85 x 10^{-8} Mol were available.

3- bR was diluted in a 1 ml 10 mM Tris-HCl solution (pH7)

- The bR concentration was:

$$\frac{3.85 * 10^{-8}\ \text{Mol}}{1 * 10^{-3}\ \text{L}} = 3.85 * 10^{-5}\ \text{Mol/L} \qquad \text{(Equation C-1)}$$

The primary solution combined DPhyPC with N-decane. N-decane is a solvent that helped dissipating the lipid as a solution. For this purpose, 25 mg DPhyPC were purchased from Avanti Lipid and mixed with 2.5 ml N-Decane to obtain a 1 % w/v solution, calculated as follows.

1- DPhyPC Mol mass = 846.252 g [2],

2- 25 mg DPhyPC => 25 x 10^{-3} g / 846.252 g = 2.95 x 10^{-5} Mol were available.

3- DPhyPC powder was diluted in 2.5 ml N-Decane to obtain a final concentration of

$$\frac{3.95*10^{-5}\ \text{Mol}}{2.5 * 10^{-3}\ \text{L}} = 0.012\ \text{Mol/L} \sim 1\%\ \text{W/V} \qquad \text{(Equation C-2)}$$

Targeting a ratio of approximately 1/200 between bR and DPhyPC, the mixture bR + DPhyPC was made of 50 % DPhyPC solution, and 50 % bR solution. 50 µl of each solution for example would contain:

$$\frac{5.91*10^{-7}\ \text{DPhPC}}{1.92*10^{-9}\ \text{bR Molecules}} = 307 \qquad \text{(Equation C-3)}$$

A 0.1 M sodium chloride (NaCl) was used in both chambers as electrolyte solution because of its conductivity. Phosphate Buffered saline was used as buffer to supply the solution with free charge while keeping the pH around 7. The mixture leading to the 0.1 M NaCl was obtained as follows.

1- NaCl Mol mass = 58 g,

2- Diluting 5.8 g of NaCl in 1L DI water.

- a 0.1 Mol/L solution is obtained

References

1. G. Varo "Analogies Between Halorhodopsin And Bacteriorhodopsin" Biochemical et Biophysical Acta (BBA) - Bioenergetics Vol.1460. 1, 2000, pp. 220-229.

2. V. Drachev and N. Frolov, "Reconstitution of Biological Molecular Generators of Electric Current" The Journal of Biological Chemistry Vol. 251, pp. 7059-7065, 1976.

Appendix D. Deriving the Capacitance Equation

The charge Q of a capacitor is proportional to its zero charge Q_0 multiplied by the charges movements following impulse excitation 1/RC within a defined period "t".

$$Q = Q_0\,(1 - e^{-\frac{t}{RC}}) \qquad \text{(Equation D-1)}$$

A differentiation of the charge expression by the time "t" leads to the equality:

$$\frac{dQ}{dt} = \frac{Q_0}{RC}\, e^{-t/RC} \qquad \text{(Equation D-2)}$$

The current can then be defined as:

$$I = I_0\, e^{-t/RC} \qquad \text{(Equation D-3)}$$

An integral of the charge variation yield the direct relationship between charge and capacitance "C"

$$Q = \int_0^t I\, e^{-\frac{t}{RC}} = I_0 RC\,[1 - e^{-\frac{t}{RC}}] = I_0\, RC\,[\,1 - \left(1 - \frac{t}{RC}\right)] \qquad \text{(Equation D-4)}$$

The capacitance "C" can thus be extracted as:

$$\Rightarrow \quad C = \frac{\Delta Q}{\Delta V} = I_0\, \frac{\Delta t}{\Delta V} \qquad \text{(Equation D-5)}$$

Appendix E. Supporting Figures

1. Sun based technologies

The most popular use of sun-based technology is without doubt the solar cell. Solar cells were developed since the 1960s as alternative means to generate power alongside the existing fossil fuel types. The growing awareness of the human responsibility in climate change, leading to the necessity to revisit the energy production made it possible for the solar cell technology to benefit from enormous attention.

Similarly, to solar cells, solar energy plants use solar panels to mirror sun heat toward a tower that uses the collected heat to drive a steam turbine, and to produce electricity. Both, solar energy plant and solar cell plant are often used in combination.

Photosynthesis is so far one of the still undeveloped technology to harvest and use solar energy. Applications include mostly glucose (sugar), and oxygen production as depicted in Figure E. 1.

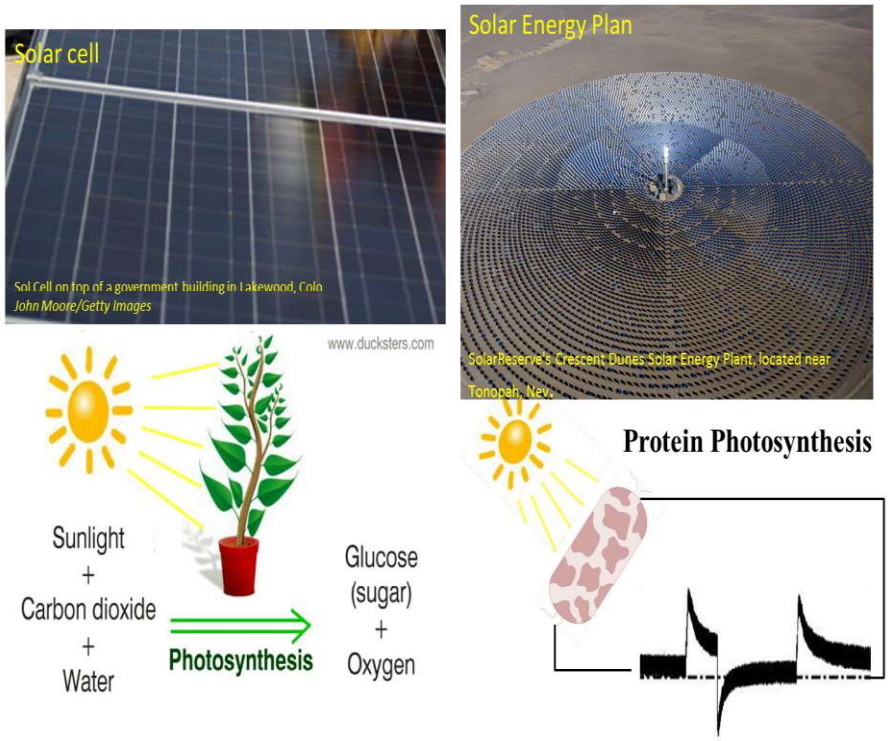

Figure E. 1: Popular sun based technologies.

2. Bacteriorhodopsin and Halorhodopsin

Bacteriorhodopsin and halorhodopsin occurs mostly as patches on the membrane of the halobacterium salinarum. The halobacterium salinarum is a bacterium with high saline environment affinity. Figure E. 2 shows salt ponds in San Franscisco, California. With considerably high salinity, salt ponds offer the best environmental and living condition for the bacteria. The proteins are found as purple patches on the bacteria membrane (Figure E. 2 (B)).

Figure E. 2: Natural occurrence of bR and hR.

3. Optical set-up

The optical set-up used in this experiment is presented in Figure E. 3. The set-up included a microscope, which allowed operators to see the inside of the experimental chamber. The set-up also included the lasers, which were described and characterized in Section 5.3.4 and Section 6.1. A power meter was borrowed from Dr. Yong Wang's group (University of

Arkansas, Physics Department) to calibrate the lasers and identify the power decay.

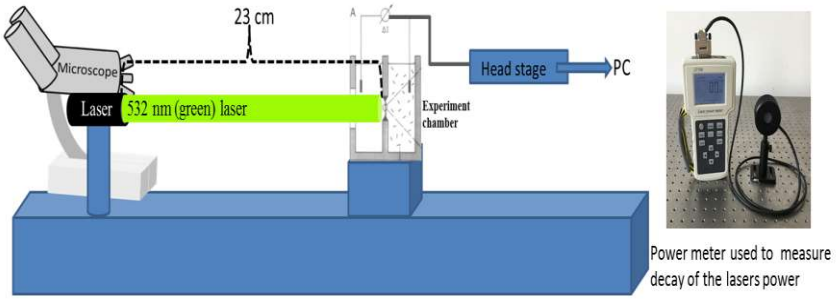

Figure E. 3: Optical set-up of the experiment.

Appendix F. Local Research Groups Activities in Research Area

The following research groups at the University of Arkansas are focusing on theme related to the presented work. No other research groups active on protein generated photocurrent (Protein Photosynthesis) was found on the University of Arkansas, Fayetteville campus.

Professors name	Department	Related research interest
Dr. Roger Koeppe	Chemistry	Membrane Biochemistry,
Dr. Paul Adams	Chemistry	Physical chemistry of Proteins and Membranes
Dr. Ingrid Fritsch*	Chemistry	Energy conversion and Storage
Dr. Frank Millet	Chemistry	Proton and electron Translocation
Dr. Hameed Naseem	Electrical Engineering	Solar cell, photovoltaic
Dr. Surendra Singh*	Physics	Laser: optic and characterization
Dr. Yong Wang	Physics	Super-resolution fluorescence microscopy
Dr. Mourad Benamara	Nano Institute	Transmission Electron Microscopy

* Dissertation committee members

Collaboration and consultations with the most of these research groups contributed to better experiment and interpretation of the results.

Appendix G. Description of Research for Popular Publication

Bio-Avenger: The revolution of Biological species

By Joel Kamwa

For several decades, biological species have been disregarded from application in most technologies including: semiconductors, electronics, medical device technology, and more. The progress of the science shows that biotechnology is on the rise as never before. Bacteriorhodopsin and halorhodopsin, two purple membrane-proteins, with the capability to create electricity when exposed to sunlight (photo activity), were found to be great candidate for numerous bio-scientific applications. When captured in a lipid membrane and illuminated with specific light intensities, bacteriorhodopsin and halorhodopsin can absorb the energy of the incident light, and use it to change their structure and start acting as pumps. Under this new configuration bacteriorhodopsin and halorhodopsin absorb electrically charged particles (ions) from the front side and pump them into the backside. This pumping process, also known as "vectoral charge transport", bears tremendous uncovered potential.

Human eyes are equipped with a protein called retinal. It was demonstrated that the retinal contained in bacteriorhodopsin and halorhodopsin exhibits a similar working principle as in the human retinal. Bacteriorhodopsin and halorhodopsin can, thus, be used to mimic and eventually to replace the retinal in human eyes. It was also demonstrated that the binary code 0/1 used in the development of flash drive devices can be mimicked with bacteriorhodopsin and halorhodopsin capability to pump charges under illumination. This could be achieved by replacing the code 0 with the no-pump structure (dark) and the code 1 with the pumping structure (light). This principle can serve as basis for the development of so called bio-flash drives. It was further demonstrated that the transfer principle in bacteriorhodopsin and halorhodopsin, resemble the G-protein working principle. Since the G-protein is the target of choice of most drugs,

bacteriorhodopsin and halorhodopsin could be used to study the interaction of newly developed drugs with the G-protein. It was finally demonstrated that by harvesting the pumped charge to, for example charge a battery, bacteriorhodopsin and halorhodopsin can act as Bio-Solar-Cells.

Investigators at the University of Arkansas in Fayetteville were able to construct an experimental set-up that can generate up to 40 x 10^{-11} Ampere using bacteriorhodopsin (bR), and up to 20 x 10^{-11} Ampere using halorhodopsin with a formed 100 x 10^{-5} m large lipid-protein membrane. As supporting elements in the experiments, the researchers used: sodium chloride (NaCl) to facilitate the charge flow toward the membrane, phosphate buffered saline (PBS) to supply the environment with charges, N-decane (alcohol) to help build the membrane, and the lipid called Di-Phytanoyl Phosphatidyl-Choline (DPhyPC) as the main membrane material into which bacteriorhodopsin and halorhodopsin were inserted.

The research showed that up to 2600 Ampere could be generated using an area of 1000 m^2 (~1/6 of a football field) as total bio-solar-surface. The generated energy would be sufficient to supply up to 13 North American households (at ~200 Ampere/household). The energy could also be used to charge batteries of most motor vehicles (~80 A to -300 A), and much more. The research also exhibits a new approach in "communicating" with cell membrane, as well as characterizing lipid-protein membrane for biomedical applications. Further development of the investigation will allow a better control of the parameters, a stabilization, and accurate prediction of the outcomes.

Appendix H. Executive Summary of Newly Created Intellectual Property

The following new intellectual property items was created in the course of this research project and should be considered from both a patent and commercialization perspective.

1. The fabricated chamber, made of polydimethylsiloxane (PDMS) presented in 0 is a particularly efficient way to transport a real current generating membrane, and to capture its structure using an imaging equipment such as TEM or AFM.
2. The rudimentary aspect of the experimental set-up makes it a unique and open possibility to use it as experimental kit for school labs.

Appendix I. Potential Patent and Commercialization Aspects of Intellectual Property

The following two aspects were considered first from the perspective of whether the process, and or items could be patented.

I.1 Patentability of Intellectual Property (Could Each Item be patented)

1. The intellectual properties associated with the fabricated chamber made of polydimethylsiloxane (PDMS) have solid patentability potential. However, the results gathered with this type of chamber at this point of the investigation, do not constitute tangible proof of concept to allow starting a patent process.
2. No kits were created or tested for this research. The rudimentary aspect of the research is just a facilitating way to perform this type of experiments and cannot be claimed as intellectual property.

I.2 Commercialization Prospects (Should Each Item Be Patented)

1. Once successfully implemented multiple times, the fabricated chamber made of polydimethylsiloxane (PDMS) will present a particularly efficient way to transport a real current generating membrane, and to capture its structure using an imaging equipment such as TEM or AFM. A commercialization strategy would be needed to ensure the distribution of this tool within the research world. However, the potential market for this type of device is reduced to a niche of the research world, which would not justify the pursuit of a patent from a financial point of view.
2. The simplicity of the experiments in this work allows the experiments to be performed in rudimentary labs, such as schools laboratories. This experiment can be developed as a kit and commercialized to bring this type of solar conversion method to a broader audience. The reduced number of potential customers, however, does not justify the development of a profitable business or the acquisition of a patent on this device.

Appendix J. Broader Impact of Research

J.1. Applicability of Research Methods to Other Problems

The results generated in this work specifically support the development of a better, more stable set-up for photocurrent generation and lipid-protein membrane characterization. The results serve as additional means to understand ions translocation and improve artificial photosynthesis. The results serve as support element for the development of bacteriorhodopsin and halorhodopsin based bioelectronics, retinal-prosthesis, bio-solar-cell, and more. The results generated in this work could also be used to support the development of new drugs (interaction with membranes), and the investigation of other types of biological charge transfer processes.

J.2. Impact of Research Results on U.S. and Global Society

The work presented here not only supports the development of bio-medical and bio-electronic devices; this research is also a welcomed alternative to conventional carbon-based energy generation methods. Additional experiments will be necessary to identify means to effectively use bacteriorhodopsin, halorhodopsin, and other types of ions-pumps as an energy harvester. The ideas developed here support the effort deployed to address global warming and the energy shortage.

J.3. Impact of Research Results on the Environment

Besides being a non-carbon-based energy generation solution, bio-compatibility and recyclability are among the best attributes of this investigation. The environmental friendliness of the experiments was central in the definition of the research. In fact, all used specimen were biocompatible. The electrophysiology measurement and handling equipment used in this work were reused for the entire period of the investigation. As a non-carbon-based energy generation solution, the developed idea would be, with 0% emission, a blessing for the environment.

Appendix K. Microsoft Project.

Appendix L. Identification of Software Used in Research and Dissertation Generation

1- Computer #1: DELL

Model Number: Dell Optiplex 390

Serial Number: 7215609313

Location: PHYS119

Owner: Prof. Jiali Li

Software #1:

Name: Microsoft Office 2007

Purchased by: University of Arkansas physics Department.

Software #2:

Name: pClamp 10 from AxoScope

Purchased by: Prof. Jiali Li

Software #3:

Name: Clampfit 10 from AxoScope

Purchased by: Prof. Jiali Li

Software #3:

Name: Adobe Acrobat Professional 10.0

Purchased by: University of Arkansas Site License 68

Software #3:

Name: Microsoft project

Purchased by: Microelectronics-Photonics graduate program, University of Arkansas

2- Computer #2: DELL

Model Number: Dell Optiplex 390

Serial Number: JHKMRH1

Location: PHYS125

Owner: Prof. Jiali Li

Software #1:

Name: Microsoft Office 2007

Purchased by: University of Arkansas physics Department.

Software #2:

Name: pClamp 10 from AxoScope

Purchased by: Prof. Jiali Li

Software #3:

Name: Clampfit 10 from AxoScope

Purchased by: Prof. Jiali Li

Software #3:

Name: Adobe Acrobat Professional 10.0

Purchased by: University of Arkansas Site License 68

Appendix M. All Publications Published, Submitted and Planned

1) Kamwa, S. Singh, J. Li. “Photo-Current and TEM Imaging Characterization of Light-Gated Ion Pump Proteins in Lipid Membranes” Biophysical Journal, Volume 110, Issue 3, Supplement 1, February 2016, pp. 313a.